The Abdus Salam
International Centre for Theoretical Physics

United Nations
Educational, Scientific and
Cultural Organization

IAEA
International Atomic Energy Agency

2272-6

Joint ICTP-IAEA School on Synchrotron Applications in Cultural Heritage and Environmental Sciences and Multidisciplinary Aspects of Imaging Techniques

21 - 25 November 2011

Ion Beam Analysis Techniques for Cultural Heritage and Environmental Applications

Massimo Chiari
INFN, Florence
Italy

Strada Costiera 11, 34151 Trieste, Italy - Tel.+39 040 2240 111; Fax +39 040 224 163 - sci_info@ictp.it

Ion Beam Analysis Techniques for Cultural Heritage and Environmental Applications

Massimo Chiari / *I.N.F.N. Florence*

chiari@fi.infn.it

max0068

Joint ICTP-IAEA School on "Synchrotron Applications in Cultural Heritage and Environmental Sciences and Multidisciplinary Aspects of Imaging Techniques", Trieste - Italy, 21 - 25 November 2011

IBA techniques basics

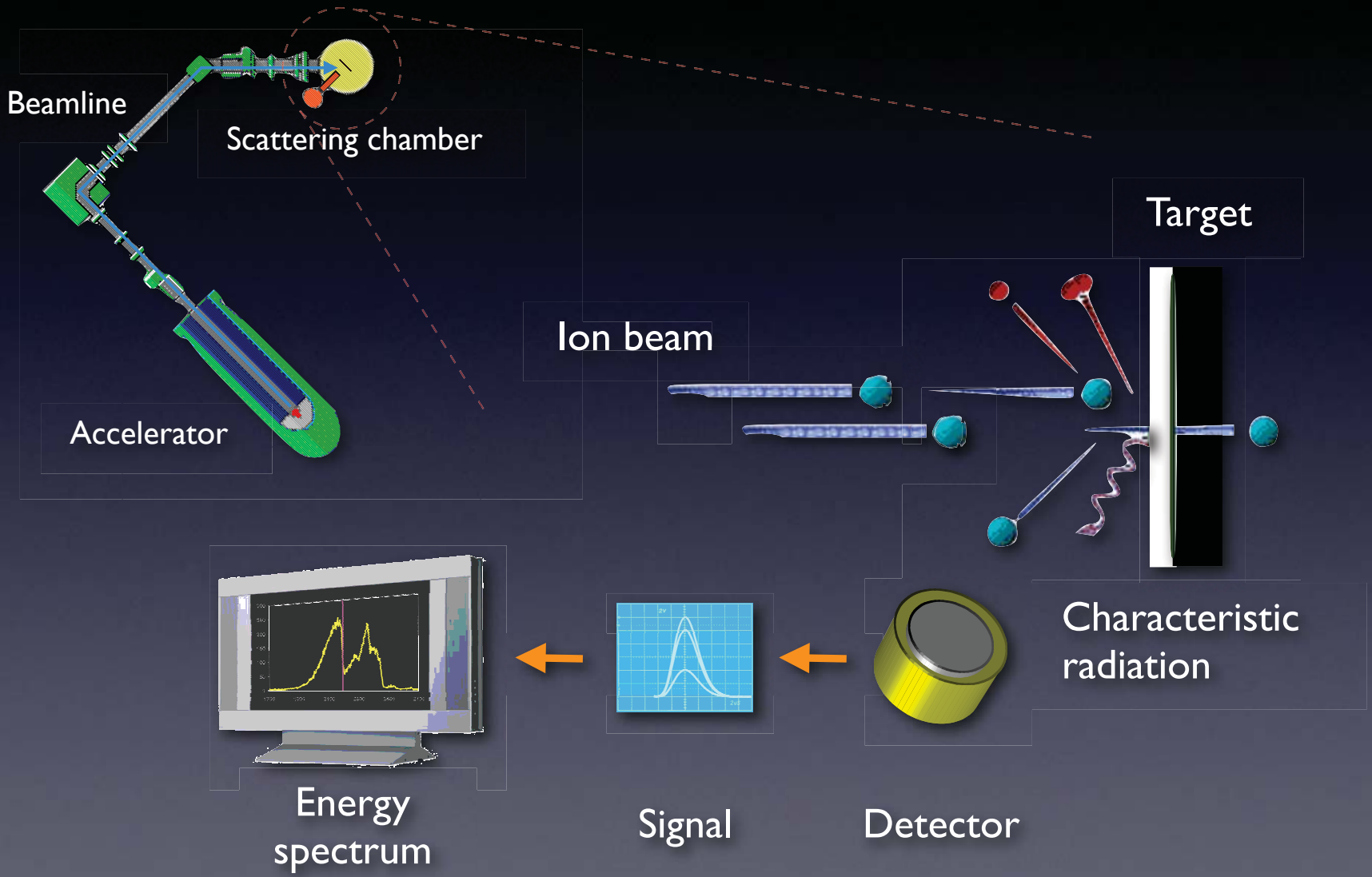

Stopping power

The "stopping power" (the energy lost per unit lenght, *dE/dx*) is a macroscopic and measurable quantity, describing the average interaction of the ion with the material:

$$-\frac{dE}{dx} = \frac{4\pi}{m_e c^2} \cdot \frac{nz^2}{\beta^2} \cdot \left(\frac{e^2}{4\pi\varepsilon_0}\right)^2 \cdot \left[\ln\left(\frac{2m_e c^2 \beta^2}{I \cdot (1-\beta^2)}\right) - \beta^2\right]$$

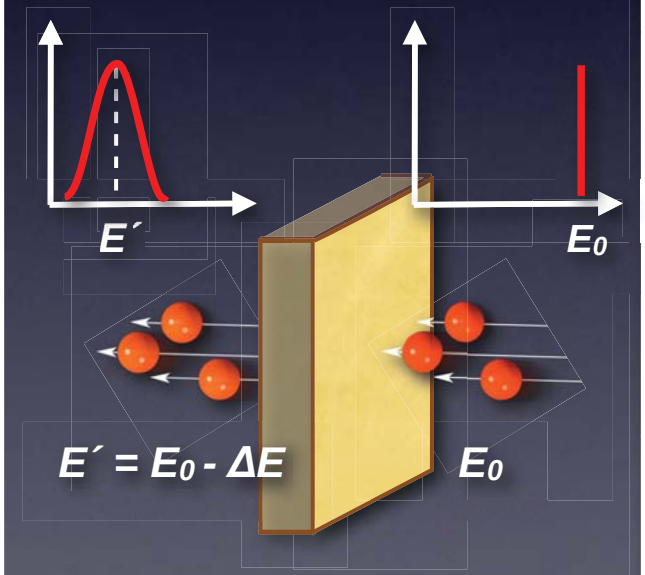

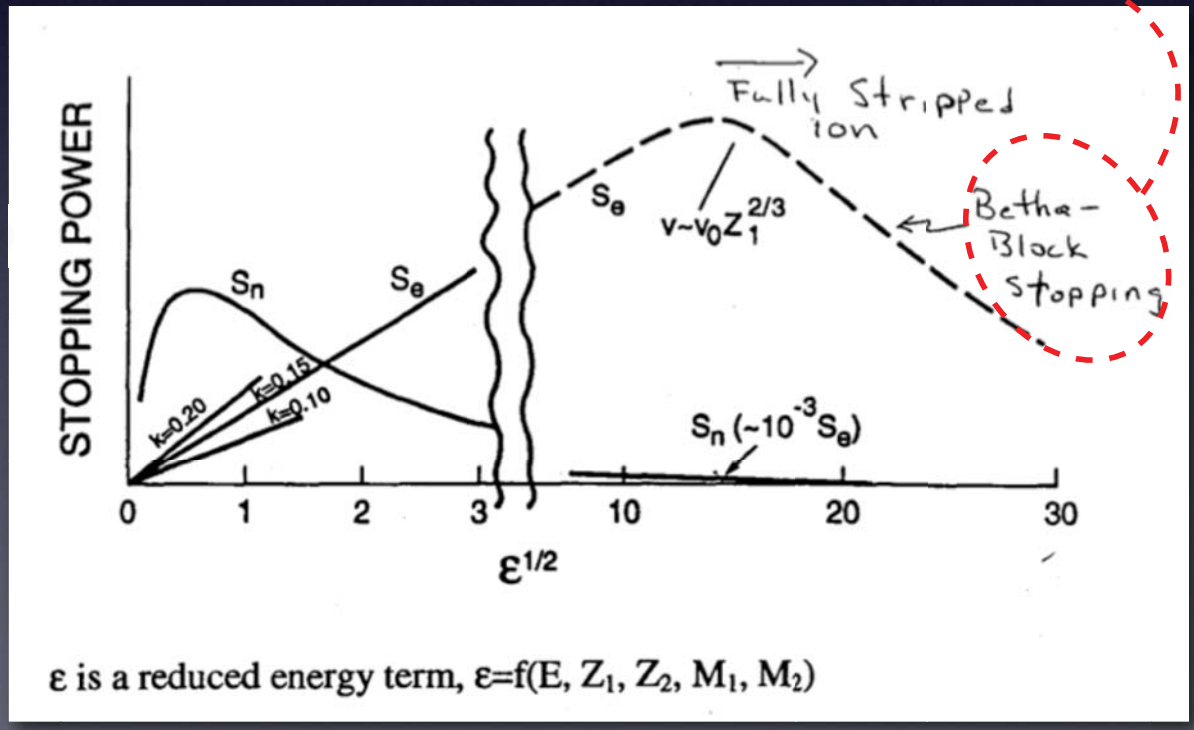

IBA

Ion Beam Analysis

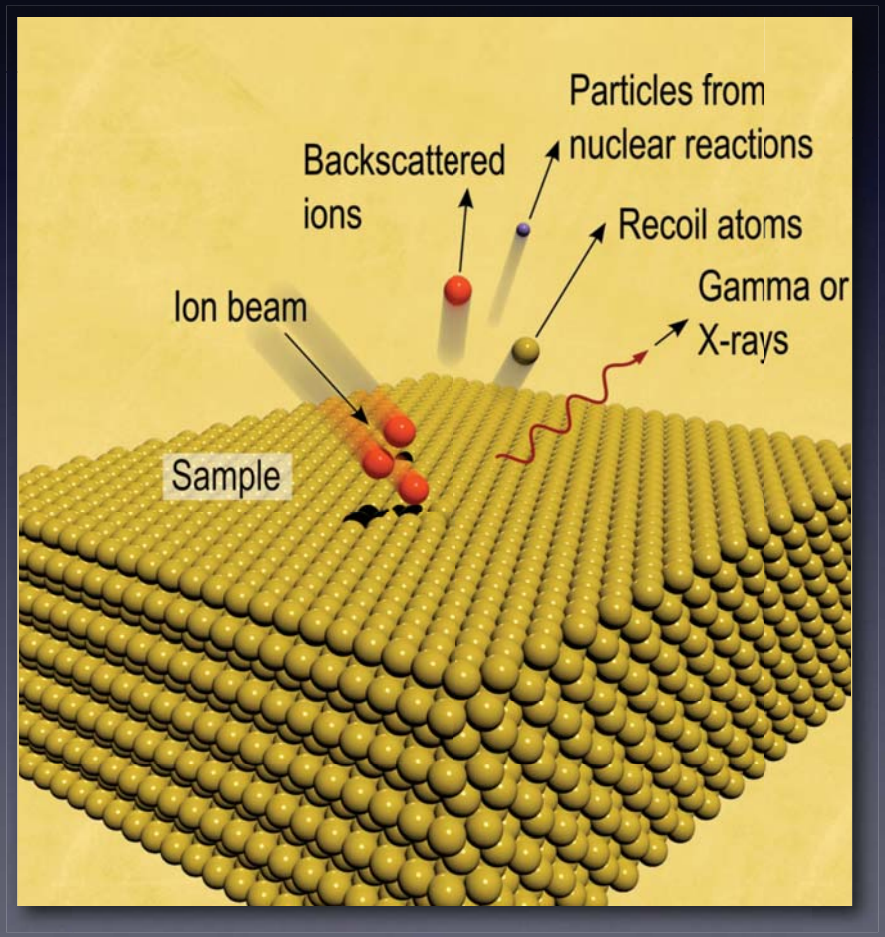

Beam IN	Beam OUT	Analytical technique
ion	ion	RBS, NRA
ion	target	ERDA, SIMS, SNMS
ion	X-ray	PIXE
ion	Gamma-ray	PIGE, Activation Analysis
ion	hν	Ionoluminescence (IL)

General features of IBA

- Multielemental
- Quantitative analysis ("traceability")
- High sensitivity (1-100 ppm in at/cm^3; 10^{11}-10^{12} in at/cm^2)
- Surface analysis (10 Å - 10 µm)
- Depth profiling
- Non-destructive
- No sample pre-treatment
- Microanalysis (lateral resolution <1 µm)
- 2D mapping

External beam

Advantages

- direct analysis of artefacts having any shape and any size
- no sampling
- no charging, no preparation (conductive coating etc.)
- no heating, reduced damage risk
- easy sample positioning
- fast and efficient

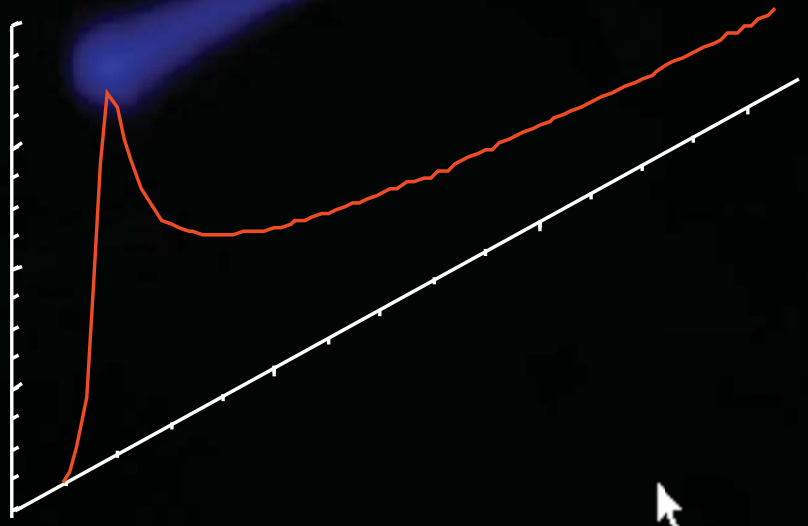

Disadvantages

- energy loss
- energy straggling
- beam lateral spread

The LABEC laboratory in Florence

3 MV Tandetron accelerator
3 independent ion sources
6 beam lines for IBA (3 external-beam lines)
1 beam line for AMS

The external-beam lines at LABEC

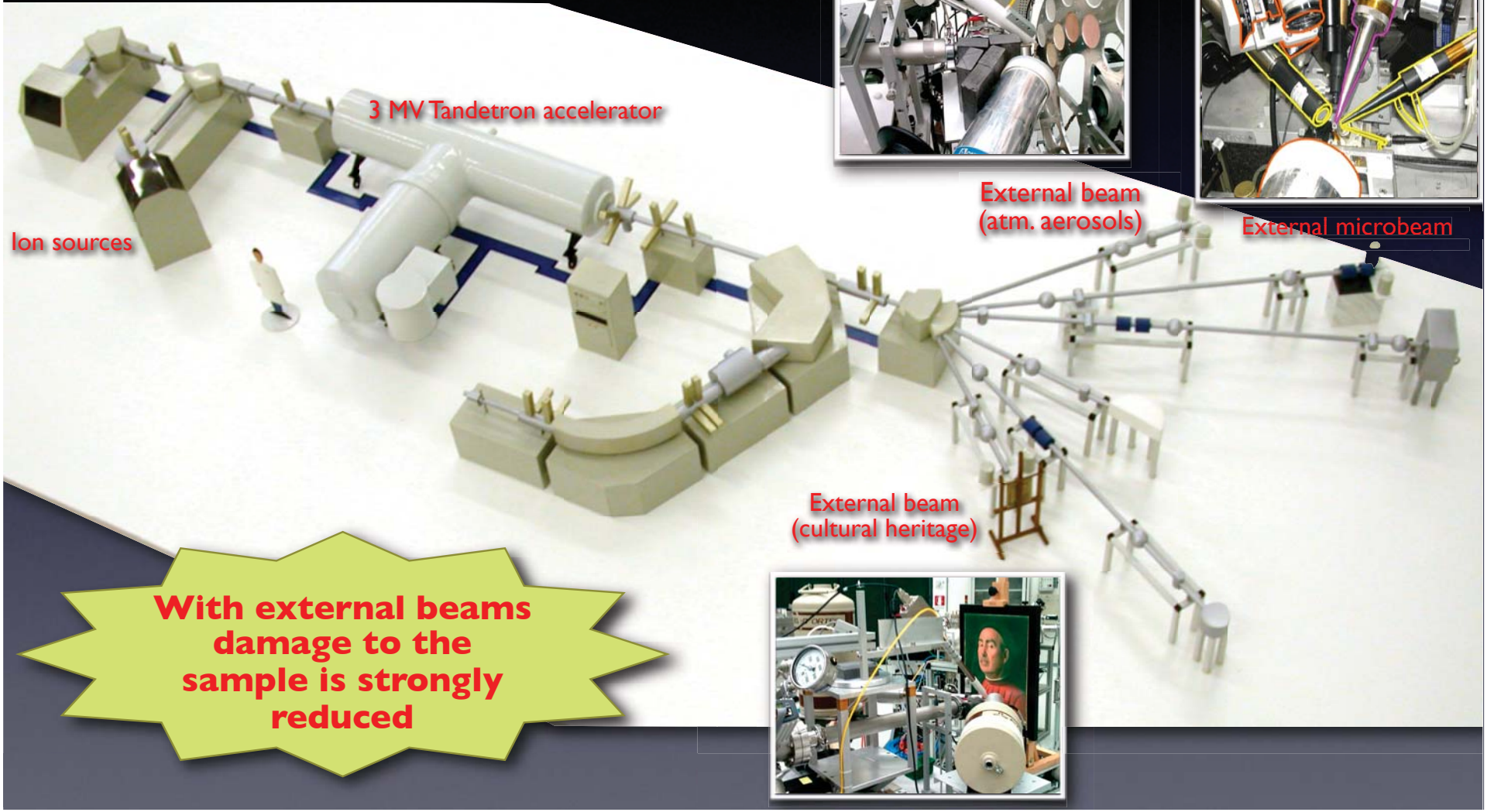

With external beams damage to the sample is strongly reduced

External-beam set-ups

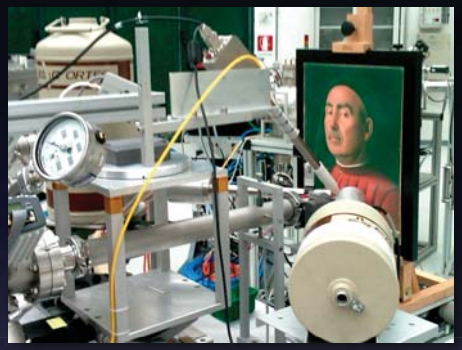

Cultural Heritage
-45° beamline

- PIXE (x2)
- PIGE
- RBS

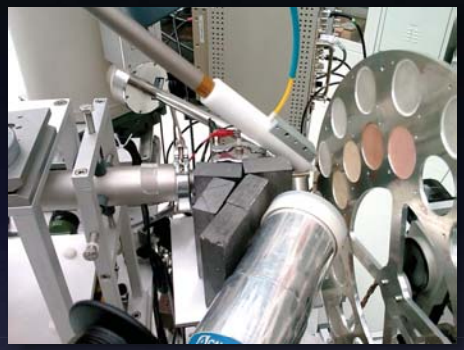

Atmospheric aerosol
+45° beamline

- PIXE (x2)
- PIGE
- PESA

Microbeam
+30° beamline

- 10 μm @ 3MeV p
- PIXE (x2)
- PIGE
- RBS
- PESA/ERDA
- IBIL

The external microbeam line

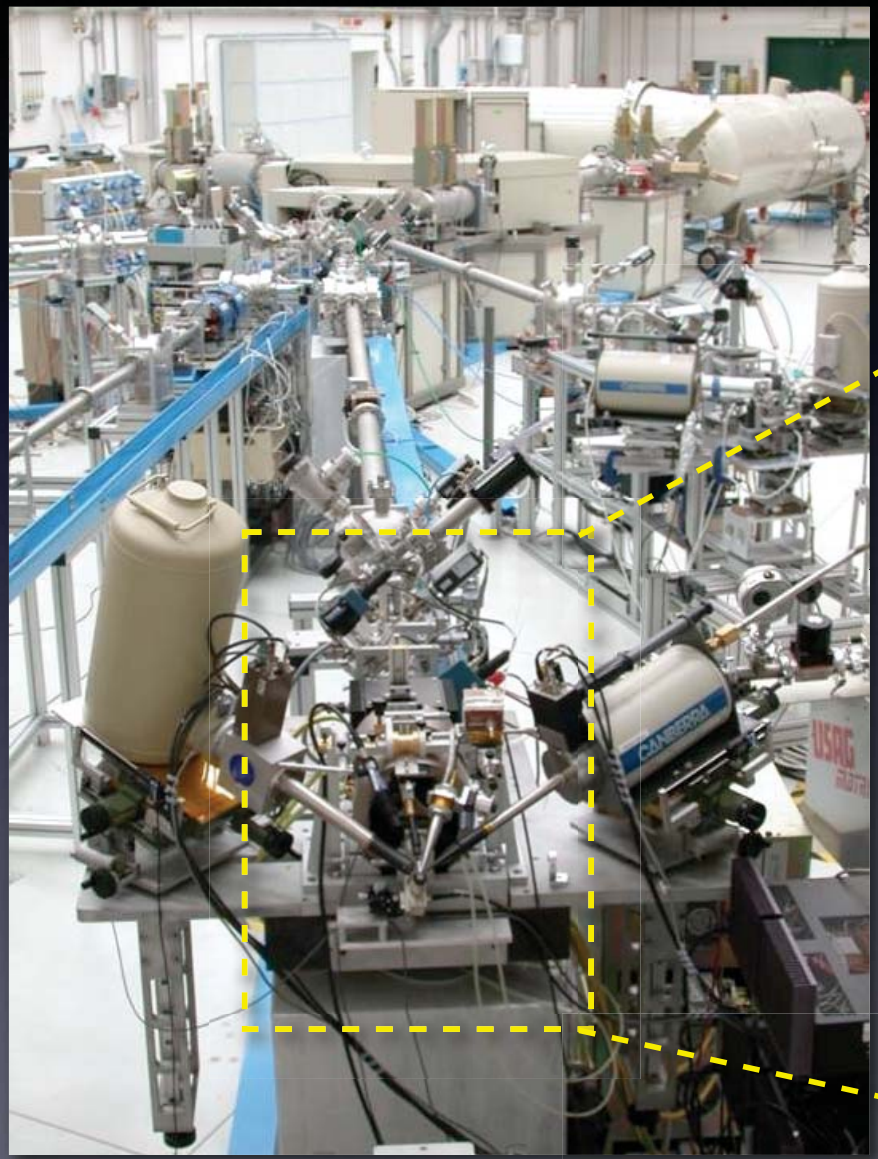

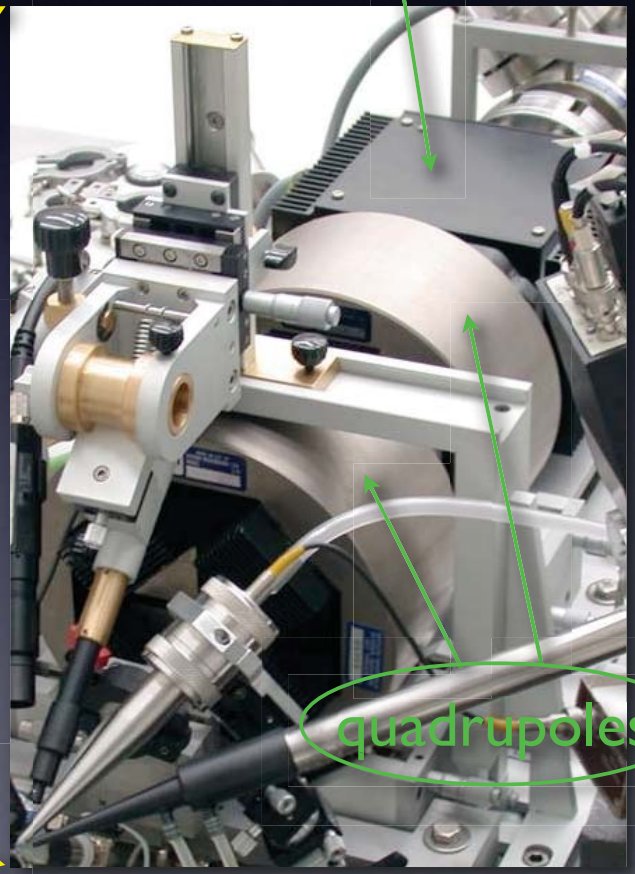

Microbeam experimental set-up

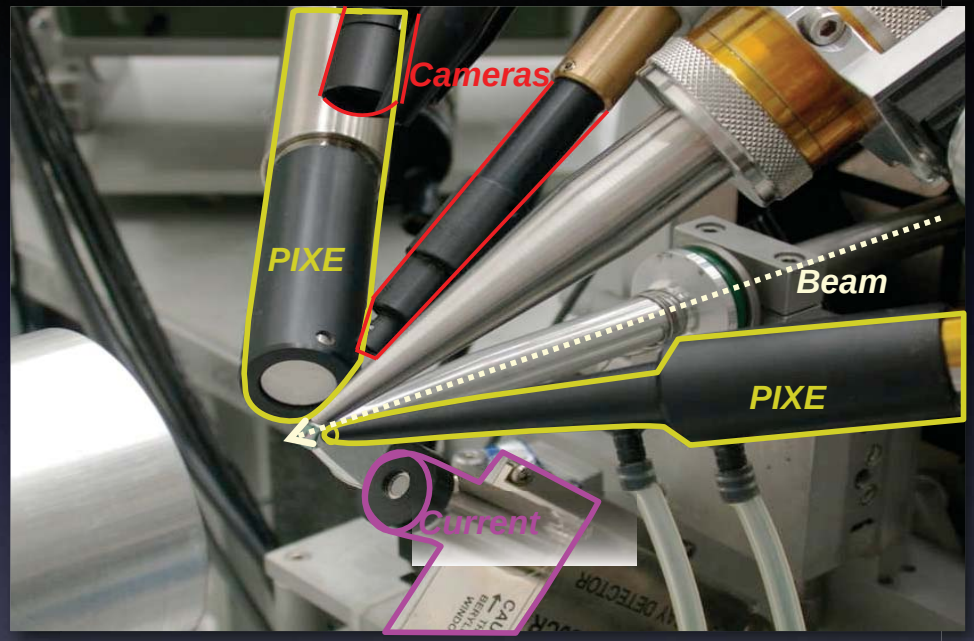

Standard two detectors set-up, (“small” and “big”) optimized for low and medium-high energy X-rays detection

(+ PIGE, RBS, STIM, IBIL)

- Si_3N_4 extraction window (100, 200 or 500 nm thick)
- Target at 2-3 mm from the exit window, path saturated with helium
- 3 MeV protons:
  10 µm spatial resolution
  ~10 keV energy straggling

External beam PIXE-PIGE facility

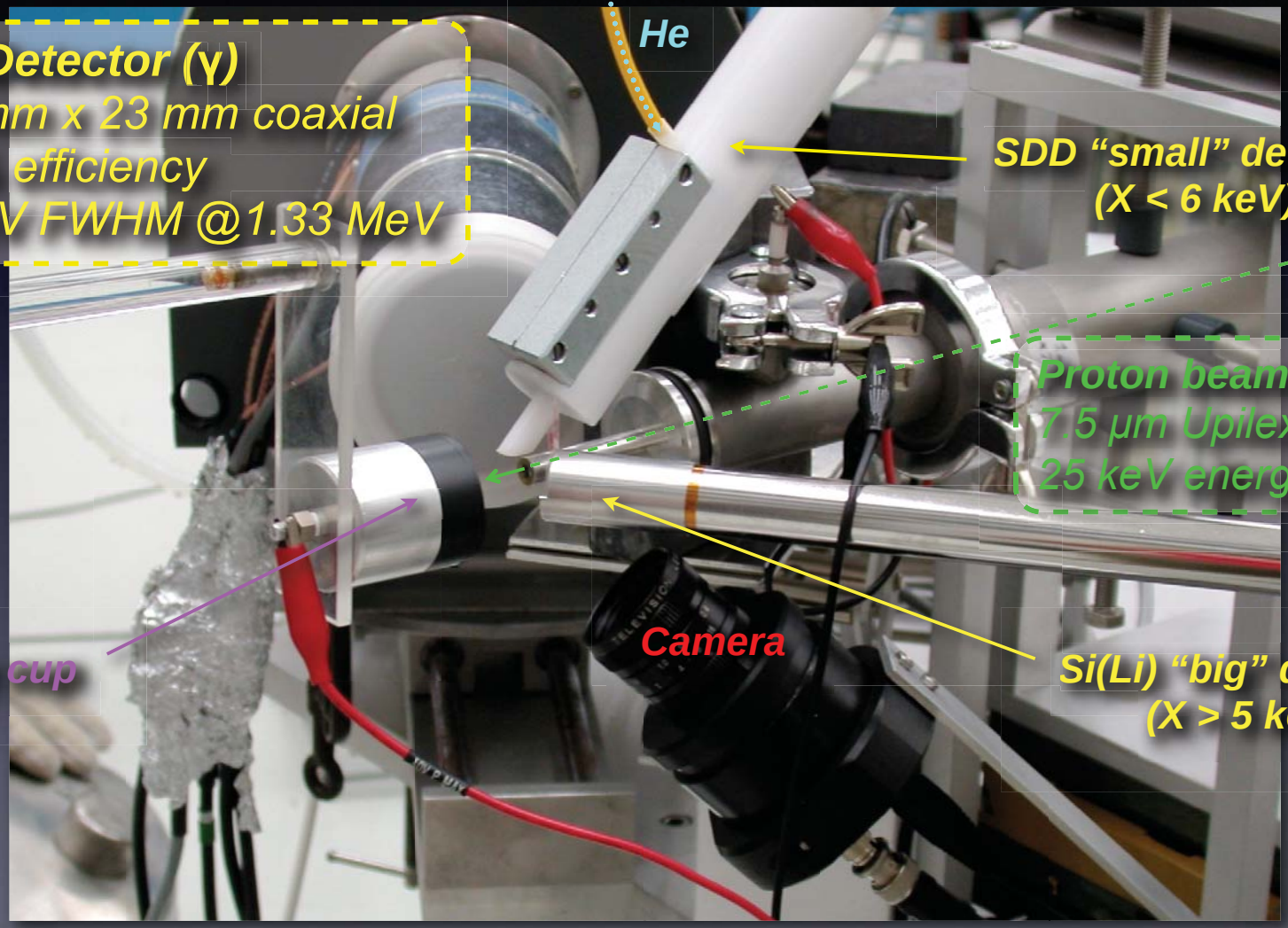

PIXE

Particle Induced X-ray Emission

Emission of characterisic X-rays following ioniziation from incident ions

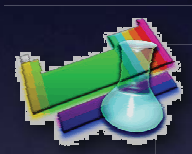

Z>10

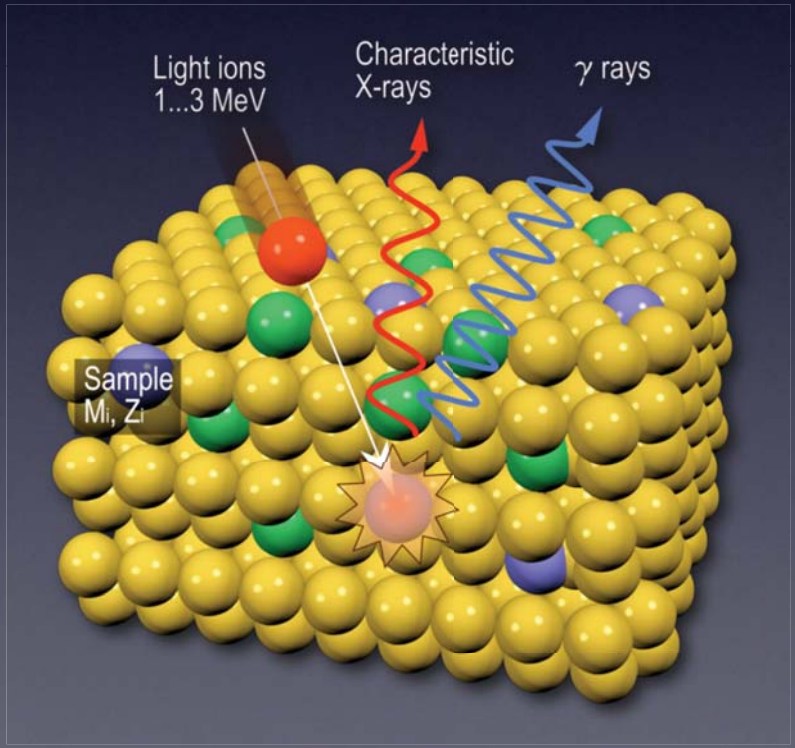

Energy of characteristic X-rays

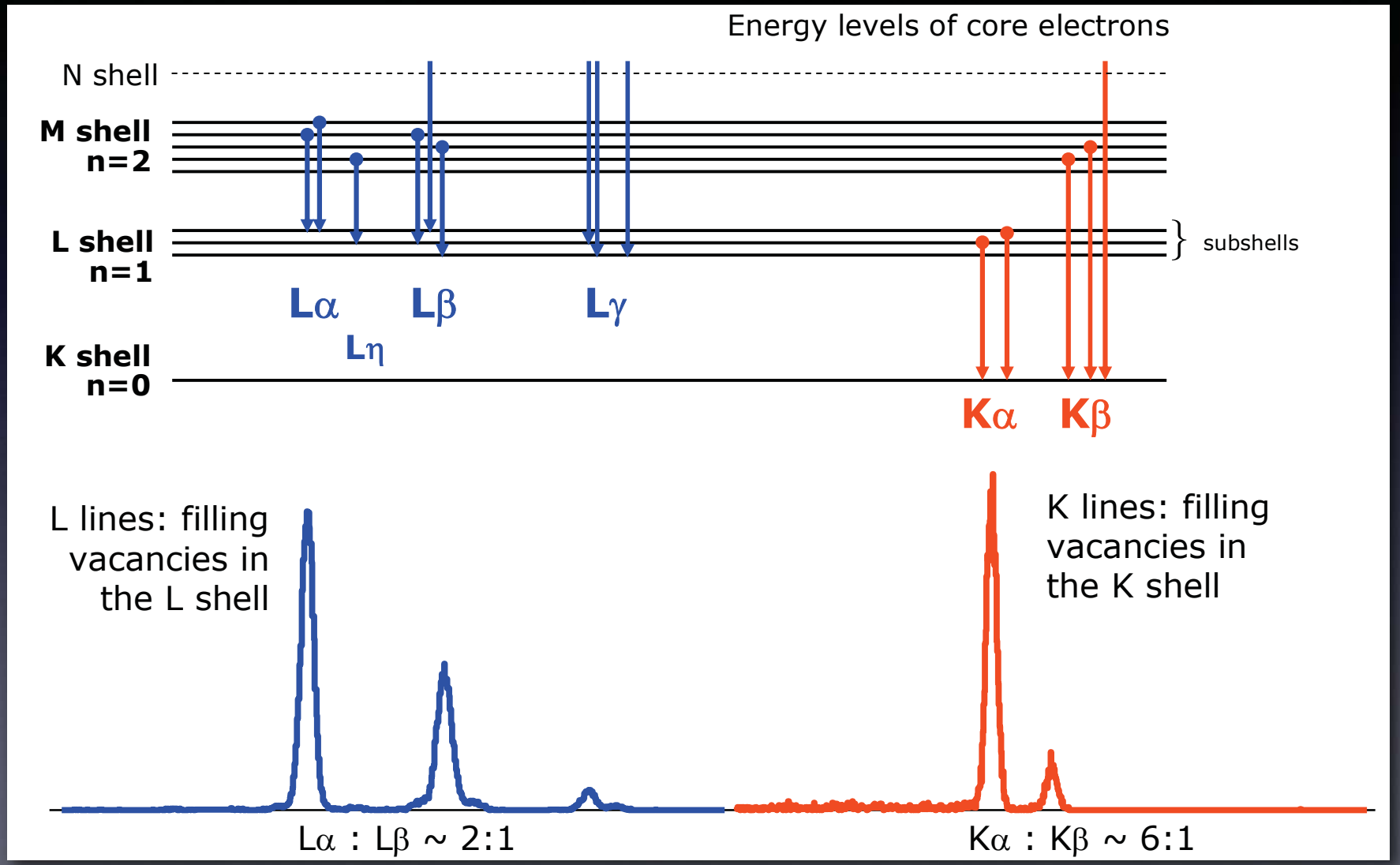

Energy of characteristic X-rays

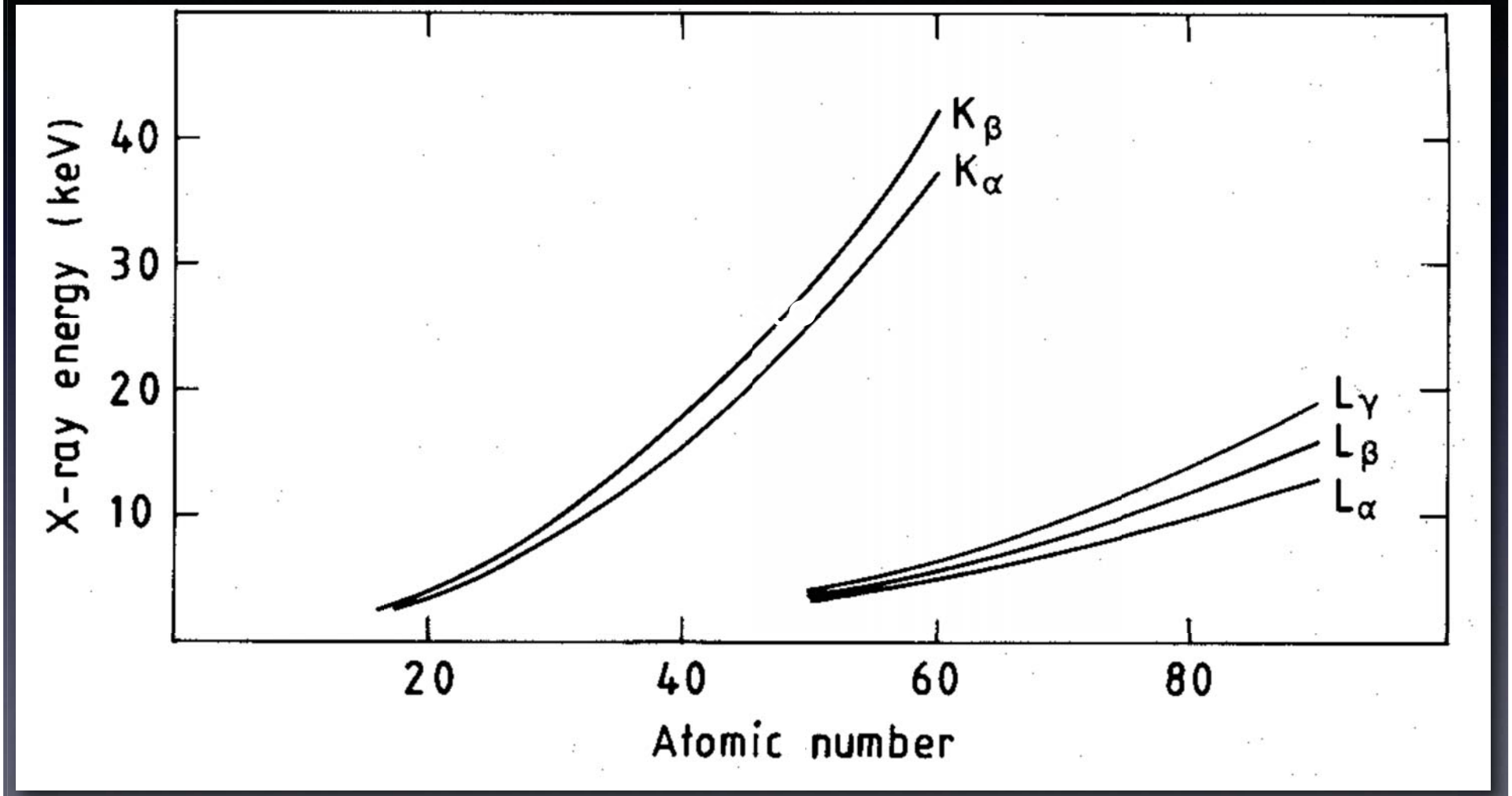

X-ray production cross sections

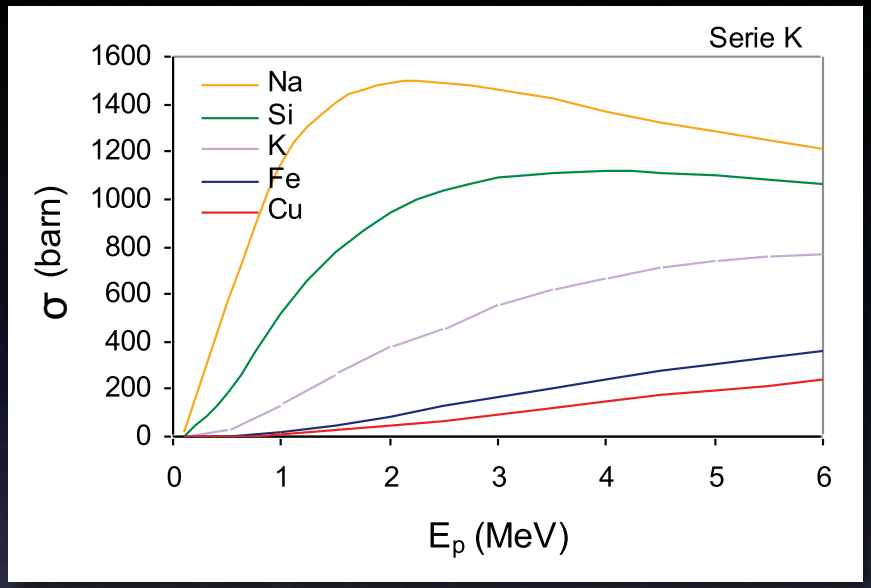

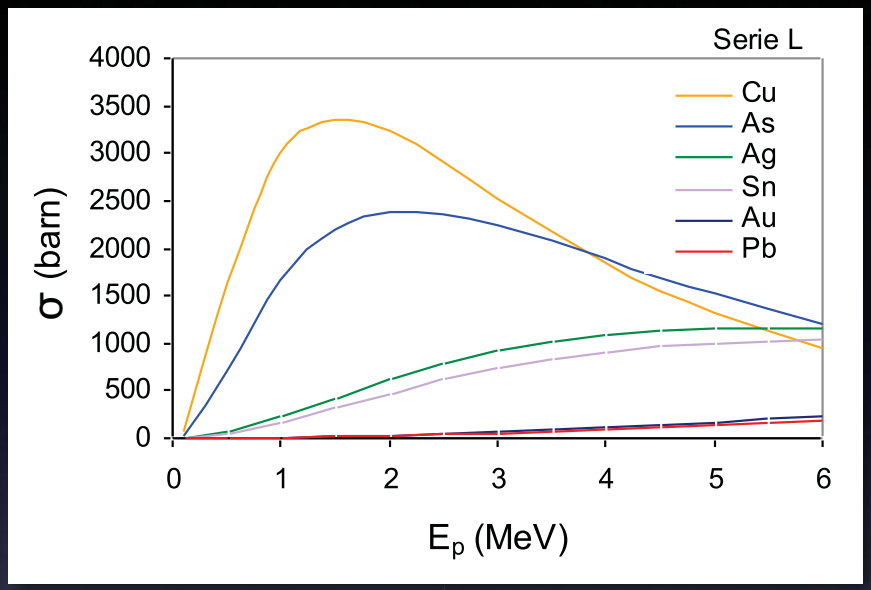

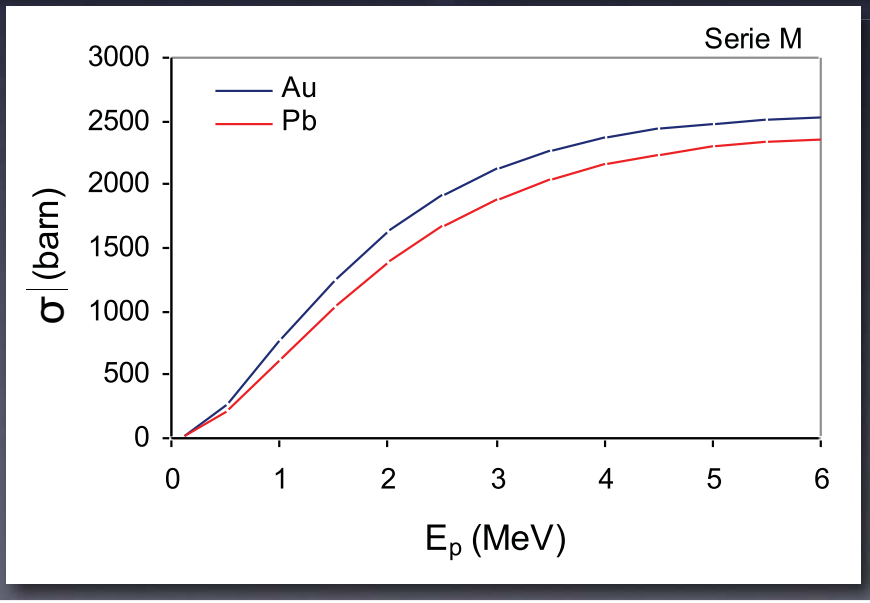

Adavantages of PIXE

- very fast, high-sensitivity, **non-destructive** analysis
- **quantitative** analysis
- minimum energy of detected X-rays tipically ~1 keV

➡ *all the elements with $Z \geq 11$ are quantifible simultaneously*

Limitations of PIXE

- no information on the organic components
- no direct information on chemical bonds

but… hypothesis on stoicheometry through quantitative and multielemental anaylisis

- no direct information on the stratigrapgy and the depth distribution of the elements

but… Differential PIXE

Example of PIXE spectra: aerosol particles

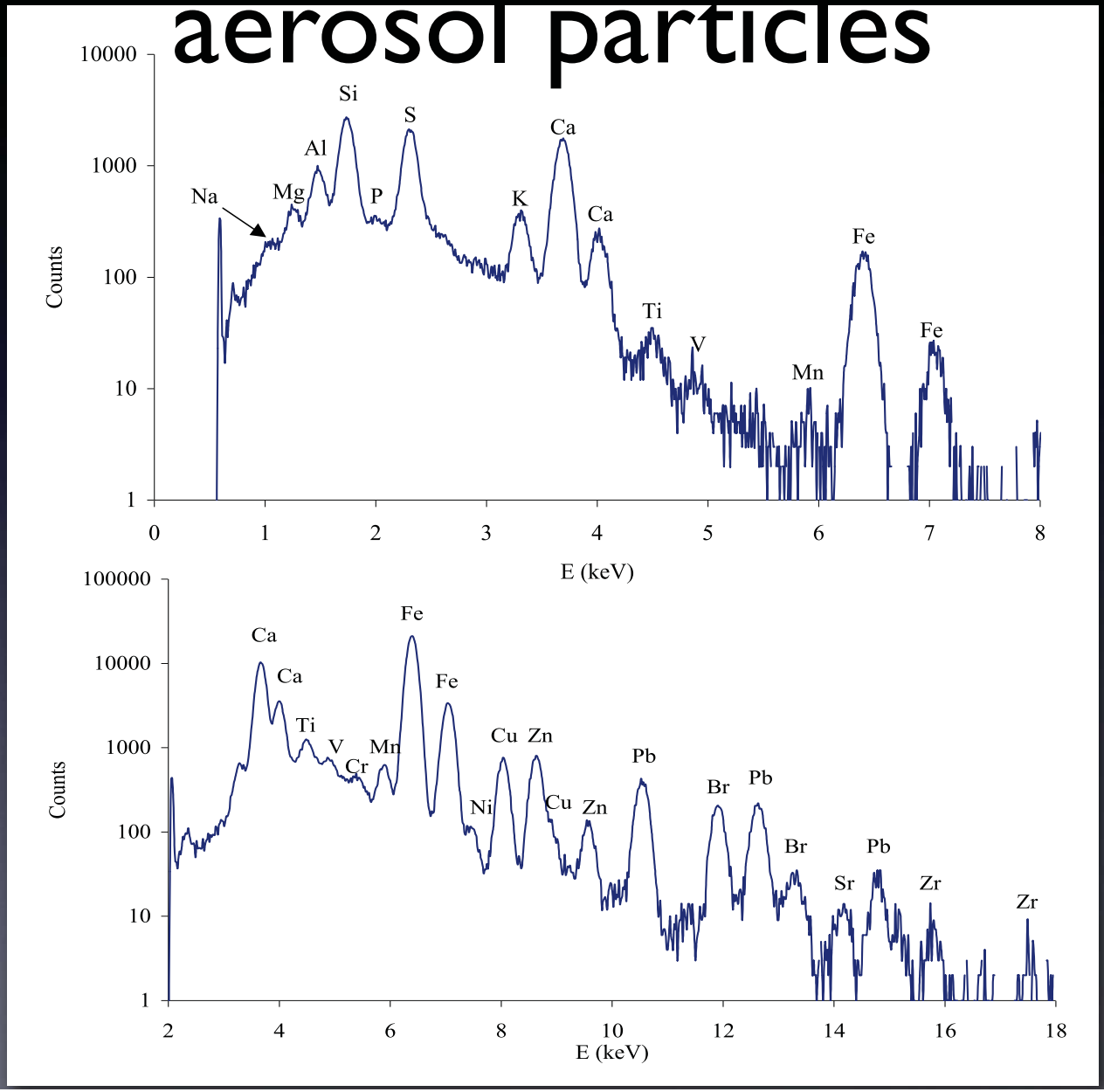

Quantitative analysis (thin target)

$$Y_0(Z) = N_P \cdot N_Z \cdot t \cdot \sigma_{Z,E0} \cdot (\alpha_Z \cdot \varepsilon_Z \cdot \Delta\Omega/4\pi)$$

$$Y_0(Z) = (Q/e)(N_A/A)(\rho_Z t) \cdot \sigma_{Z,E0} \cdot (\alpha_Z \cdot \varepsilon_Z \cdot \Delta\Omega/4\pi)$$

with $$\eta_Z = (1/e)(N_A/A) \cdot \sigma_{Z,E0} \cdot (\alpha_Z \cdot \varepsilon_Z \cdot \Delta\Omega/4\pi)$$

$$Y_0(Z) = \eta_Z \cdot Q \cdot (\rho_Z t)$$

$$\mathbf{(\rho_Z t) = Y_0(Z) / (\eta_Z \cdot Q)}$$

Thick targets

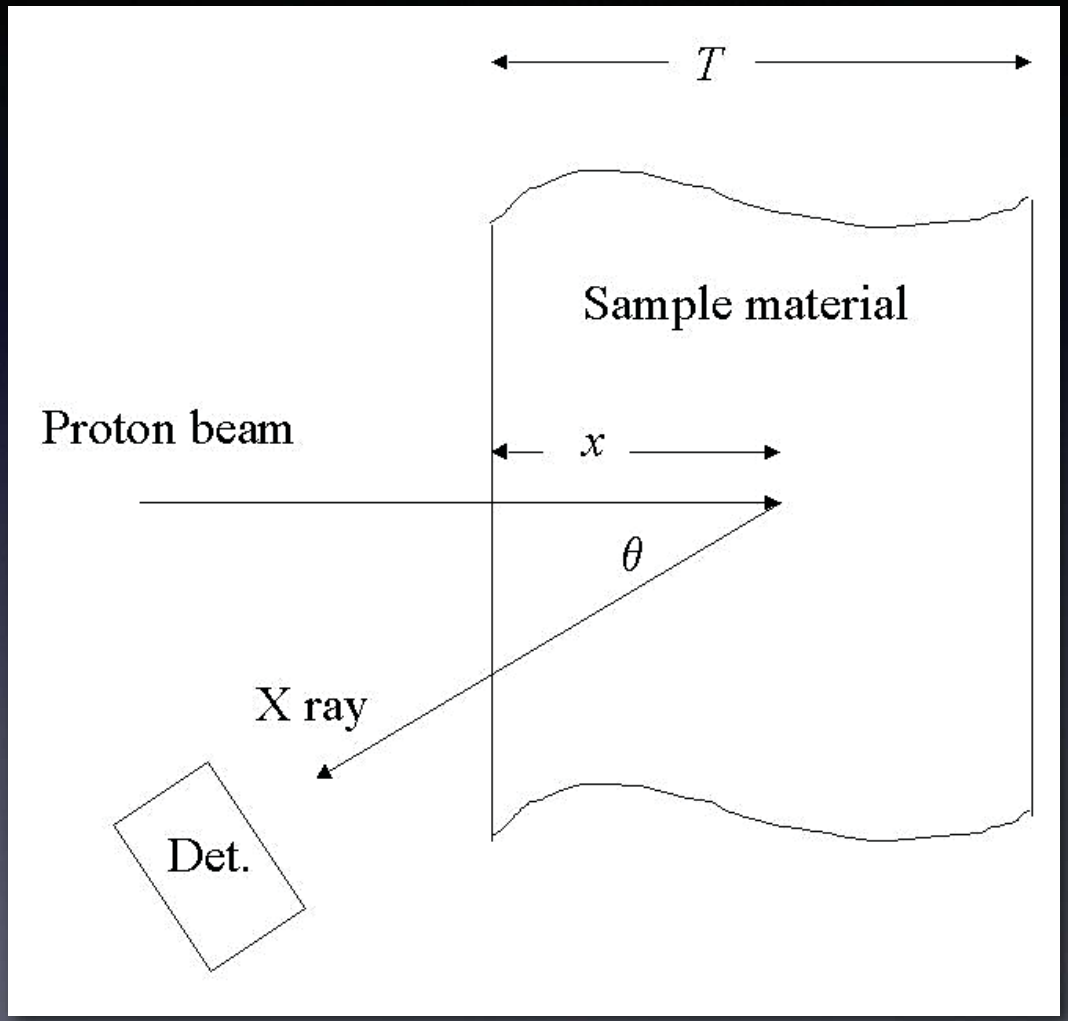

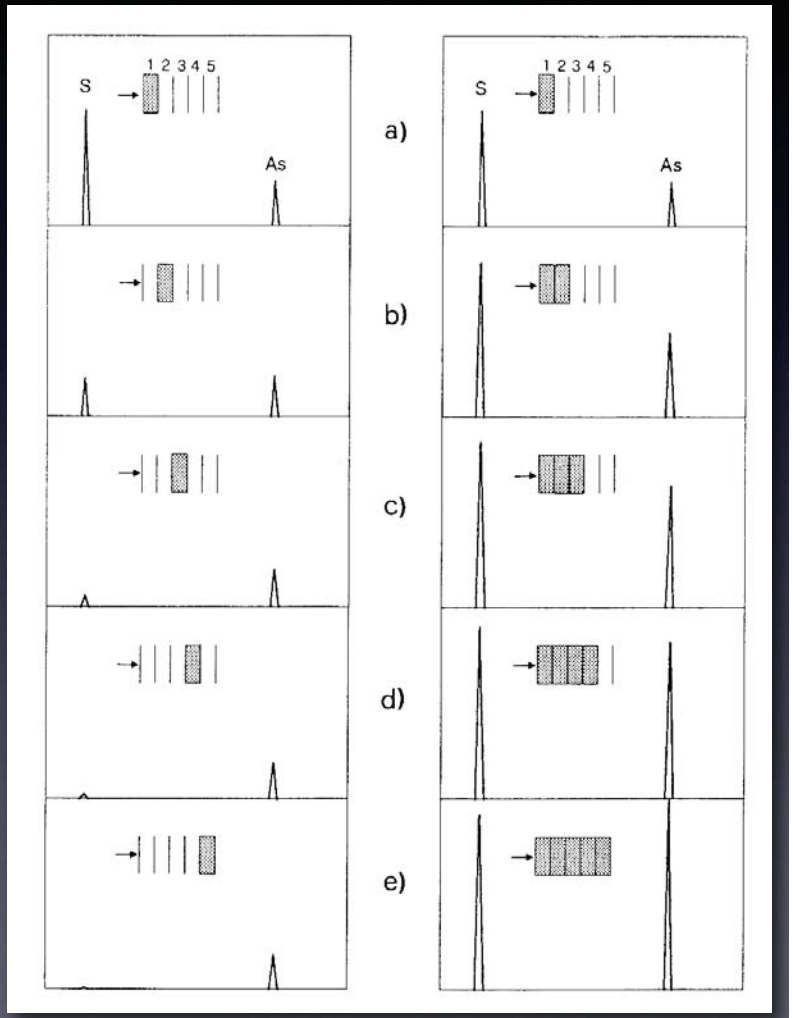

Quantitative analysis (thick targets)

$$Y(Z) = (Q/e)(N_A/A)(\alpha_Z \cdot \varepsilon_Z \cdot \Delta\Omega/4\pi) \cdot \rho_Z \int_0^T \sigma_{Z,E} \cdot exp(-\mu \cdot x/cos\theta) \cdot dx$$

$$Y(Z) = (Q/e)(N_A/A)(\alpha_Z \cdot \varepsilon_Z \cdot \Delta\Omega/4\pi)(\rho_Z/\rho) \int_E^F \sigma_{Z,E} \cdot exp(-\mu \cdot x/cos\theta) \cdot dE/S(E)$$

$$F(Z) = Y_0(Z)/Y(Z) = \frac{\rho \cdot T \cdot \sigma_{Z,E0}}{\int_E^0 \sigma_{Z,E} \cdot exp(-\mu \cdot x/cos\theta) \cdot dE/S(E)}$$

$$\mathbf{(\rho_Z t) = F(Z) \cdot Y(Z) / (\eta_Z \cdot Q)}$$

2-detectors PIXE set-up

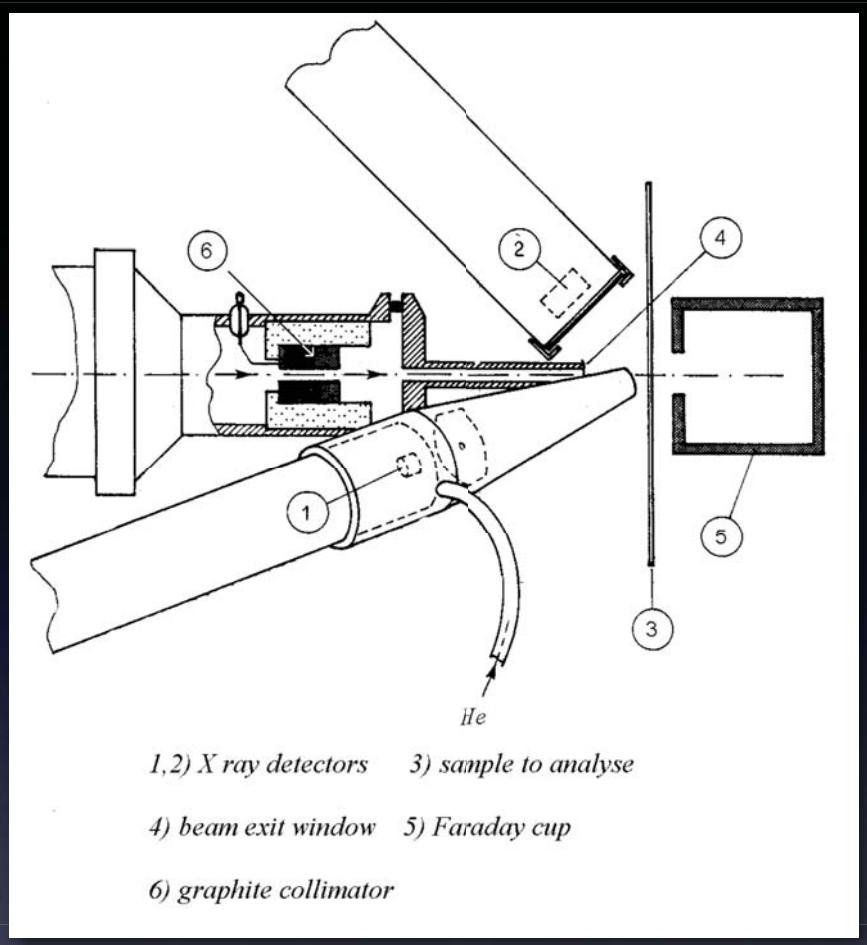

1,2) X ray detectors *3) sample to analyse*

4) beam exit window *5) Faraday cup*

6) graphite collimator

Target	X-rays	What is needed	Detector features
Low-Z elements	Low energy High cross sections	Minimum dead layers Small solid angles	Thin entrance window Small active area
Medium-high-Z elements	High energy Low cross sections	Large solid angles Efficiency	Large active area Large active thickness

Detection efficiency for a 2-detectors PIXE set-up

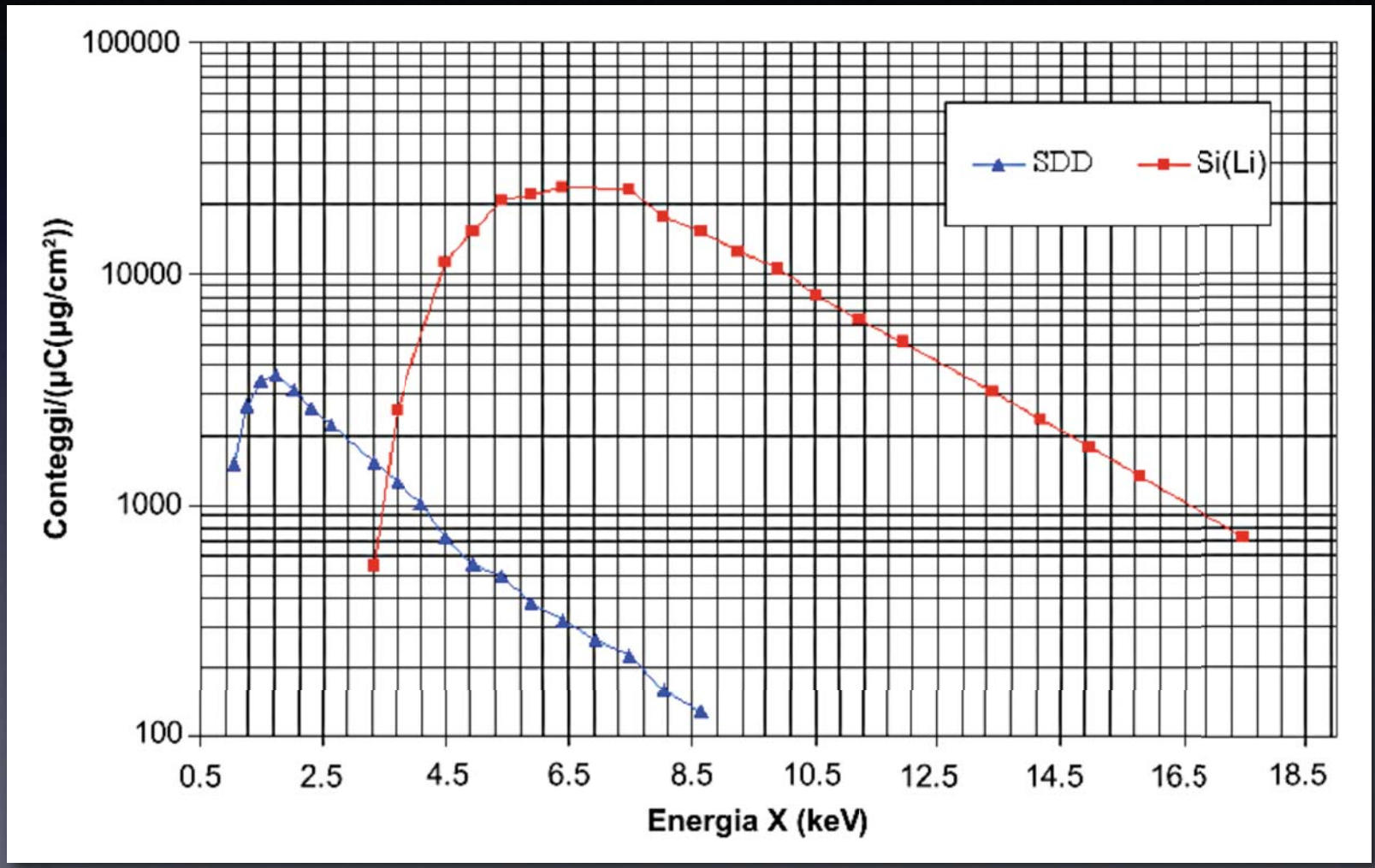

PIGE

Particle Induced Gamma-ray Emission

Prompt emission of gamma-rays during the ion beam irradiation

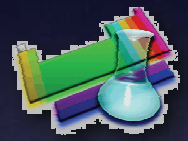

Li, B, F, Na, Al...

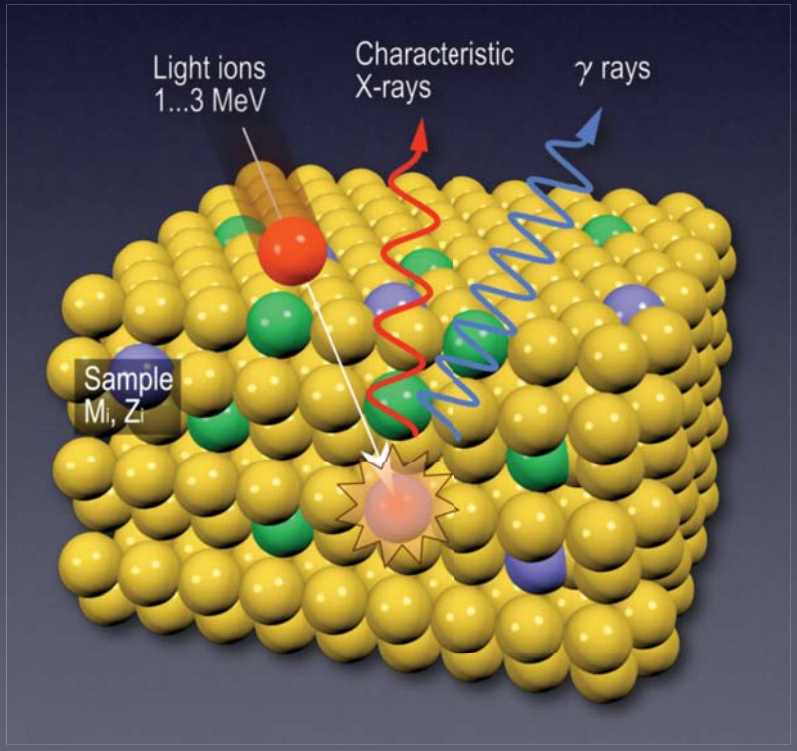

Nuclear reactions with prompt emission of gamma -rays

Radiative capture (direct reaction)	$a + A \rightarrow B^* \rightarrow B + \gamma$	$^{27}Al(p,\gamma)^{28}Si$
Inelastic scattering	$a + A \rightarrow A^* + a'$ $\searrow$ $A + \gamma$	$^{27}Al(p,p'\gamma)^{27}Al$
Rearrangement collisions	$a + A \rightarrow C^* + c$ $\searrow$ $C + \gamma$	$^{27}Al(p,\alpha\gamma)^{24}Mg$

List of proton-induced reaction

Element	E_γ (keV)	Nuclear origin	Transition	Detection limit (%)	Possible interferences
Li	429	$^{7}Li(p,n\gamma)^{7}Be$	429 → 0	0.01	As(427), B(429)
	478	$^{7}Li(p,p'\gamma)^{7}Li$	478 → 0	5×10^{-4}	Be(478), Mn(478)
Be	415	$Be^{9}(p,\gamma)B^{10}$	2154 → 1740		Ag(415)
	718	$Be^{9}(p,\gamma)B^{10}$	718 → 0		B(718)
	1023	$Be^{9}(p,\gamma)B^{10}$	1740 → 718		Ti(1022)
	1437	$Be^{9}(p,\gamma)B^{10}$	3590 → 2150		
	3562	$Be^{9}(p,\alpha\gamma)Li^{6}$	3562 → 0	0.1	
B	429	$^{10}B(p,\alpha\gamma)^{7}Be$	429 → 0		As(427), Li(429)
	478	$^{10}B(p,\alpha\gamma)^{7}Be \rightarrow {}^{7}Li$	478 → 0		Li(478), Mn(478)
	718	$^{10}B(p,p'\gamma)^{10}B$	718 → 0		Be(718)
	2124	$^{10}B(p,p'\gamma)^{10}B$	2124 → 0	5×10^{-3}	
	4433	$^{11}B(p,\gamma)^{12}C$	4433 → 0		N(4433)

List of proton-induced reaction

Element	E_γ (keV)	Nuclear origin	Transition	Detection limit (%)	Possible interferences
C	2357	$^{12}C(p,\gamma)^{13}N$	2357 → 0	1	
N	1400	$^{14}N(p,\gamma)^{15}O$			Cr(1400)
	4433	$^{15}N(p,\alpha\gamma)^{12}C$	4433 → 0		B(4433)
O	110	$^{18}O(p,\gamma)^{19}F$	110 → 0		F(110), W(111)
	197	$^{16}O(p,\gamma)^{19}F$	197 → 0		F(197),Co(197),Ni(197), Ga(197),Ti(199),Ge(199)
	496	$^{16}O(p,\gamma)^{17}F$	496 → 0	5	Ga(493)
F	110	$^{19}F(p,p'\gamma)^{19}F$	110 → 0	2×10^{-4}	O(110), W(111)
	197	$^{19}F(p,p'\gamma)^{19}F$	197 → 0	5×10^{-5}	Co(197), Ni(197), Ga(197) Ti(199), Ge(199), O(197)
Na	439	$^{23}Na(p,p'\gamma)^{23}Na$	439 → 0	10^{-3}	Se(439)
	1368	$^{23}Na(p,\gamma)^{24}Mg$	1368 → 0		Mg(1368), Al(1368)
	1633	$^{23}Na(p,\alpha\gamma)^{20}Ne$	1633 → 0		

List of proton-induced reaction

Element	E_γ (keV)	Nuclear origin	Transition	Detection limit (%)	Possible interferences
Mg	170	$^{26}Mg(p,\gamma)^{27}Al$	1014 → 844		Al(170)
	390	$^{25}Mg(p,p'\gamma)^{25}Mg$	975 → 585		
	585	$^{25}Mg(p,p'\gamma)^{25}Mg$	585 → 0	5×10^{-3}	
	844	$^{26}Mg(p,\gamma)^{27}Al$	844 → 0		Al(844)
	975	$^{25}Mg(p,p'\gamma)^{25}Mg$	975 → 0		
	1014	$^{26}Mg(p,\gamma)^{27}Al$	1014 → 0		Ti(1012), Al(1014)
	1368	$^{24}Mg(p,p'\gamma)^{24}Mg$	1368 → 0		Na(1368), Al(1368)
Al	170	$^{27}Al(p,p'\gamma)^{27}Al$	1014 → 844		Mg(170)
	844	$^{27}Al(p,p'\gamma)^{27}Al$	844 → 0	2×10^{-3}	Mg(844)
	1014	$^{27}Al(p,p'\gamma)^{27}Al$	1014 → 0	5×10^{-3}	Ti(1012), Mg(1014)
	1368	$^{27}Al(p,\alpha\gamma)^{24}Mg$	1368 → 0		Na(1368), Mg(1368)
	1779	$^{27}Al(p,\gamma)^{28}Si$	1779 → 0		Si(1779), P(1779)
Si	1273	$^{29}Si(p,p'\gamma)^{29}Si$	1273 → 0	3	
	1779	$^{28}Si(p,p'\gamma)^{28}Si$	1779 → 0		Al(1779), P(1779)

PIGE cross sections

The cross sections are the superimposition of resonances (Breit-Wigner) on a continuum due to direct nuclear reactions

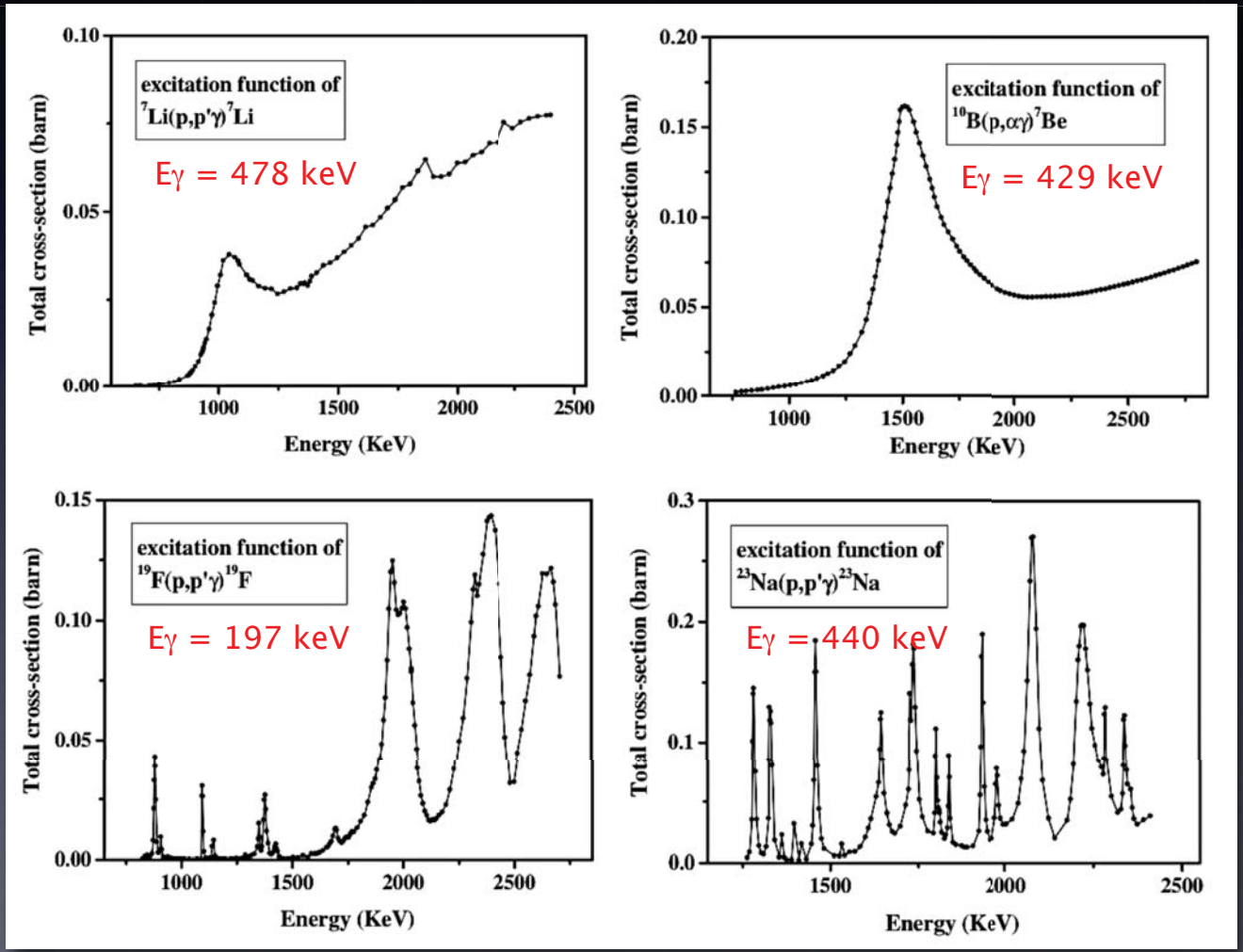

Examples of PIGE spectra

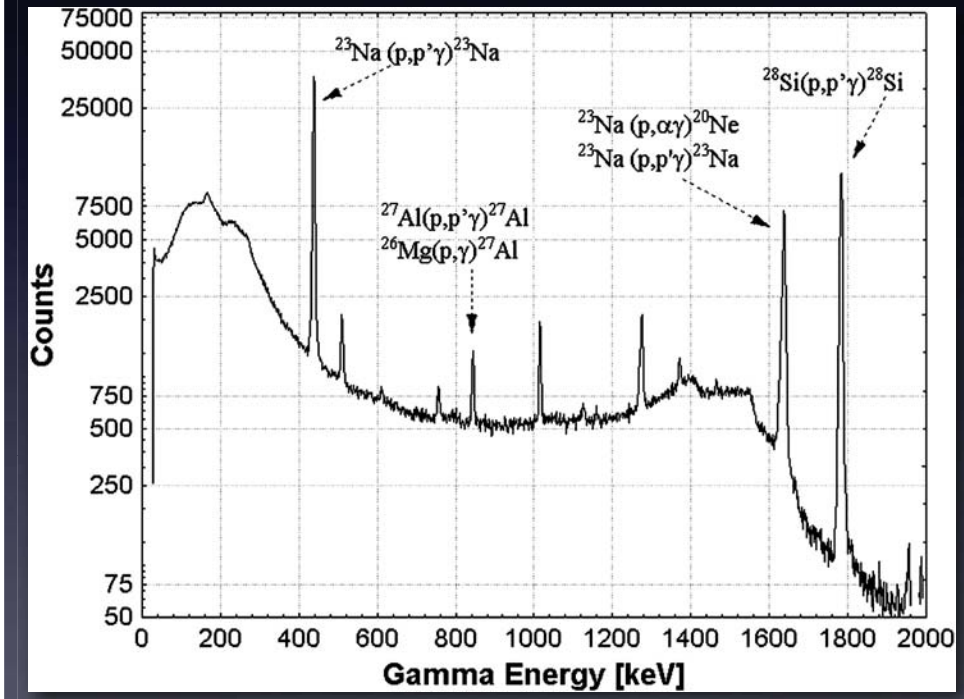

Soda-lime glass

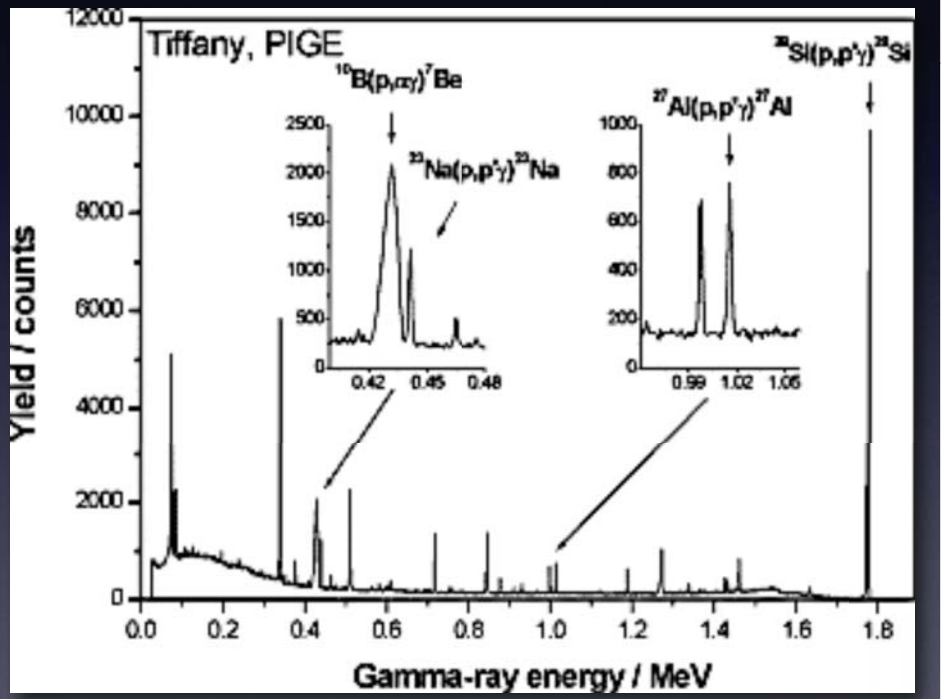

Borosilicate galss

PIGE elemental analysis

The elemental concetrations (N_T) are obtained from measured quantities (i.e. gamma-ray peak areas) using physical models implementing the sample structure and the physical microscopic data and processes:

$$Y_\gamma(E_0,\theta) = \varepsilon_{\text{abs}}(E_\gamma)\cdot N_p \cdot \int_0^{E_0} N_T \cdot \sigma(E_0,\theta)/S(E)\,\mathrm{d}E$$

The principal needed microscopic data are **stopping powers** and **differential cross sections** of the interaction (as well as the detector absolute efficiency)

Analytical applications of PIGE

Cultural Heritage
i.e. thick targets

- (Semi-)quantitative determination of light elements like Na, Al or Si in infinitely thick targets
- Unknown concentrations typically deduced by comparing the γ-ray yields with those of **thick** standards of similar composition
- Differences in stopping powers are crucial

Atmospheric Aerosols
i.e. thin targets

- Quantitative determination of light elements (F, Na or Al) with no self-absorbtion of emitted radiation inside aerosol particles
- Unknown concentrations deduced by comparing the γ-ray yields with those of a **thin** elemental standard
- Choosing the beam energy is crucial (cross-sections have to be constant over the beam energy loss in the sample)

Thick target gamma-ray yields

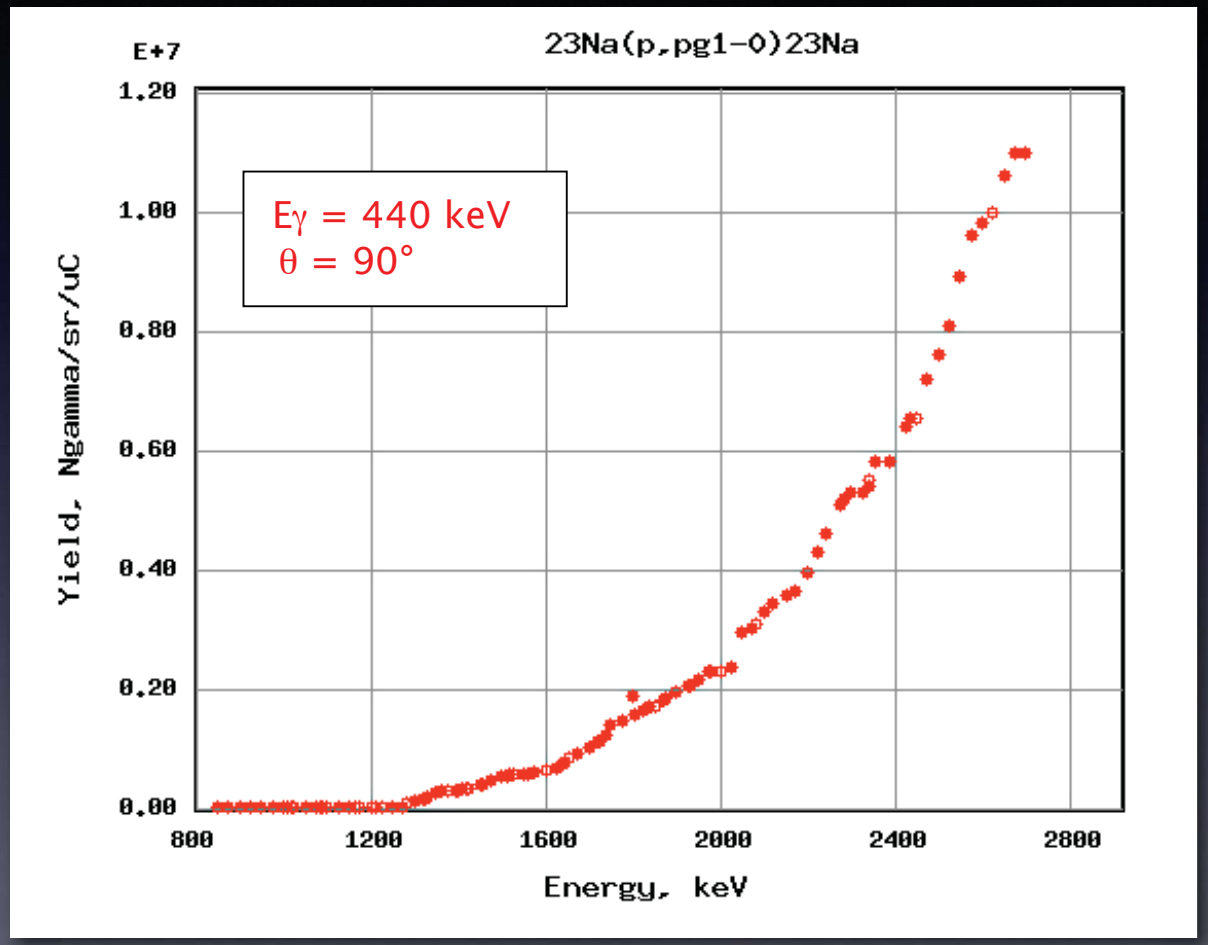

PIGE quantitative analysis: comparison with thick standards

$$C_{camp} = C_{rif} \cdot Y_{camp}(E_0)/Y_{rif}(E_0) \cdot S_{camp}(E_{1/2})/S_{rif}(E_{1/2})$$

$E_{1/2}$ such as:

$$Y(E_0) = 2 \cdot Y(E_{1/2})$$

The "$E_{1/2}$" method is valid as long as the excitation function varies slowly with the energy

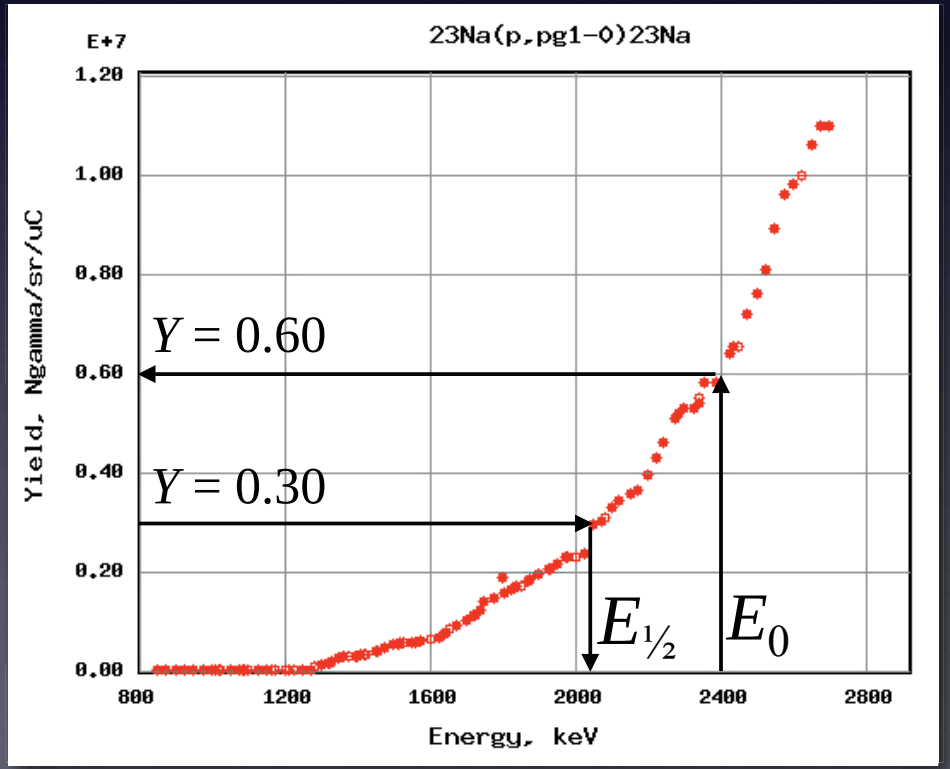

RBS

Rutherford Backscattering Spectrometry

Elastic scattering at backward angles of the impinging ions by the target nuclei

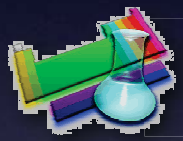

$A > A_p$

✓ depth profile

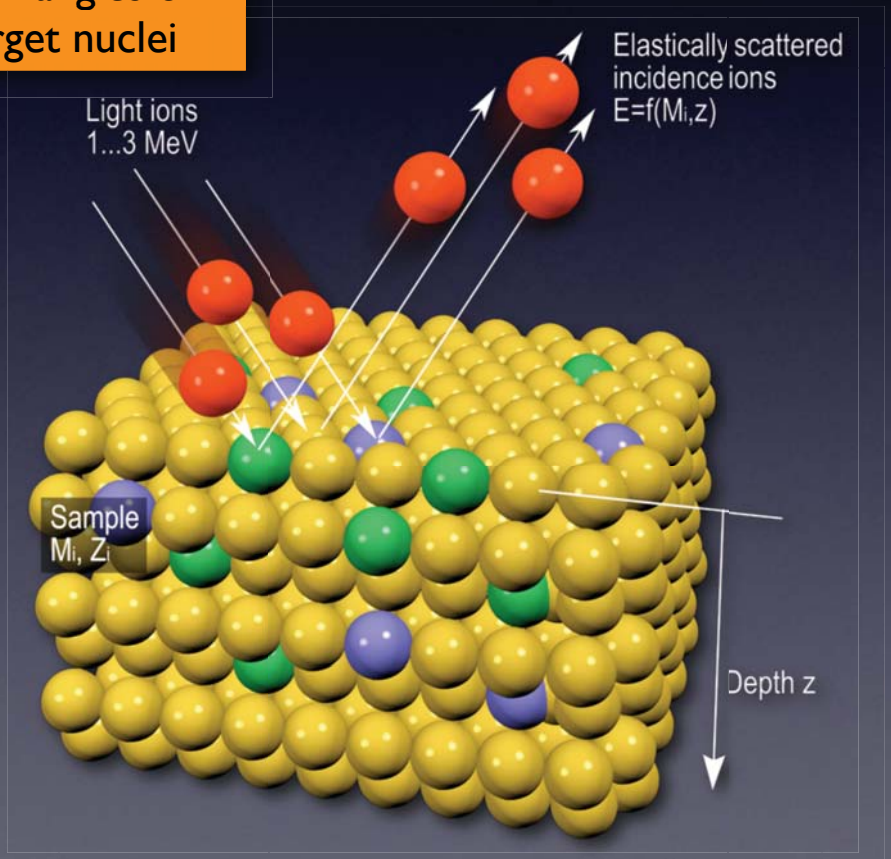

Principles of RBS

For a given scattering angle θ, the energy E_1 of the incident ion (mass M_1) after the collision is only a function of the mass M_2 of the targt nuclei

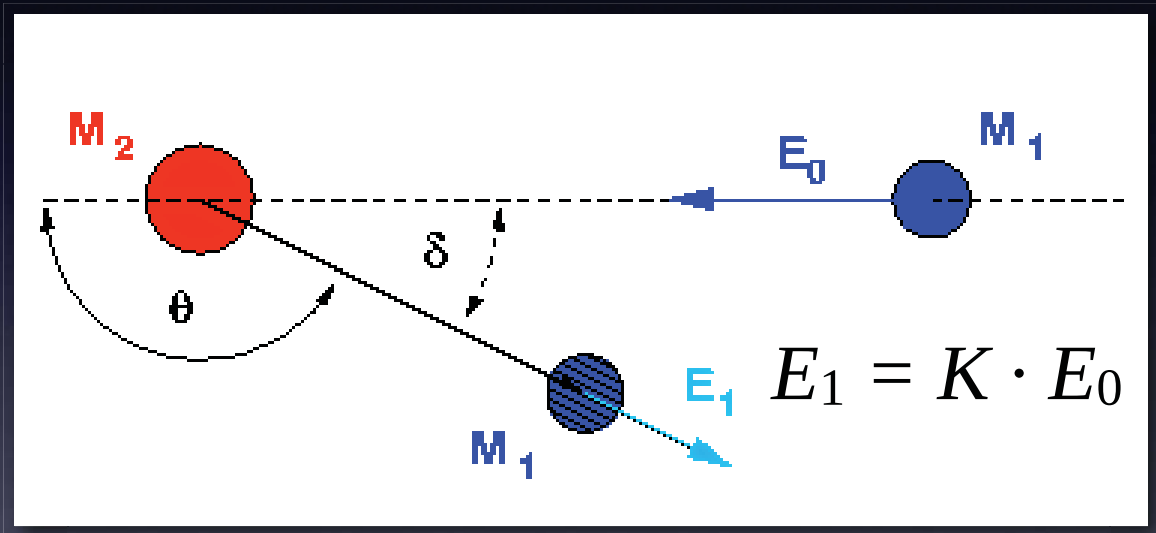

$$K = \frac{\left[\sqrt{\left(\frac{M_2}{M_1}\right)^2 - \sin^2\theta} + \cos\theta\right]^2}{\left(\frac{M_2}{M_1} + 1\right)^2}$$

larger ΔE for smaller M (light nuclei)

Larger ΔE for larger θ (backscattering)

The kinematic factor *K*

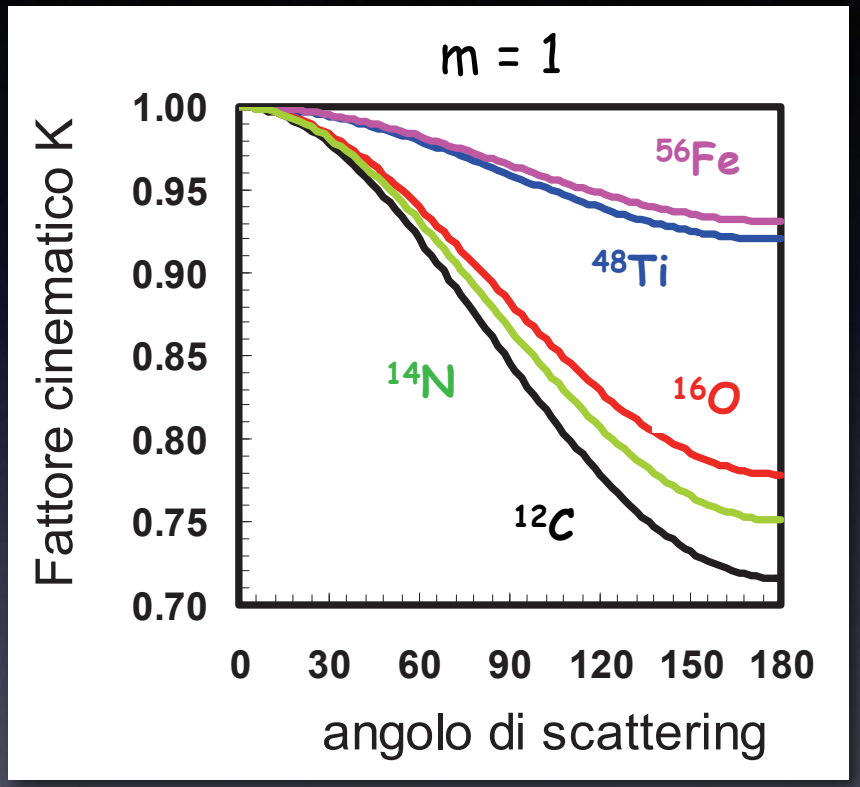

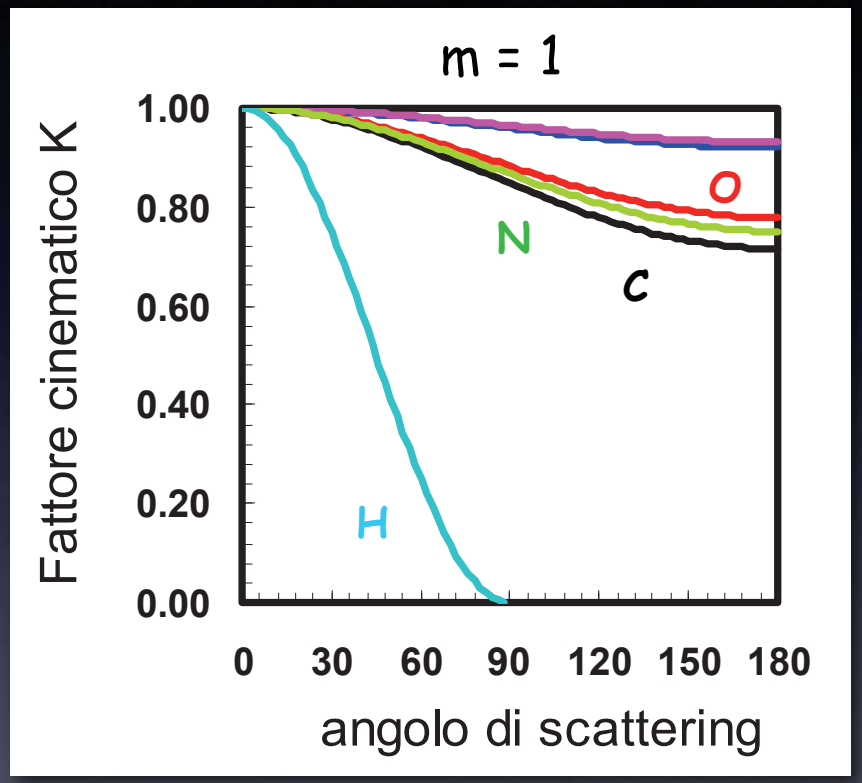

$M_2 \leq M_1 \Rightarrow$ only forward scattering (PESA)

Elastic scattering cross section

The Rutherford formula:

$$\left(\frac{d\sigma}{d\Omega}\right)_{Ruth} = \left(\frac{Z_1 Z_2 e^2}{E}\right)^2 \frac{4}{\sin^4(\theta)} \frac{\left[\sqrt{1-\left(\frac{M_1}{M_2}\sin\theta\right)^2}+\cos\theta\right]^2}{\sqrt{1-\left(\frac{M_1}{M_2}\sin\theta\right)^2}}$$

Z_1 Atomic number of the incident ion

Z_2 Atomic number of the target nucleus

E Energy of the incident ion

M_1 Mass of the incident ion

M_2 Mass of the target nucleus

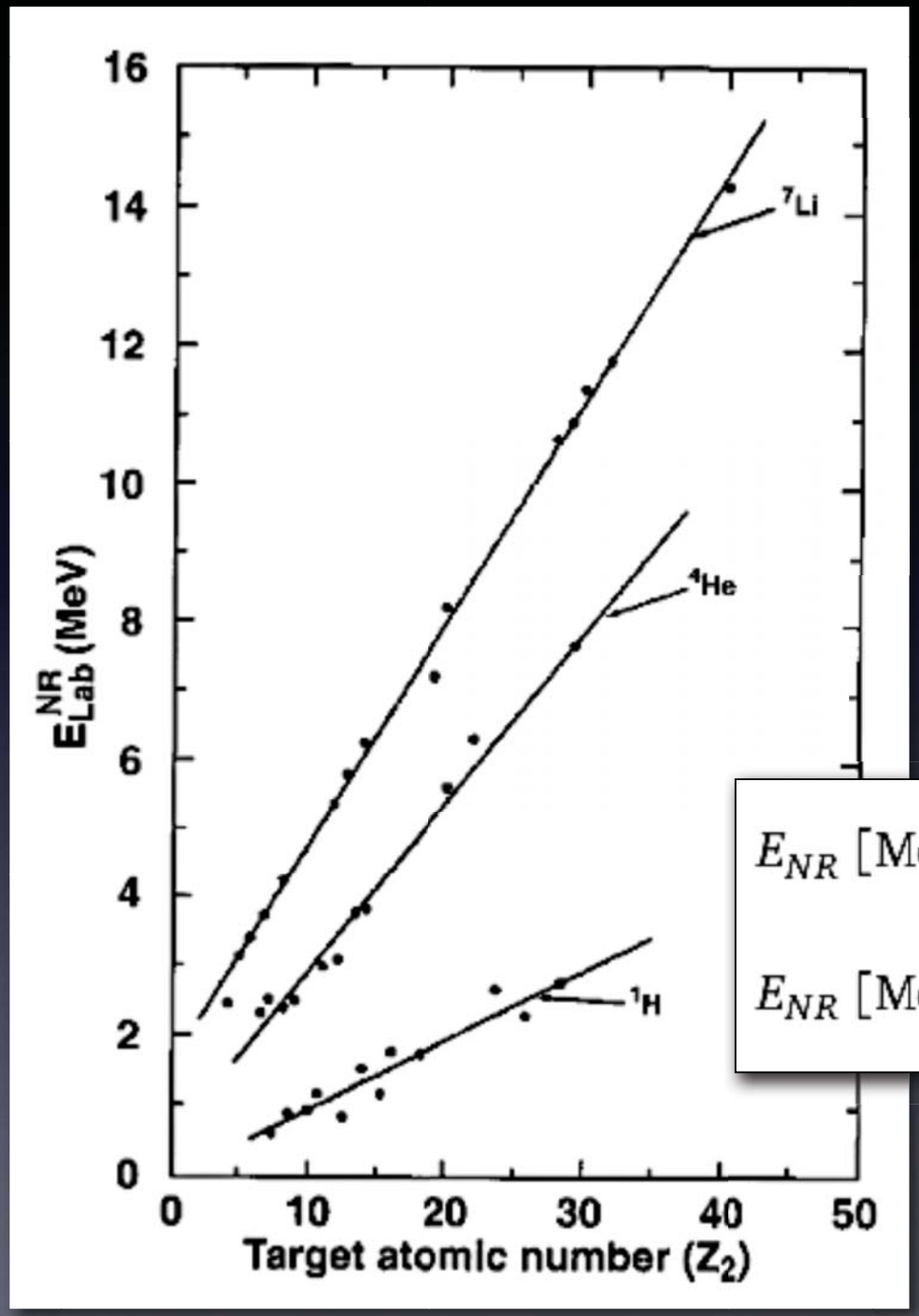

Energy (in the laboratory) at which the elastic scattering cross section deviates more than 4% from the Rutherford value
(for scattering angles > 160°)

$$E_{NR}\,[\mathrm{MeV}] = \frac{M_1 + M_2}{M_2}\frac{Z_2}{10} \quad \text{for } Z_1 = 1$$

$$E_{NR}\,[\mathrm{MeV}] = \frac{M_1 + M_2}{M_2}\frac{Z_1 Z_2}{8} \quad \text{for } Z_1 > 1$$

Non-Rutherford cross sections

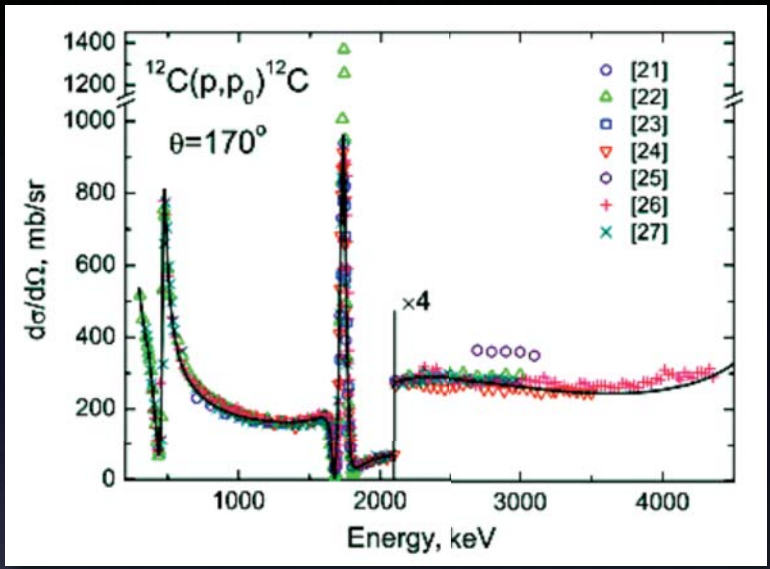

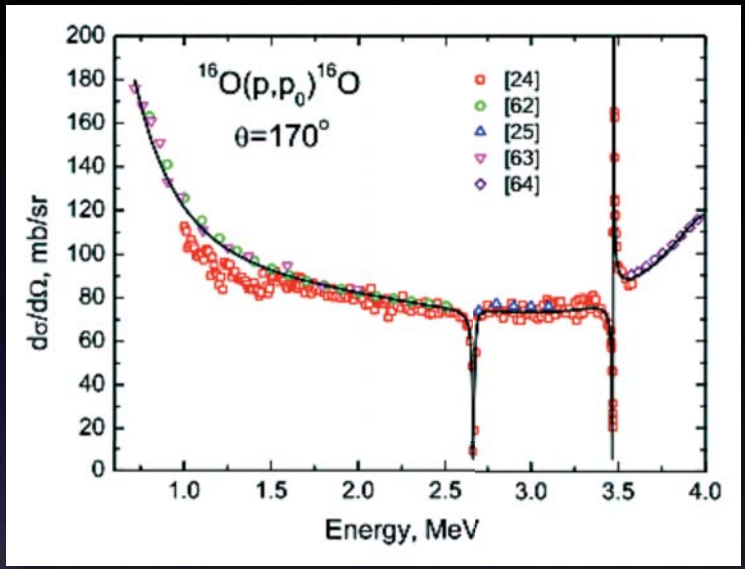

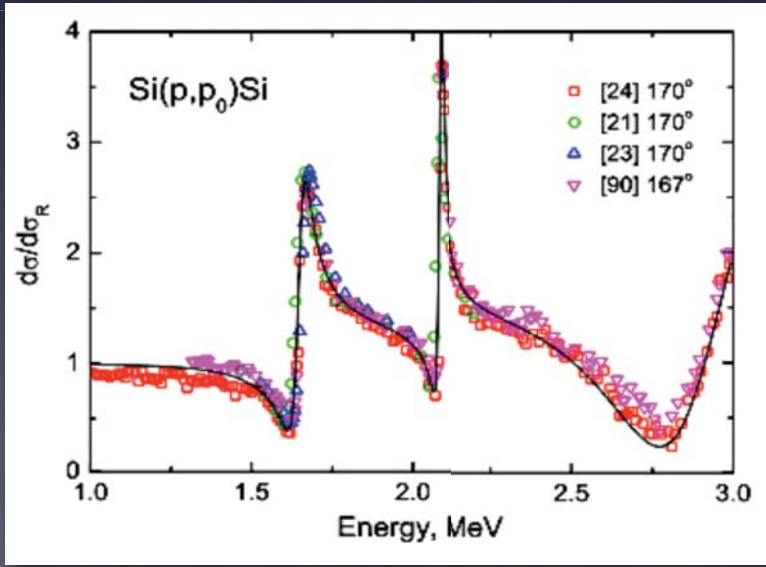

Evaluated and recommended experimental cross sections available from IBANDL web site (www-nds.iaea.org/ibandl/)

Depth scale of RBS

The signal from an atom at the sample surface will appear in the energy spectrum at a position KE_0.

The signal from atoms of the same mass below the sample surface will be shifted by the amount of energy lost while the projectiles pass through the sample, both before (ΔE_{in}) and after a collision (ΔE_{out}).

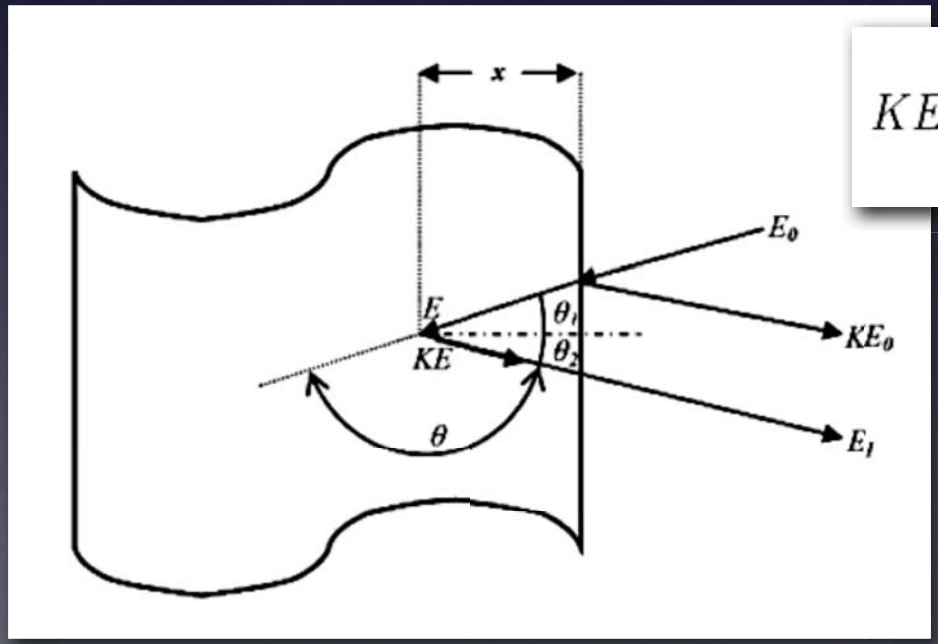

$$KE_0 - E_1 = \left[\frac{Kx}{\cos\theta_1}\cdot\left(\frac{dE}{dx}\right)_{in} + \frac{x}{\cos\theta_2}\cdot\left(\frac{dE}{dx}\right)_{out}\right]$$

There exists a relation between the measured energy E_1 and the depth x at which the scattering took place

The features of RBS spectra

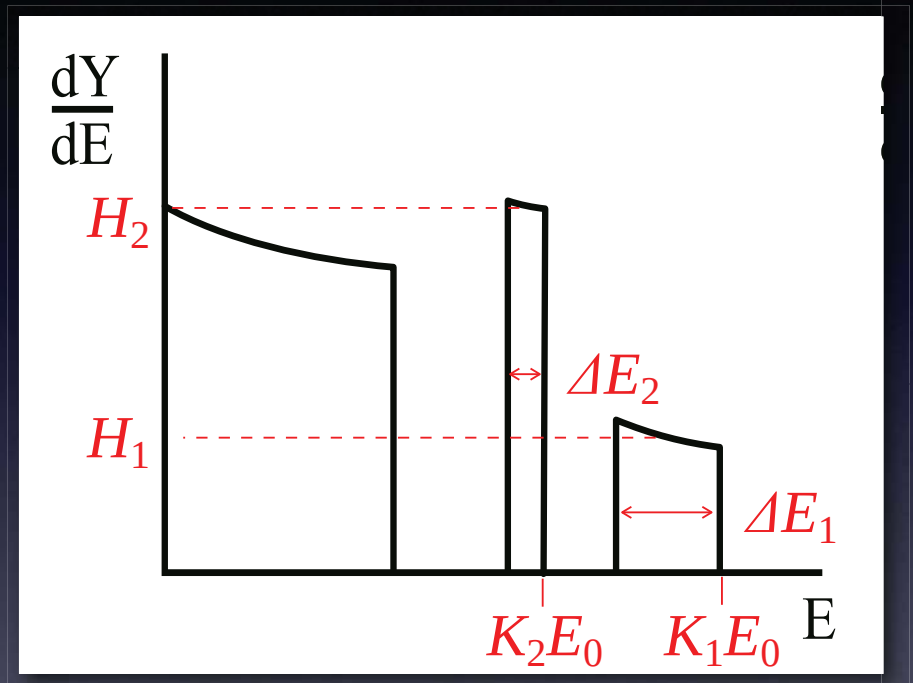

- Position of the signal (mass perception *i.e. kinematic factor*)
- Width of the signal (depth/thickness perception *i.e. stopping force*)
- Heigth of the signal (quantitative analysis of elemental composition *i.e. scattering cross section*)

Examples of RBS spectra

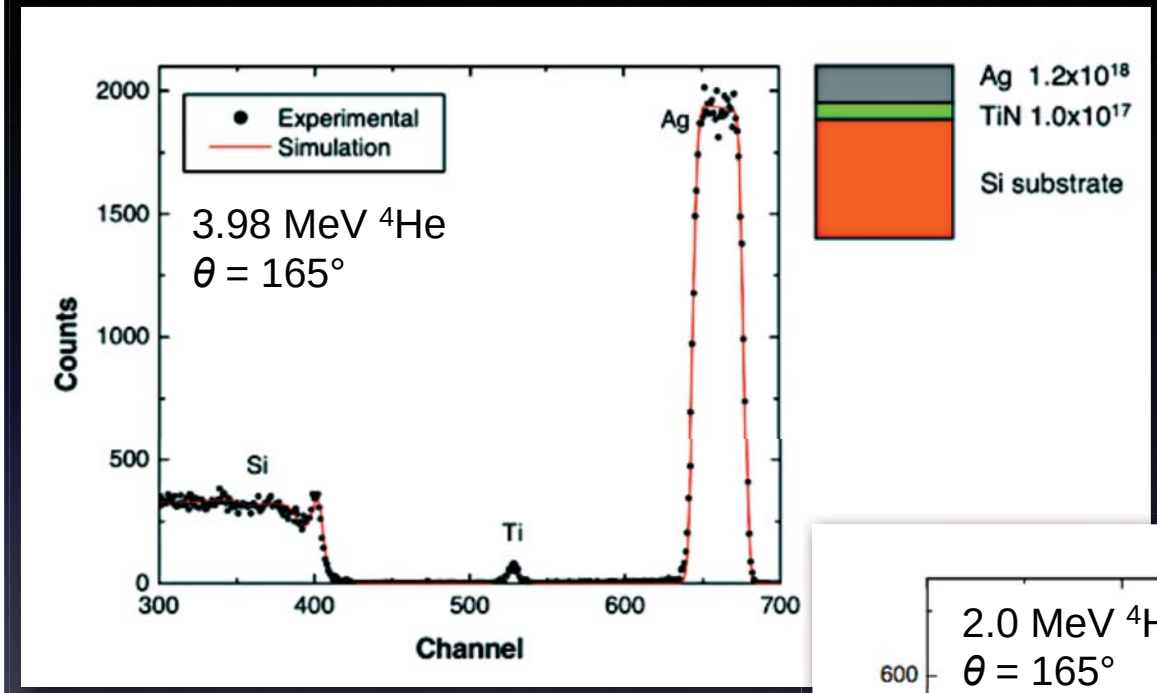

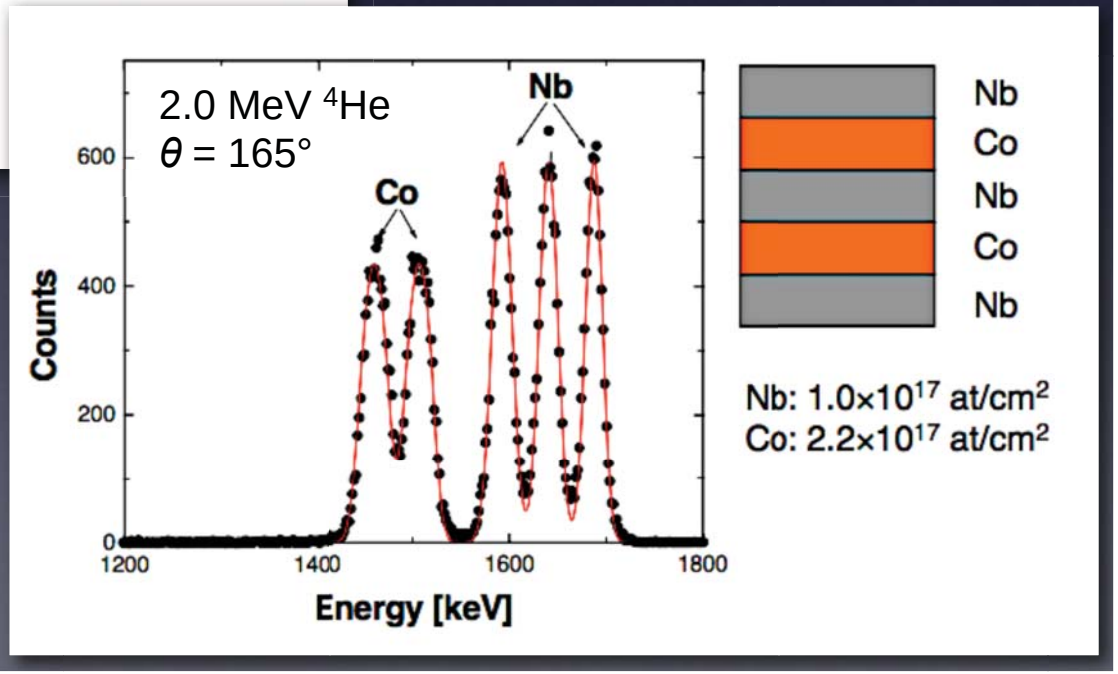

Analysis of ancient manuscripts,

PIXE analysis of the frontispiece of Pl.16,22, from Biblioteca Laurenziana in Florence

...ceramics,

Analysis of the Ritratto di fanciullo by Luca Della Robbia – before restoration at the Opificio delle Pietre Dure in Florence

… drawings,

Micro-PIXE measurements of Portrait of Lucas de Leyde by Alfred Dürer

A.Duval et al., (Louvre laboratory)

… jewels,

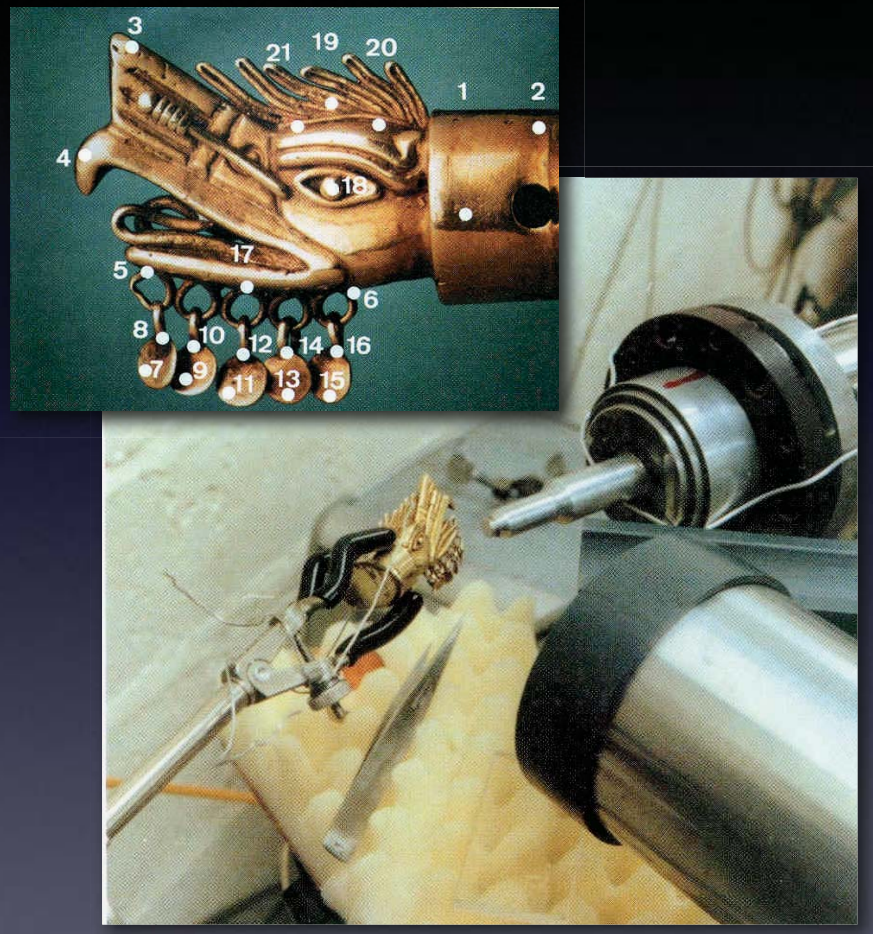

Micro-PIXE measurements of a Mexican gold alloy ornament

G.Demortier and J.L.Ruvalcaba Sil (Namur)

...paintings

PIXE analysis of a painting by
Lucas Cranach the Elder
C. Neelmeijer et al.
(Rossendorf Forschungszentrum, Dresda)

Blue Temperas

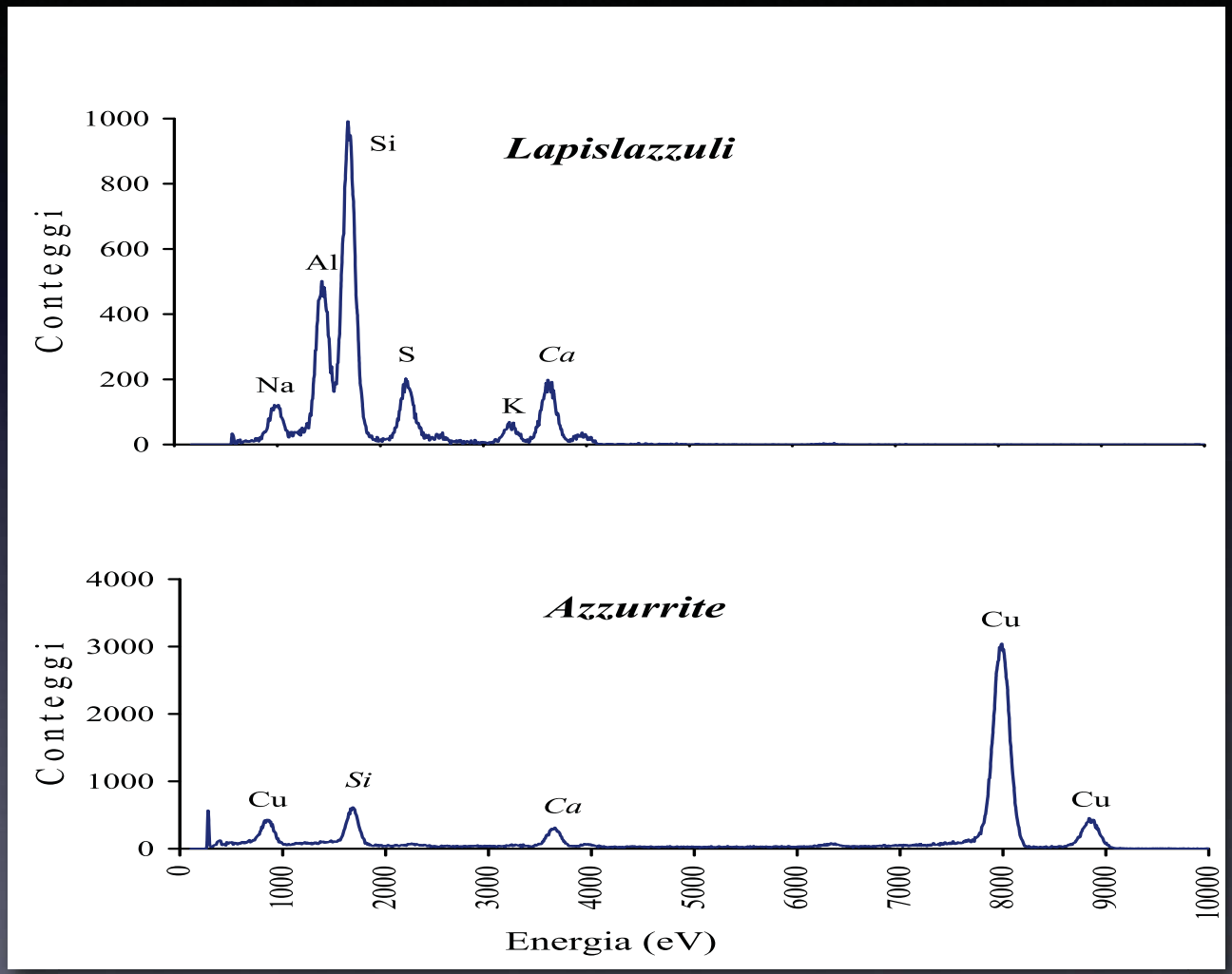

Example of PIXE spectra of two blue pigments

Blue Temperas

Extensive use of lapislazuli starting from XI century

Pluteo 48, 34, f. 66 v°

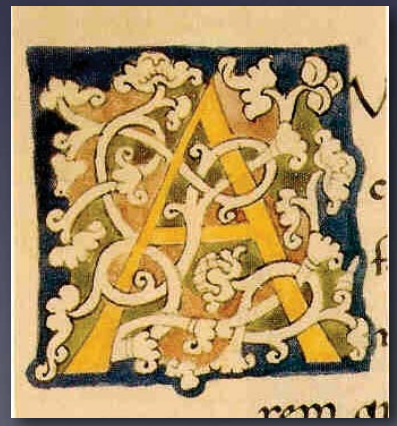

Pluteo 48, 34, f. 41 v°

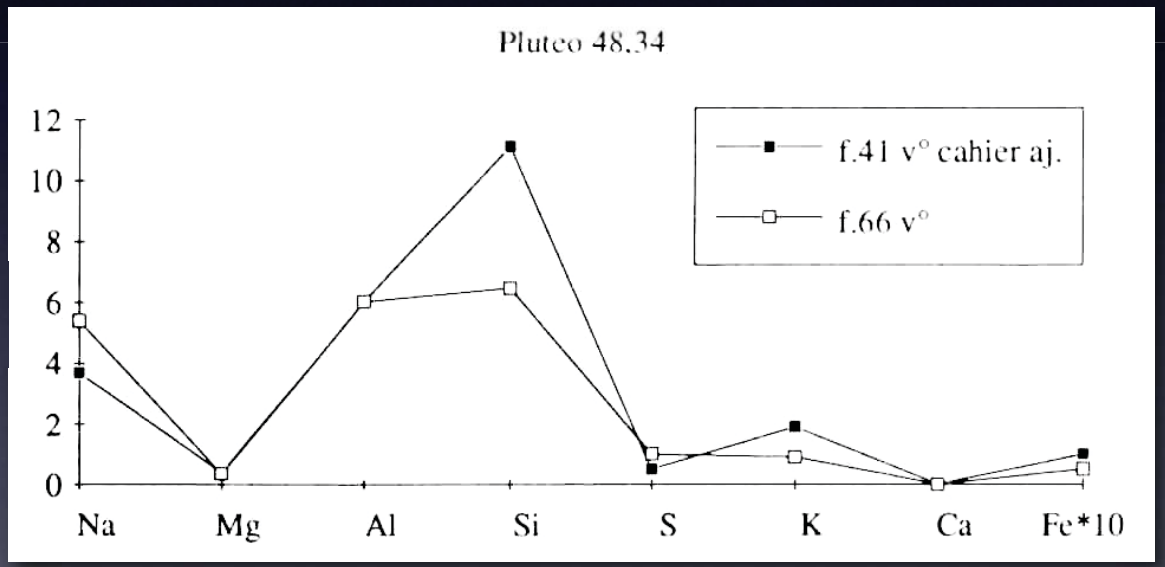

Metal point drawings

LEONARDO DA VINCI
STUDY OF A DRAPERY
Roma, Istituto Nazionale per la Grafica

metal point, lead white
red prepared paper

Characteristics of metal point drawings

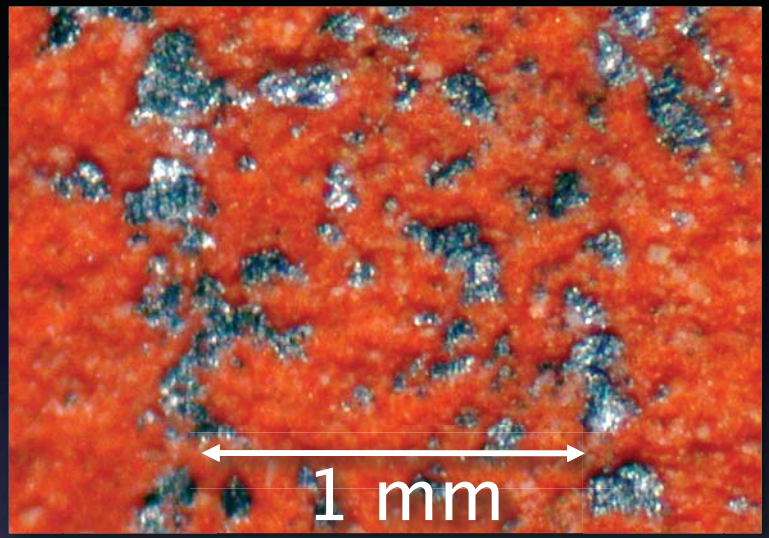

The extension of the metallic agglomerates on the surface is some tens of µm

The beam size does not allow a detailed analysis

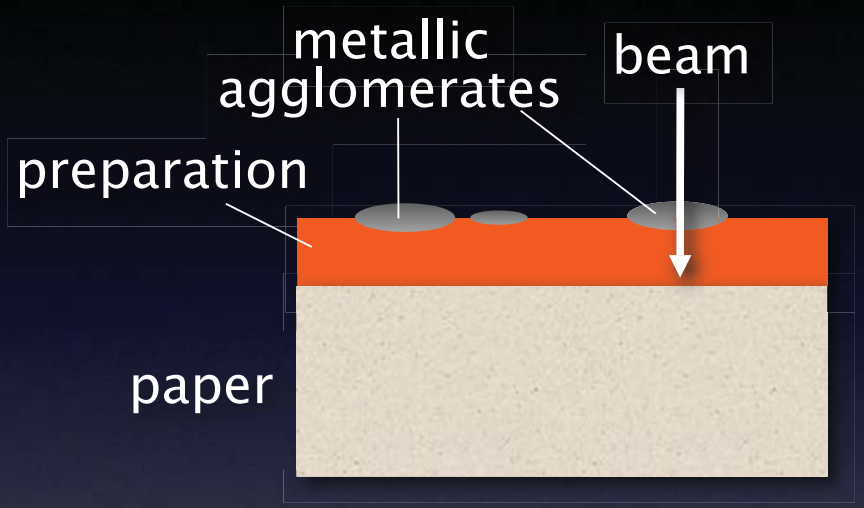

The beam can pass through the trace and hit the preaparation

The contribution of the preparation must be taken into account

MicroPIXE analysis of metal point drawings

Four metallic points:
silver, lead, gold, copper

Red preparation:
cinnaber, yellow ochre,
lead white, bone white

Au Cu Pb

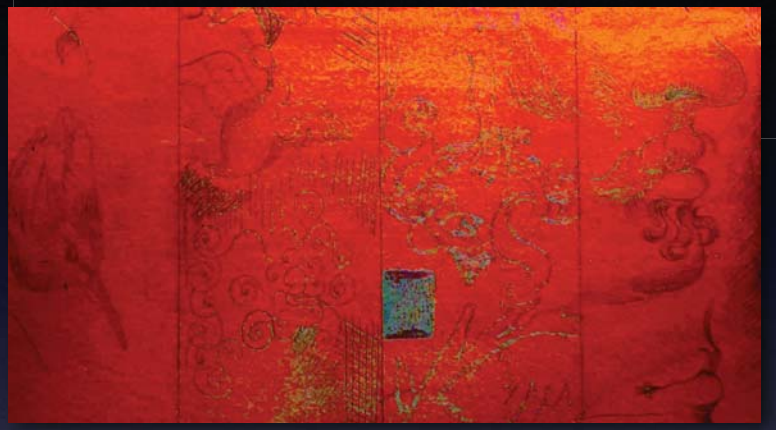

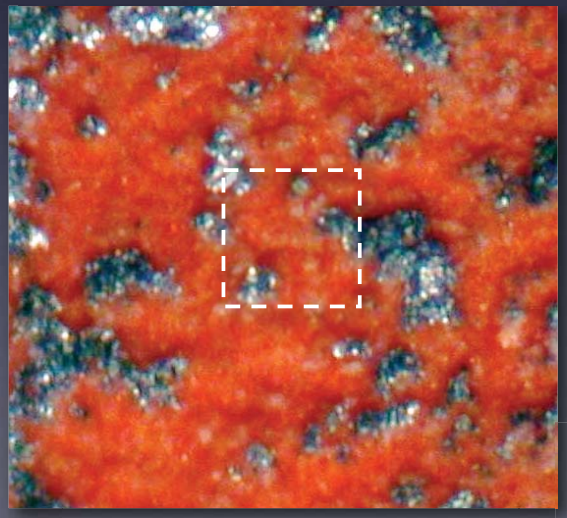

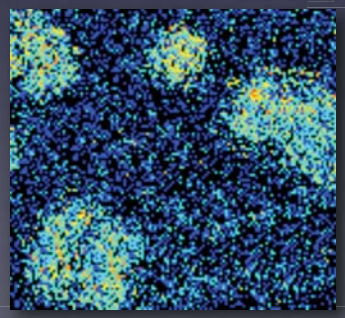

Elemental map on
0.4×0.4 mm²

Lead stylus
(**Pb**, trace of Sn)

Red preparation
(S, Hg, Pb, Fe, P, Ca)

Micro-PIXE measurements of an Achemenide pendant (IV century BC)

Micro-PIXE measurements of an Achemenide pendant (IV century BC)

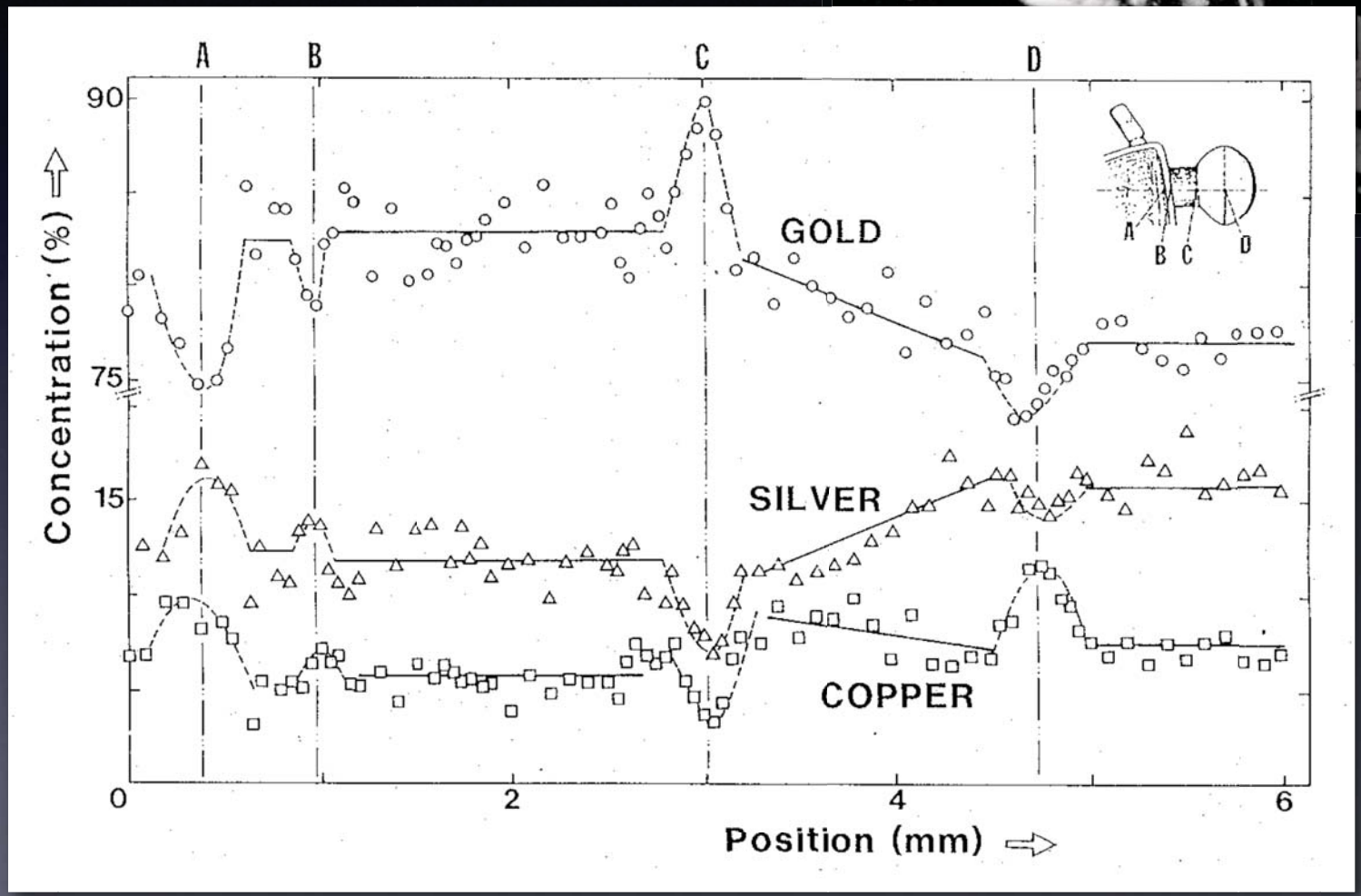

Differential PIXE

Consists in performing measurements on the same area with beams of different energies

At different energies proton beam ranges are different

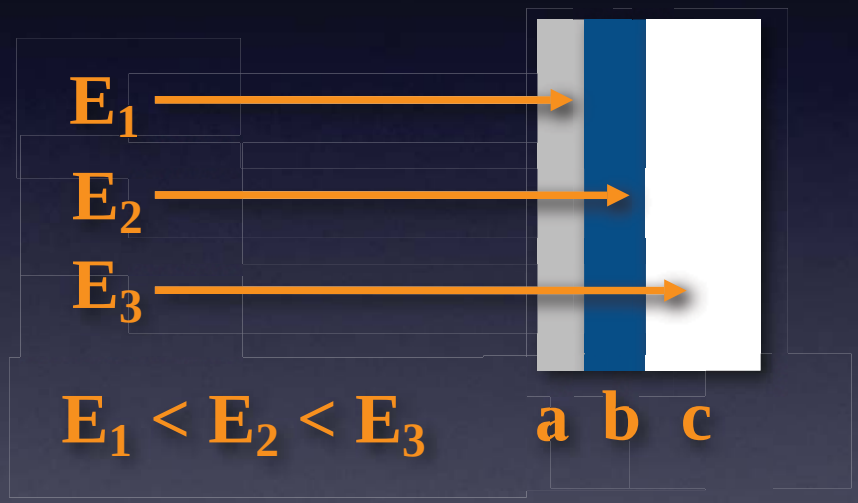

By comparing X-ray spectra taken at different energies, stratigraphic information can be obtained

PIXE spectra at different energies

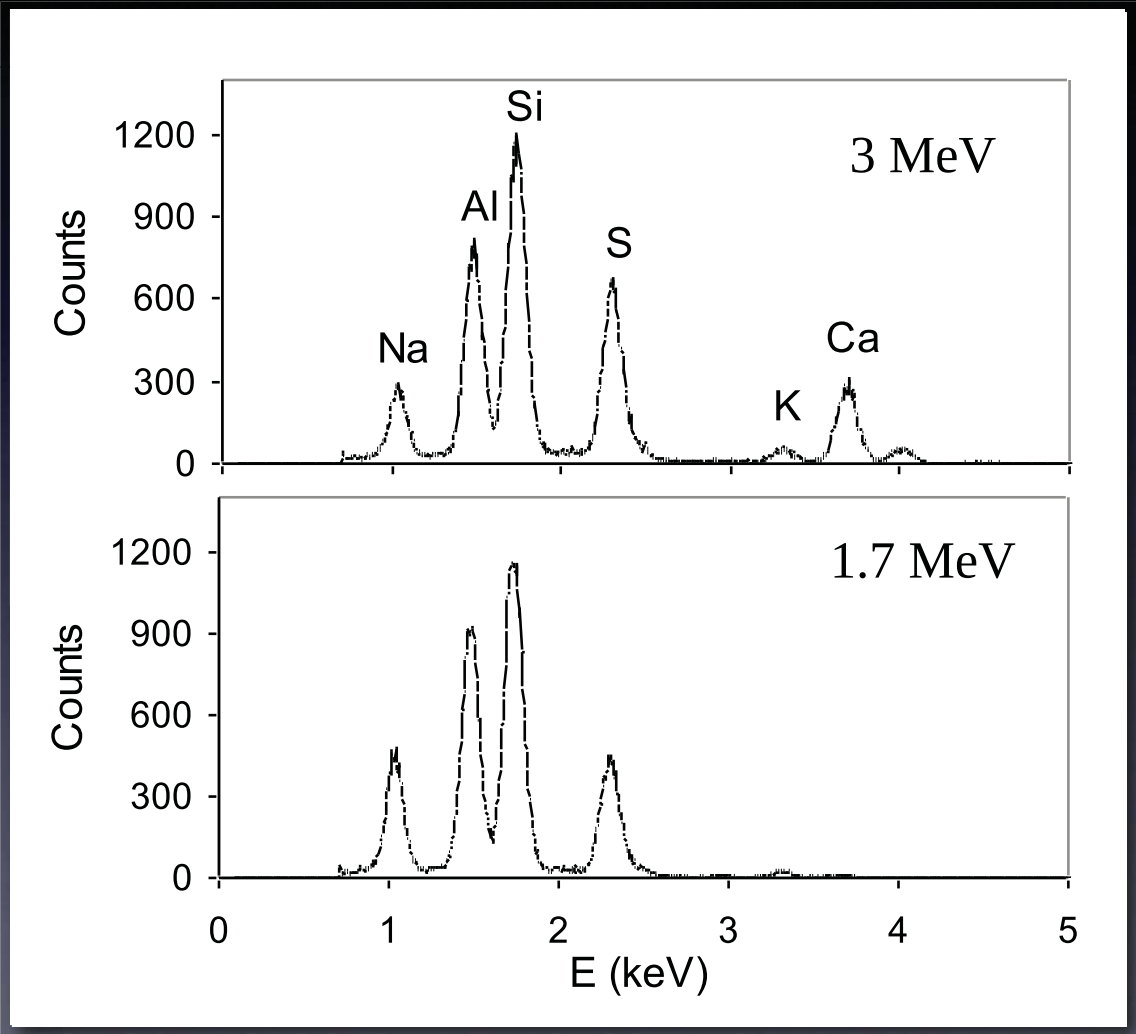

Blue paint layer (lapislazuli) on a substrate of calcium sulphate

Estimate of the paint layer thickness

$$\frac{Y_{\mathrm{Al}}}{Y_{\mathrm{Ca}}} = \frac{C_{\mathrm{Al}}}{C_{\mathrm{Ca}}} \frac{\int_{E_\mathrm{p}}^{E_\mathrm{p}-\Delta E_{\mathrm{lap}}(t)} \sigma_{\mathrm{X}}^{(\mathrm{Al})}(E)\, \mathrm{e}^{-\mu_{\mathrm{lap}}^{(\mathrm{Al})} \frac{x(E)}{\cos\theta}} \frac{\mathrm{d}E}{S_{\mathrm{lap}}(E)}}{\mathrm{e}^{-\mu_{\mathrm{lap}}^{(\mathrm{Ca})} \frac{t}{\cos\theta}} \int_{E_\mathrm{p}-\Delta E_{\mathrm{lap}}(t)}^{0} \sigma_{\mathrm{X}}^{(\mathrm{Ca})}(E)\, \mathrm{e}^{-\mu_{\mathrm{white}}^{(\mathrm{Ca})} \frac{x'(E)}{\cos\theta}} \frac{\mathrm{d}E}{S_{\mathrm{white}}(E)}}$$

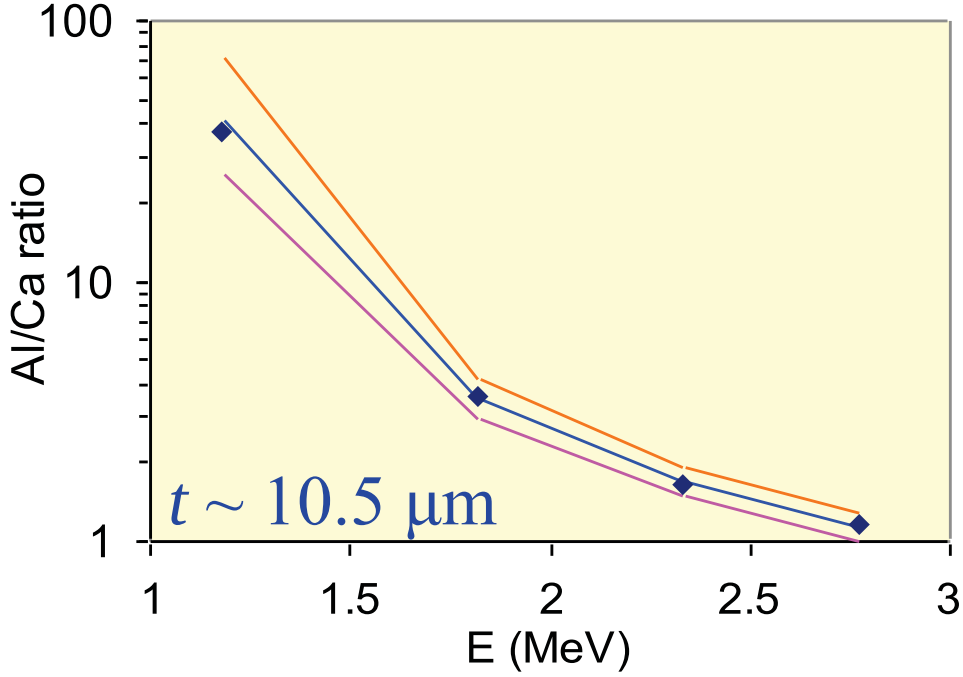

◆ Experimental

—— $t = 10.5$ µm

—— $t = 11.5$ µm

—— $t = 9.5$ µm

Metal threads (Alhambra, Granada)

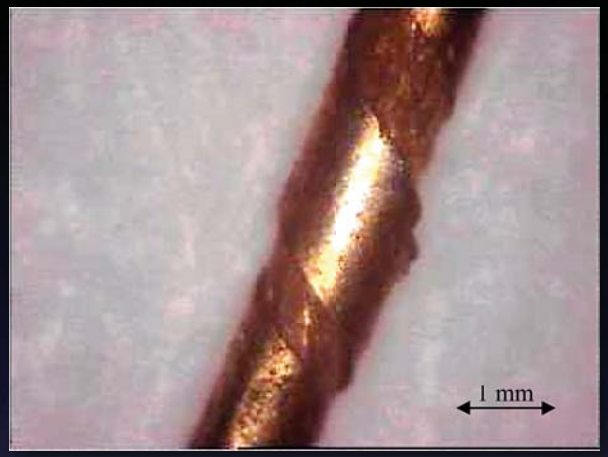

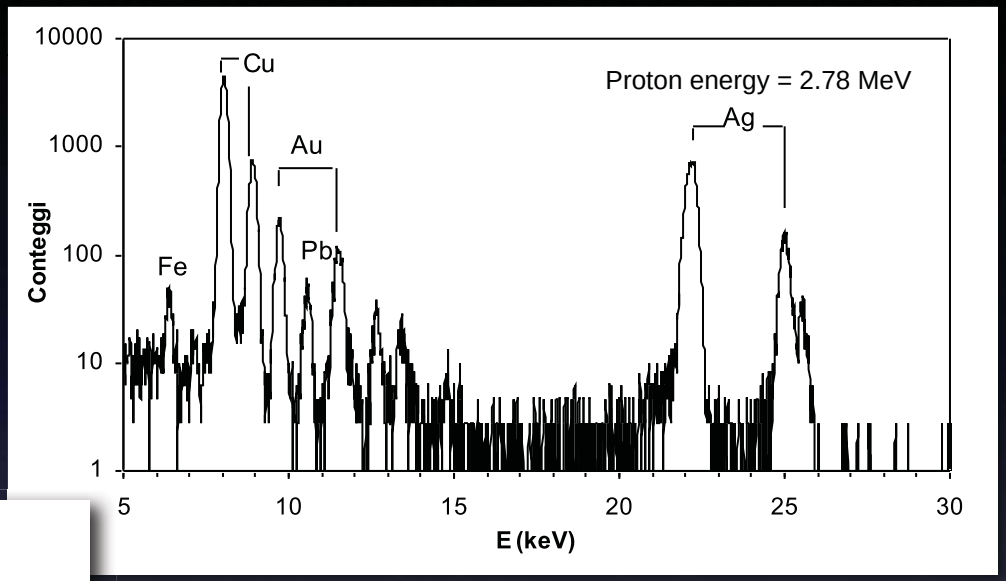

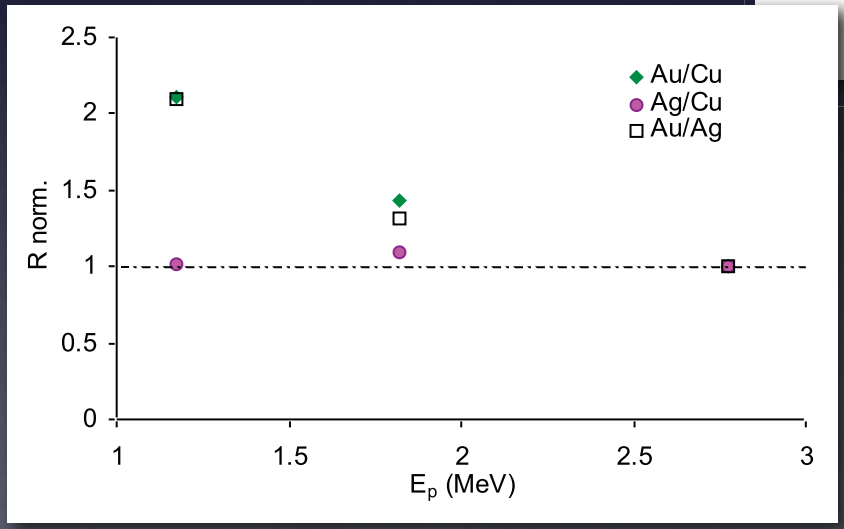

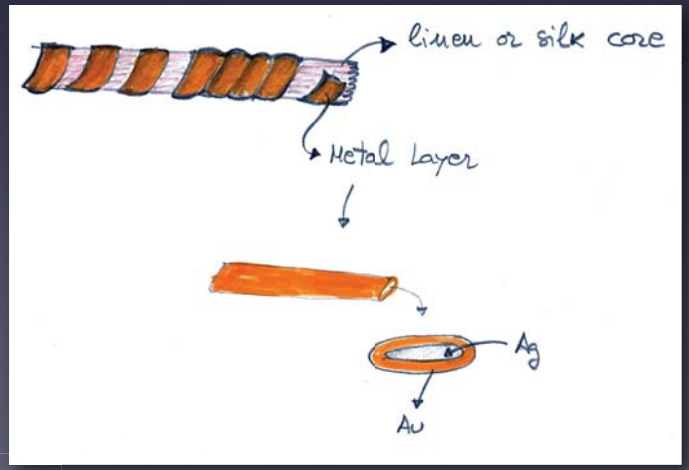

Enrichment of gold on the surface

“Incarnato”

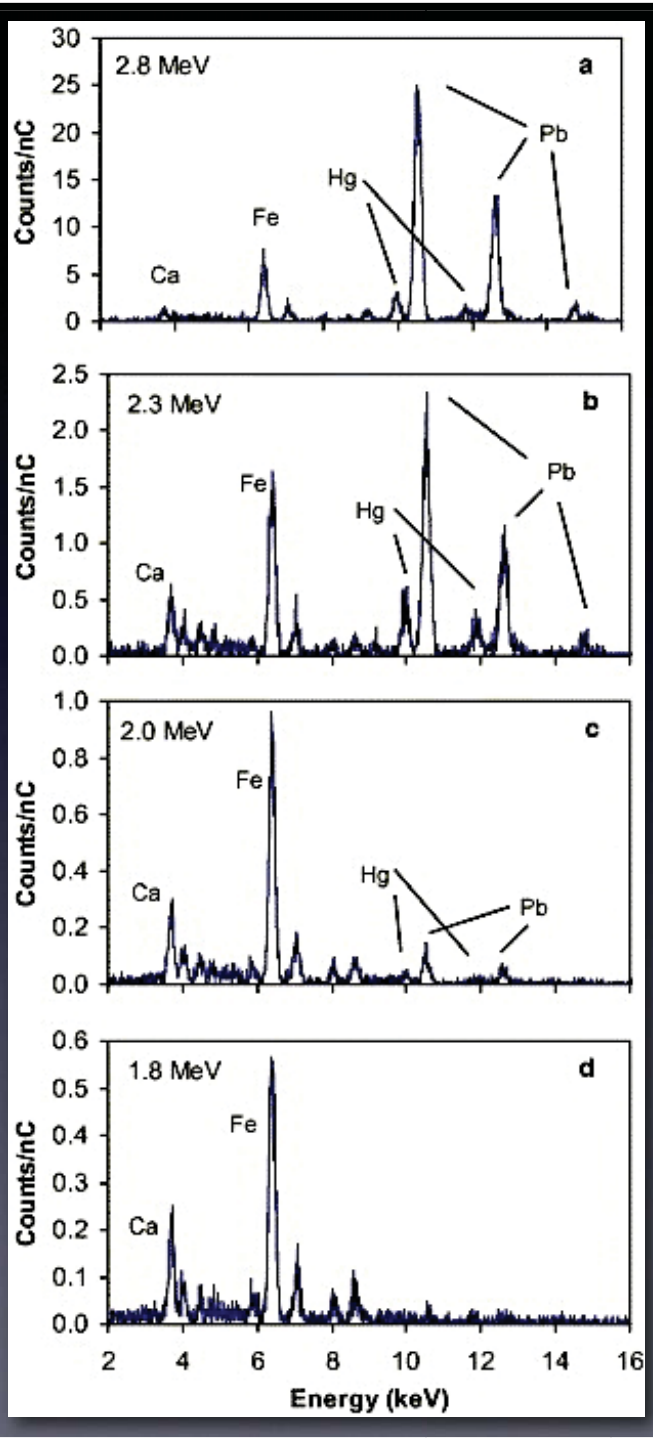

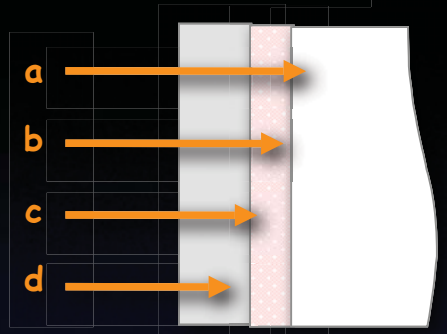

paint layer:

cinnabar (HgS, red pigment)+lead white

preparation:

lead white

Ca and Fe are in the varnish

Lapis-lazuli pigment in paint layers

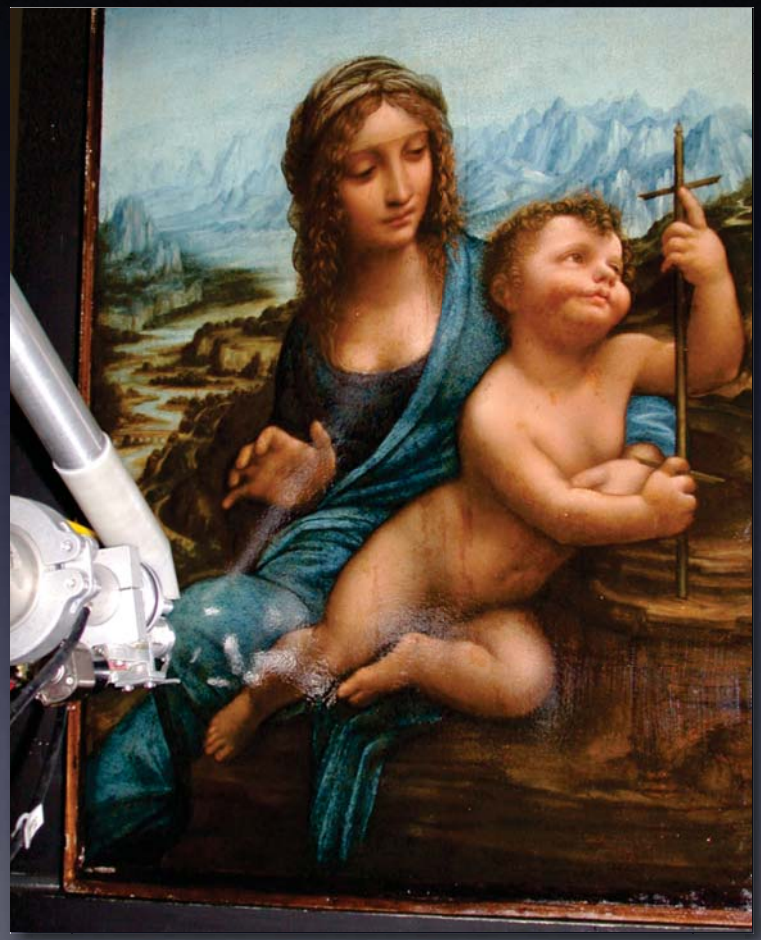

"Maddonna dei fusi", Leonardo da Vinci (1501)

Lapis-lazuli is a blue pigment, mainly composed of lazurite ($3Na_2O \cdot 3Al_2O_3 \cdot 6SiO_2 \cdot 2Na_2S$)

Limited possibility of identifying lapis-lazuli by PIXE in canvas and wood paintings:

- *low-energy X-rays absorption in the varnish and in the paint layer itself*
- *signal interference from other pigments*

Lapis-lazuli pigment in paint layers

PIXE spectra

PIGE spectra

Original

Blue pigment mixed with Lead white (Ca and Fe from the varnish)

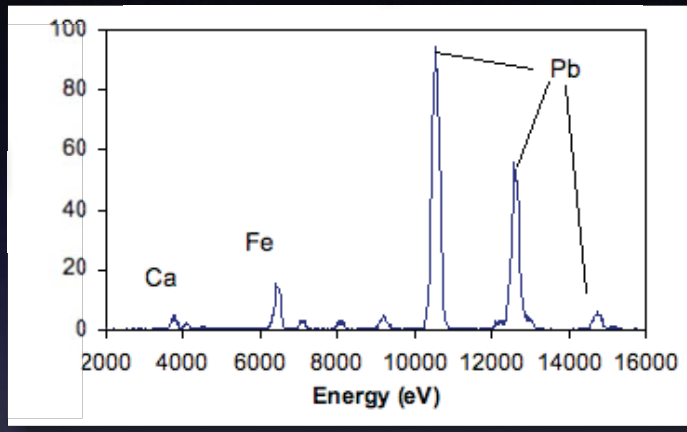

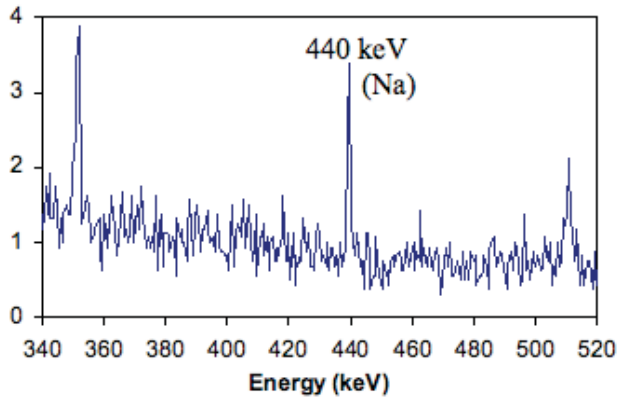

Restored

Cobalt blue and Zinc white (used only from XIX century!)

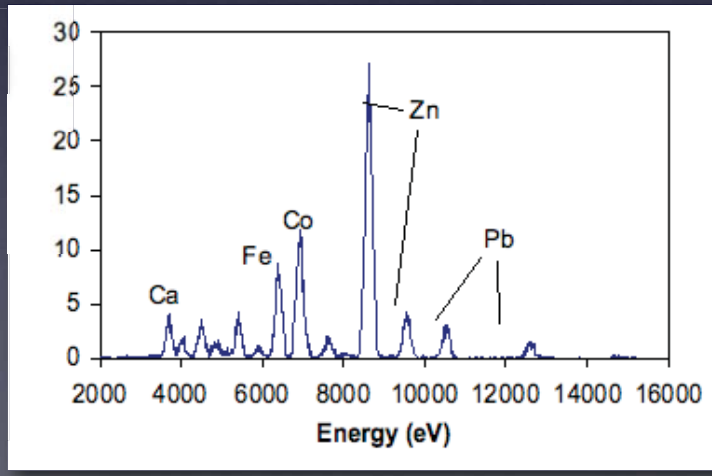

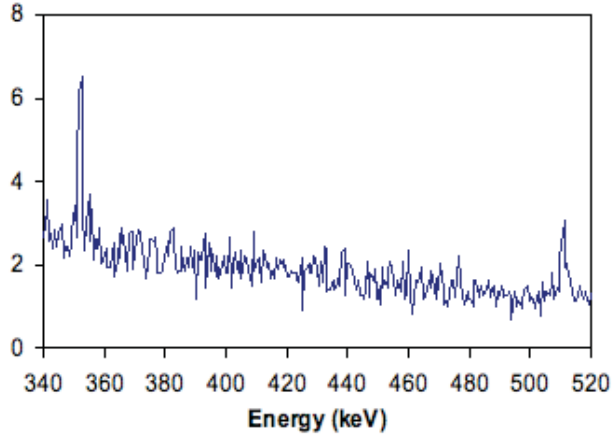

Analysis of ancient Roman glasses

Roman glass mosaic *tesserae* from Villa Adriana, Tivoli (Italy)

Quantification of Na is of great importance for the characterizaztion of ancient glasses

Two basic typologies of Western glass:

- **natron** (high Na_2O, low K_2O and MgO)
  Roman and High Middle Ages
- **plant ash** (low Na_2O, high K_2O)
  since Middle Ages

Sodium in Roman glasses

X-rays fom the lightest elements strongly absorbed by crusts and *patinae*

Roman glass mosaic *tesserae*

"freshly cut" zone

coloured but more opaque zone

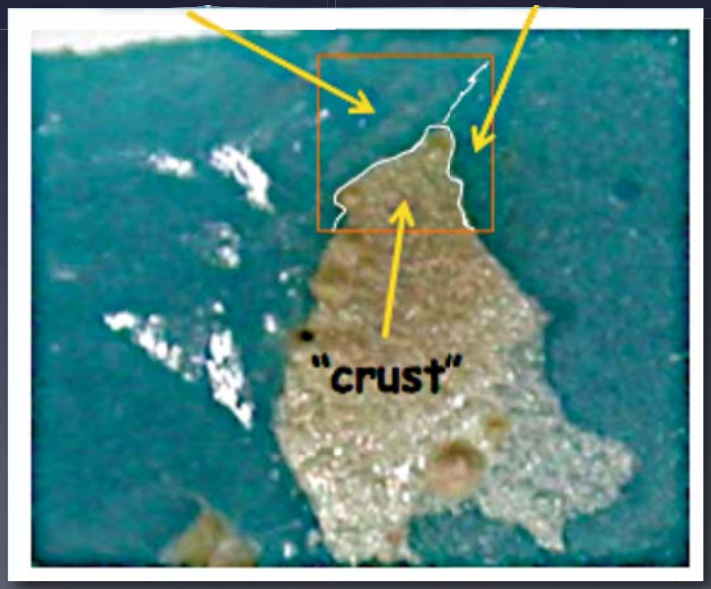

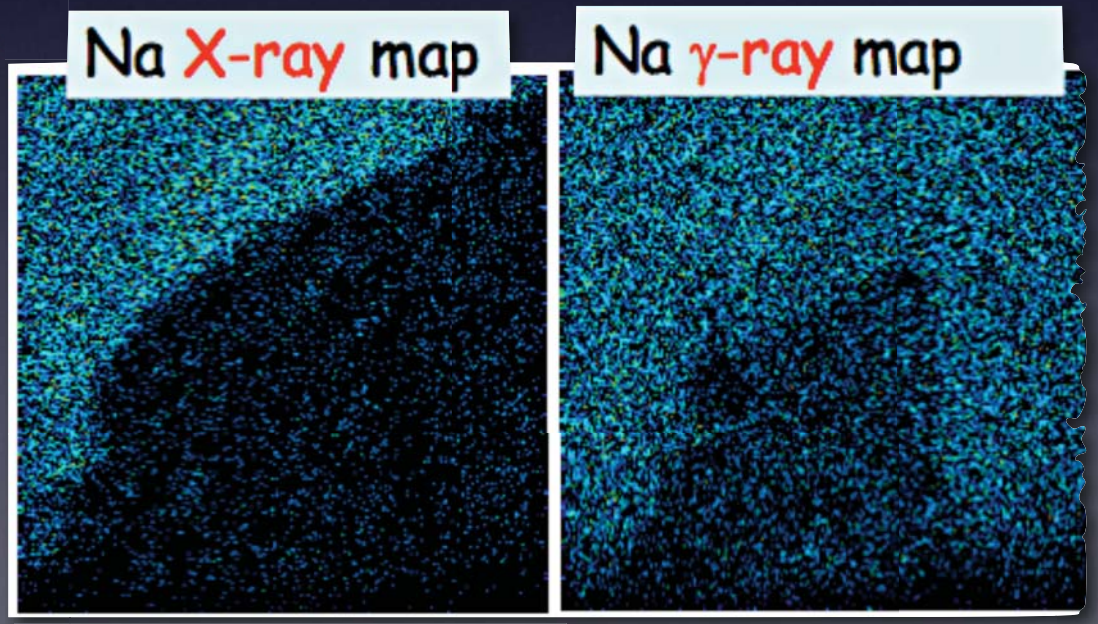

Sodium in Roman glasses

PIXE spectra PIGE spectra

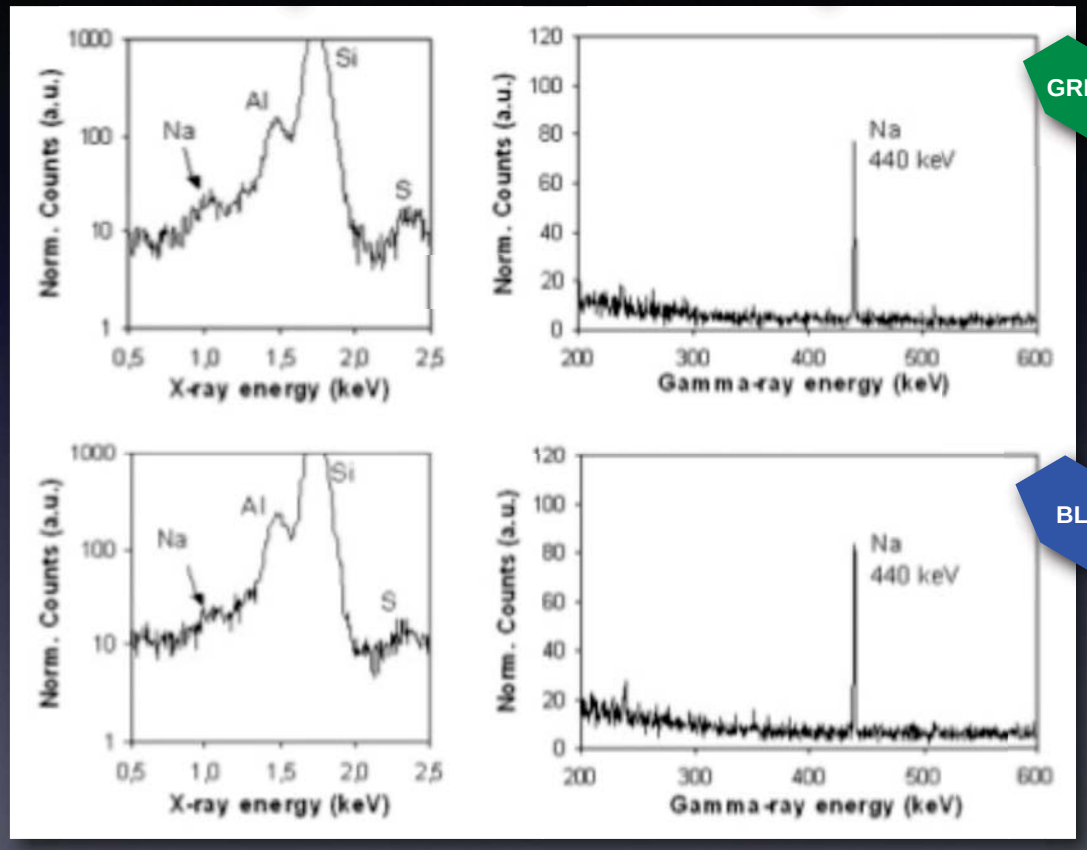

X-rays from the lightest elements strongly absorbed by crusts and *patinae*

Sodium in Roman glasses

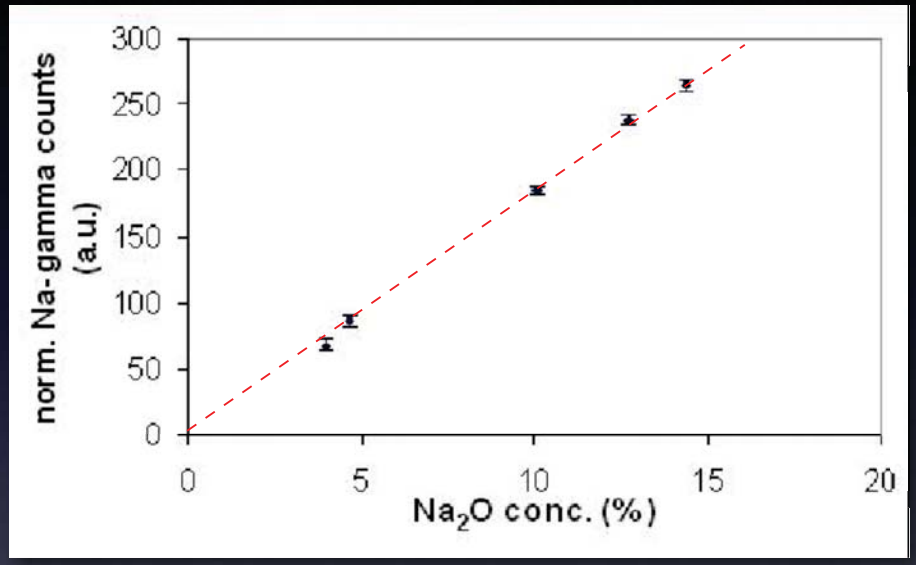

Estimate of Na content by comparing gamma-ray yields to those of thick glass standards (NIST SRM) with certified Na_2O concentration

Concentration ranges perfectly compatible with the typical Roman soda-lime-silica glass

glass colour	main oxides (%)			
	Na_2O	SiO_2	CaO	PbO
green	~20	55-60	5-9	1-3
blue	~20	60-65	5-9	<0.1
turquoise	~20	55-60	5-9	<0.3
yellow	~15	55-60	5-9	5-8
red	~10	35-40	5-9	30-35

RBS: External vs Vacuum

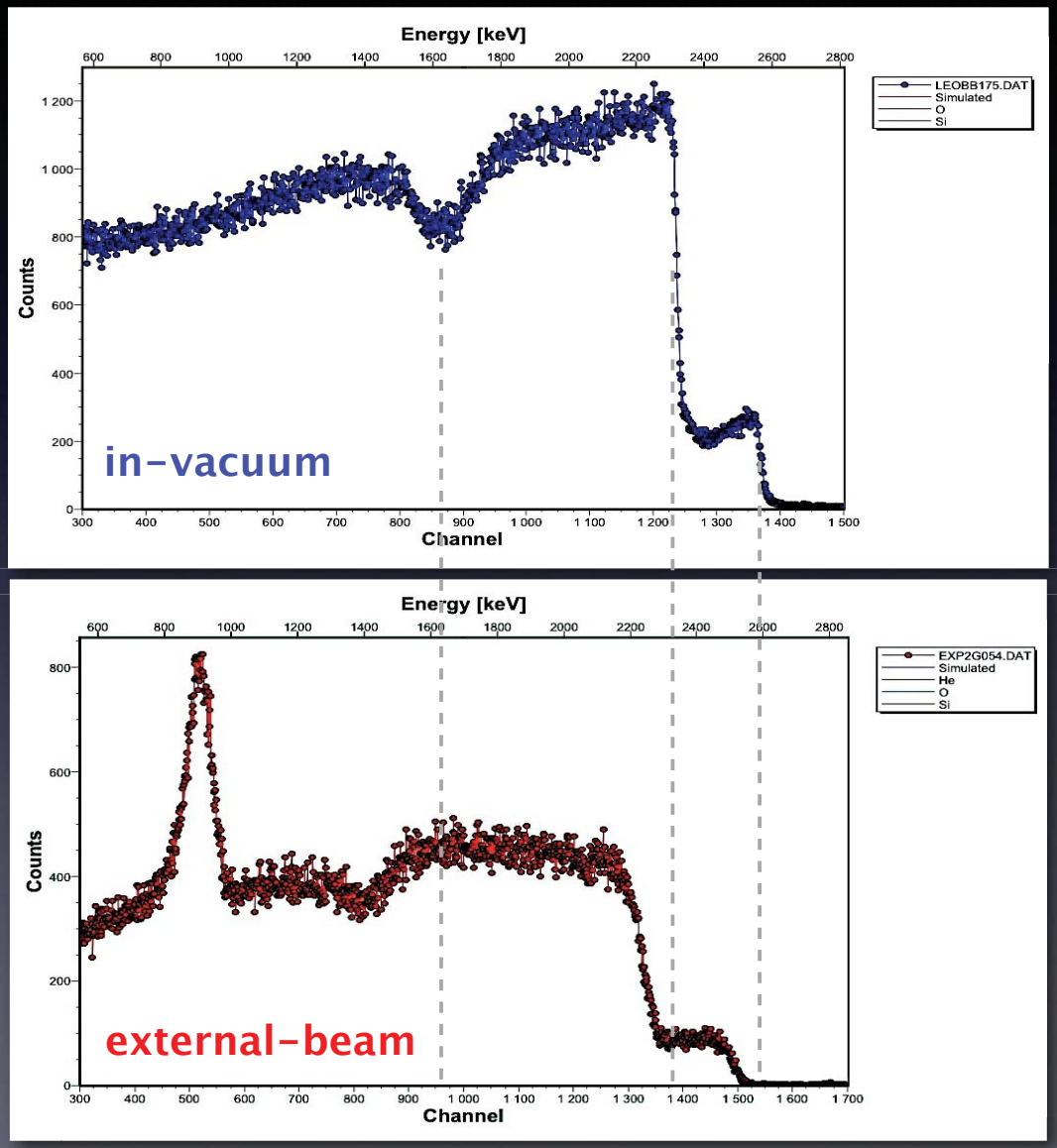

- *3 MeV protons on target*
- *θ = 150°*
- *SiO_2 target*

- Energy loss and energy straggling * in exit window and external path in atmosphere

* 25 keV FWHM for 7.5 μm Upilex + 10 mm He

Gold alloy or gilding

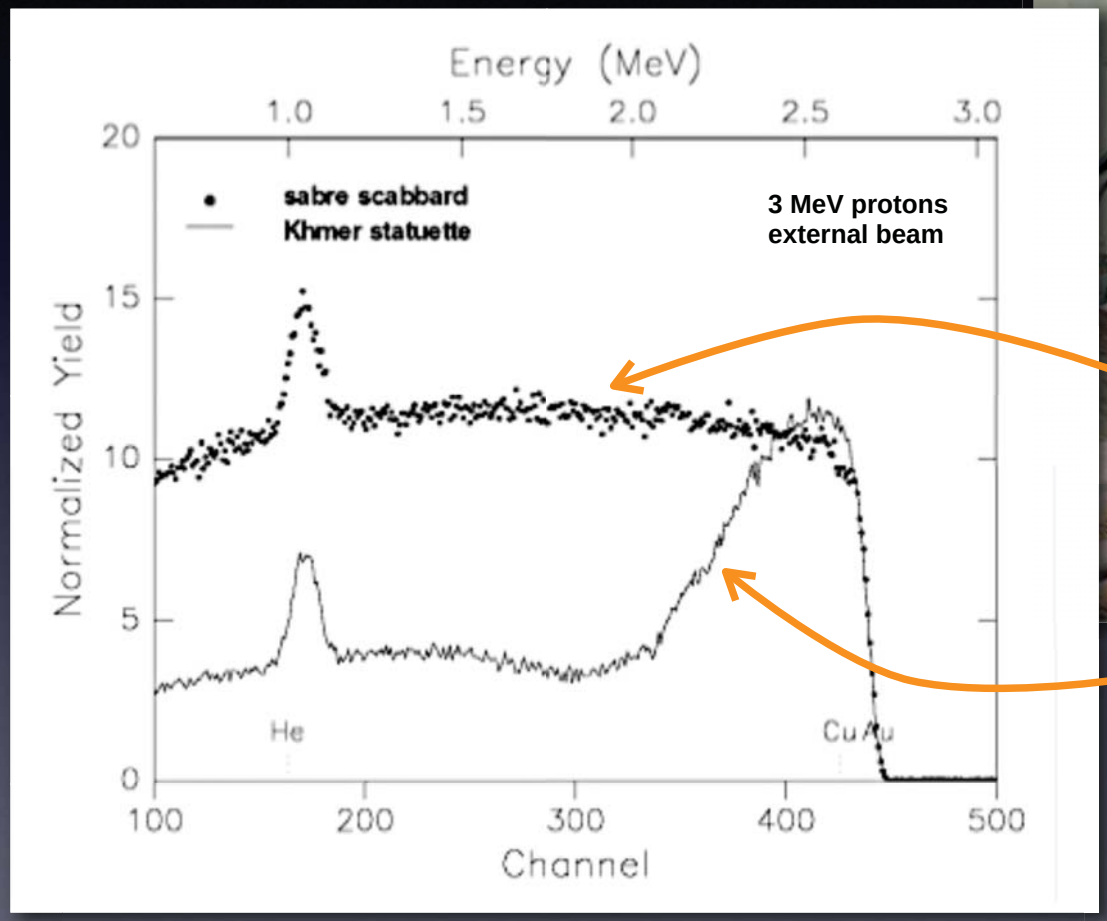

The scabbard is made of a thick Au-Cu alloy (thickness > 10 μm).

For comparison, the gilding of the statuette is about 2 μm thick.

From the width of the Au signal it is possible to obtain the thickness of the gilding (*dE/dx* is known).

RBS analysis of a gilded bronze chandelier (XI century) from the Cathedral of Hildesheim, Germany

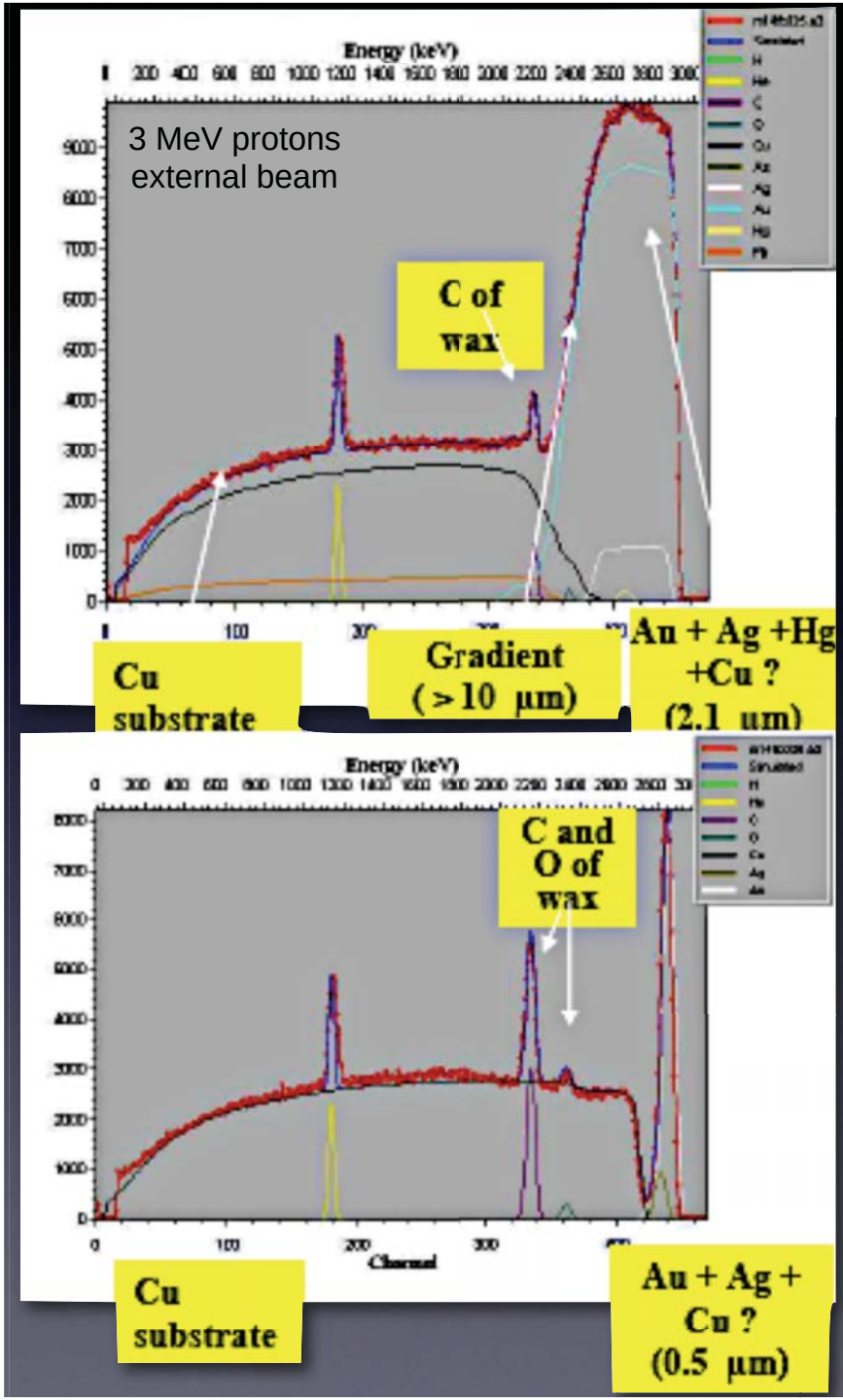

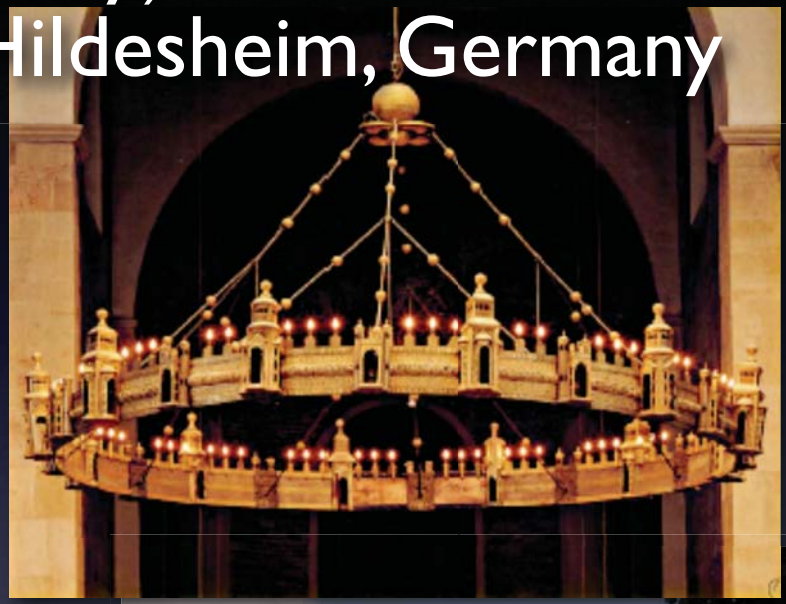

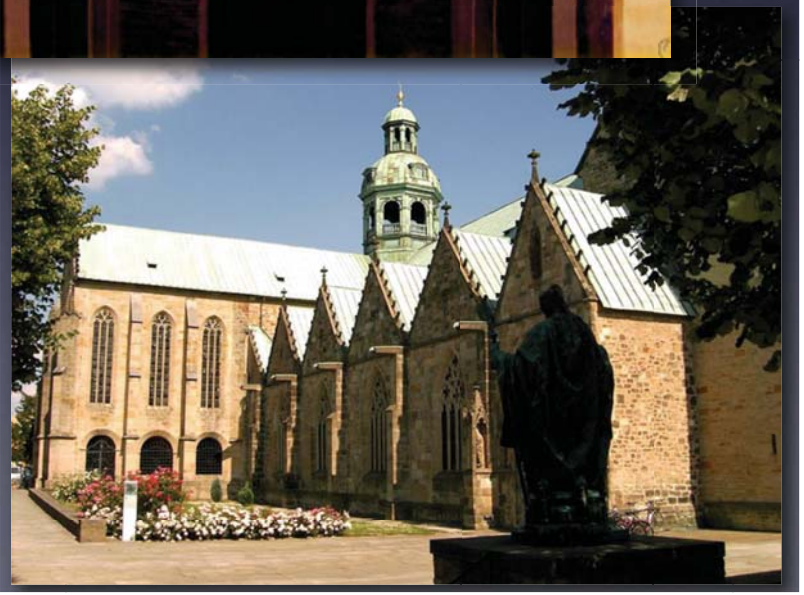

RBS study of glass corrosion

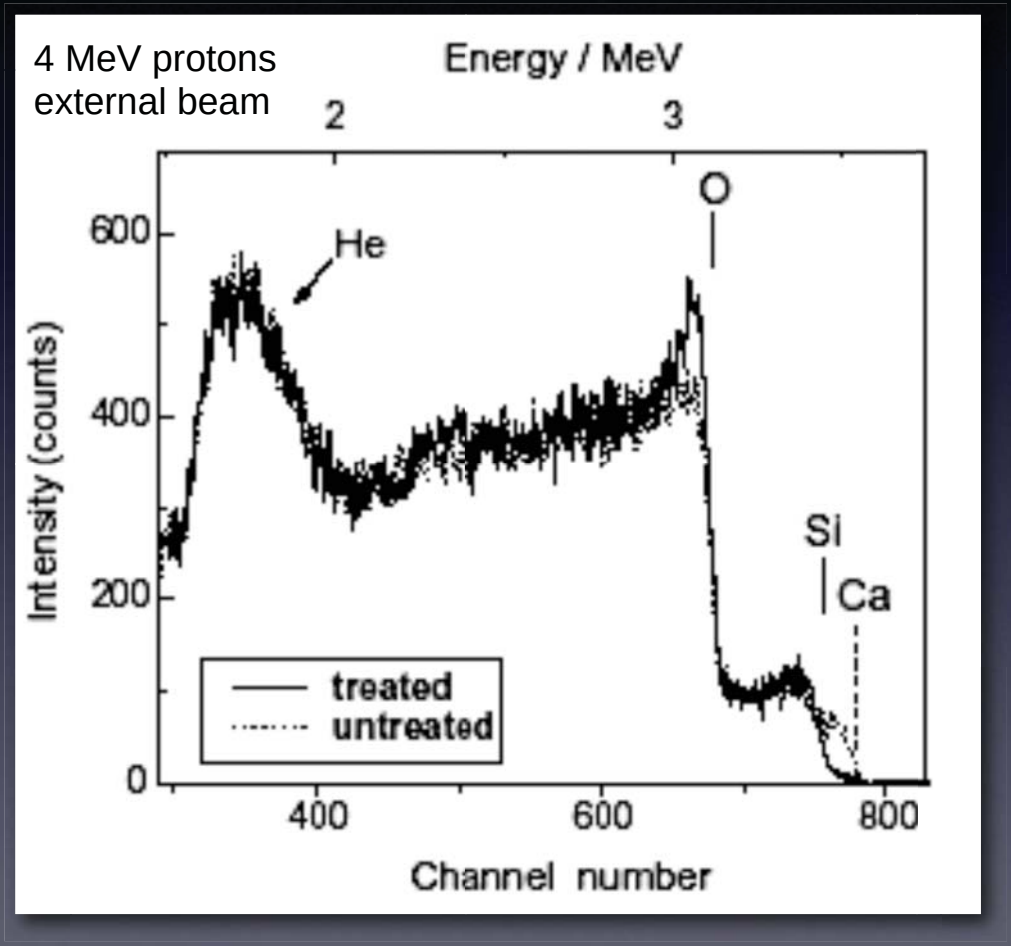

Leaching of Ca, K, Na from the interaction with moisture or water and formation of surface hydrate silicates
(cfr. PIGE analysis)

Complementary PIXE/RBS

In samples with a layered structure the elemental depth profile is needed to correctly calculate absorption effects in PIXE

PIXE strenghts

- High sensitivity
- Excellent specificity

RBS weaknesses

- Low sensitivity
- Poor mass resolution

RBS strenghts

- Traceable accuracy
- Excellent depth resolution

PIXE weaknesses

- Poor traceability
- Poor depth resolution

Characterization of paint layers by simultaneous PIXE/RBS analysis

"La Bohémienne", Frans Hals (1630)

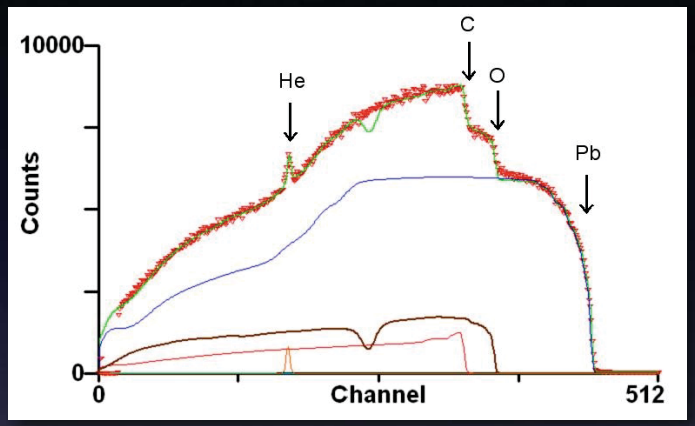

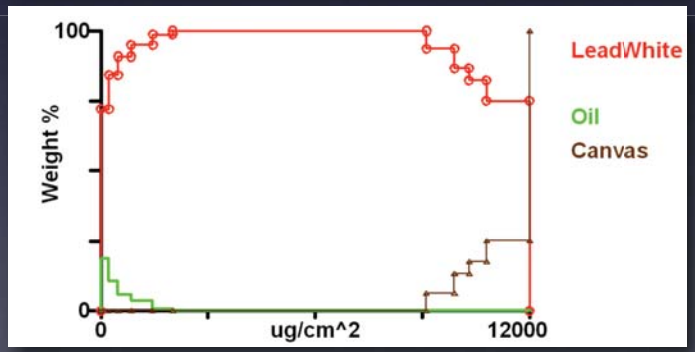

The canvas is schematized as carbon plus chalk ($CaCO_3$)

Ochre pigment (ematite) detected and quantified thanks to simultaneous PIXE/RBS measurements: $440 \cdot 10^{15}$ atoms/cm^2 Fe_2O_3 in $7000 \cdot 10^{15}$ atoms/cm^2 of oil ($C_{13}O_5$)

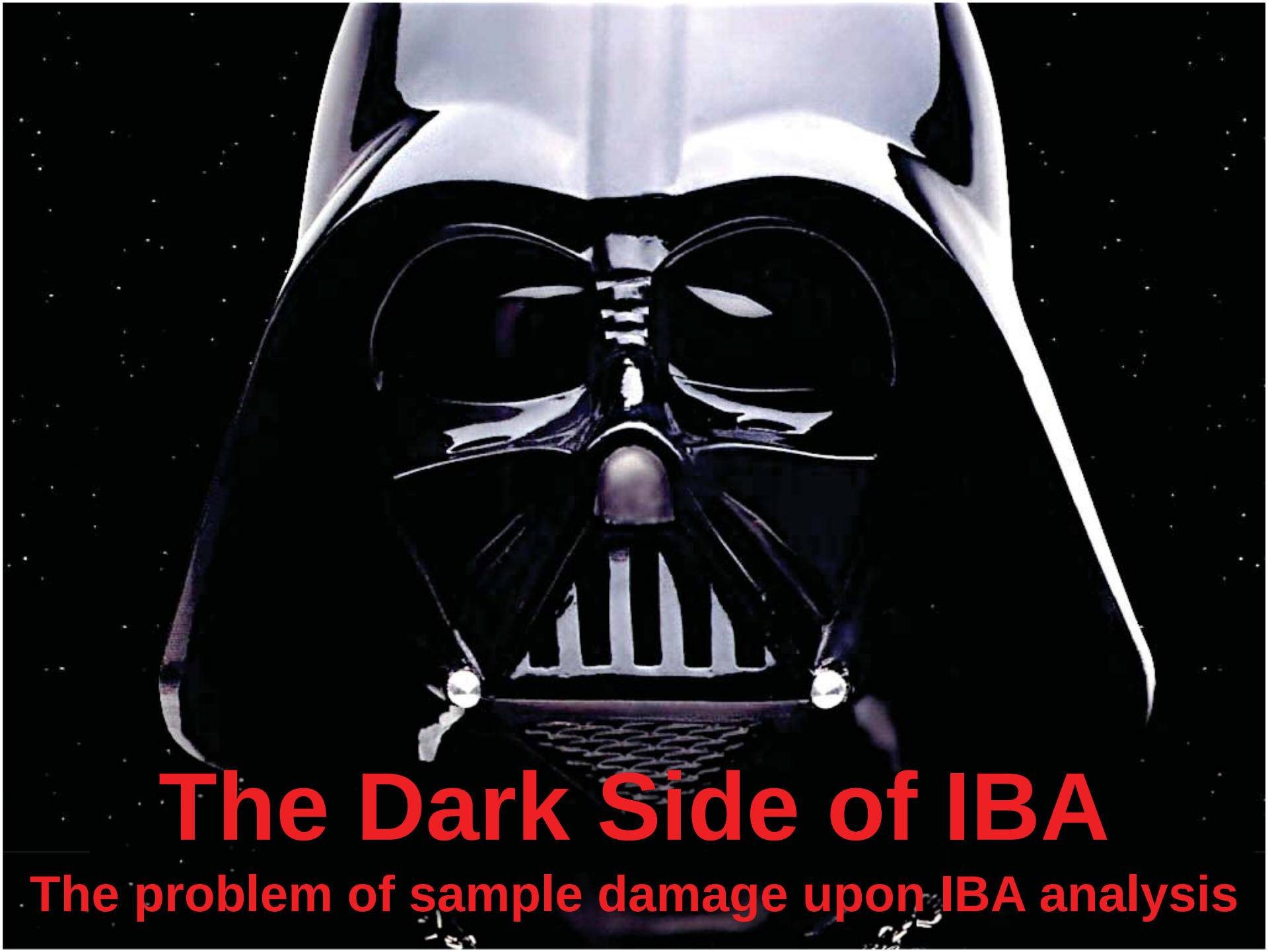

The Dark Side of IBA

The problem of sample damage upon IBA analysis

Which materials suffer ion beam induced damage ?

Ceramics

Pigments

Paper

The “dark spot” phenomenon

Appearance of dark spots during proton beam irradiation of ceramics and pigments (carbonate-based)

E = 3 MeV
i = 40 pA
t = 60 s

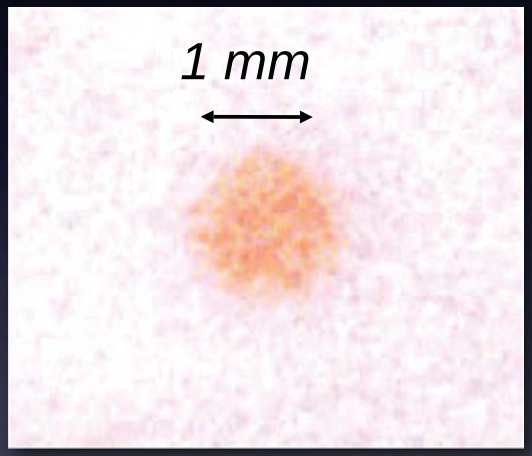

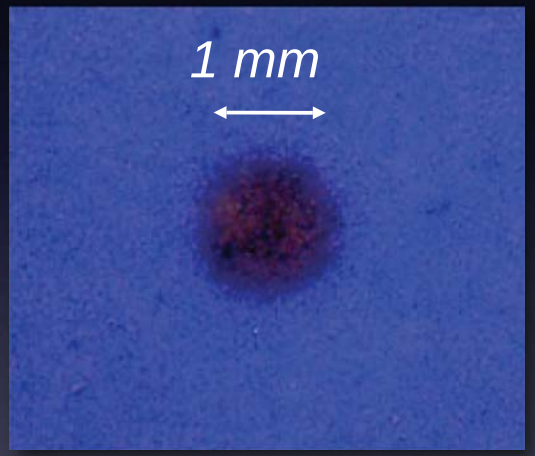

E = 2.5 MeV
i = 10 nA

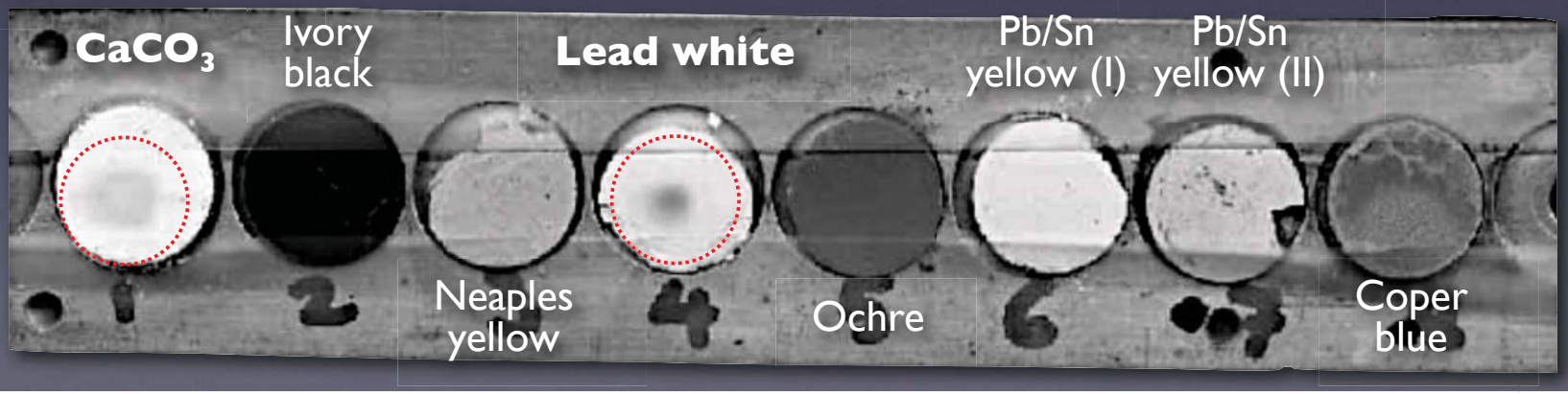

The damage and the beam dose

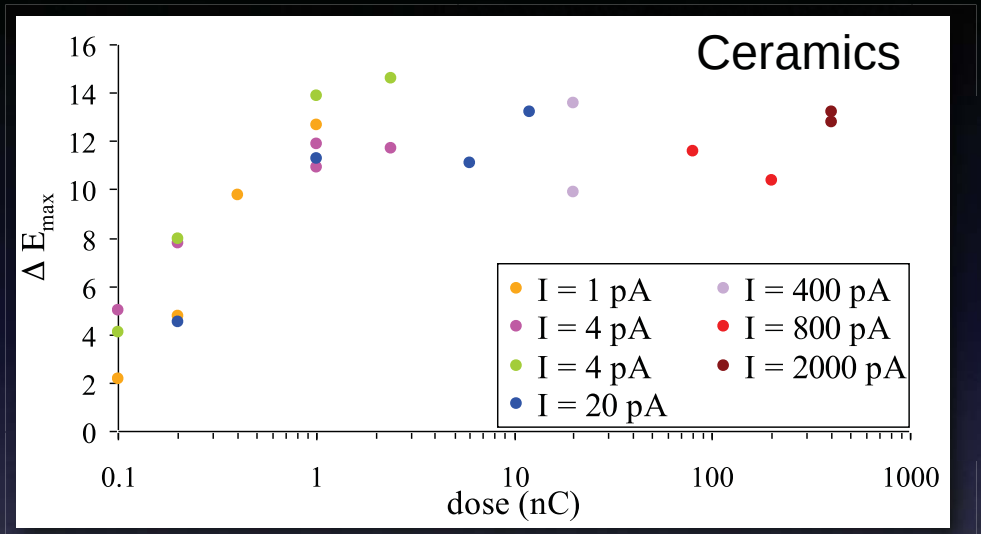

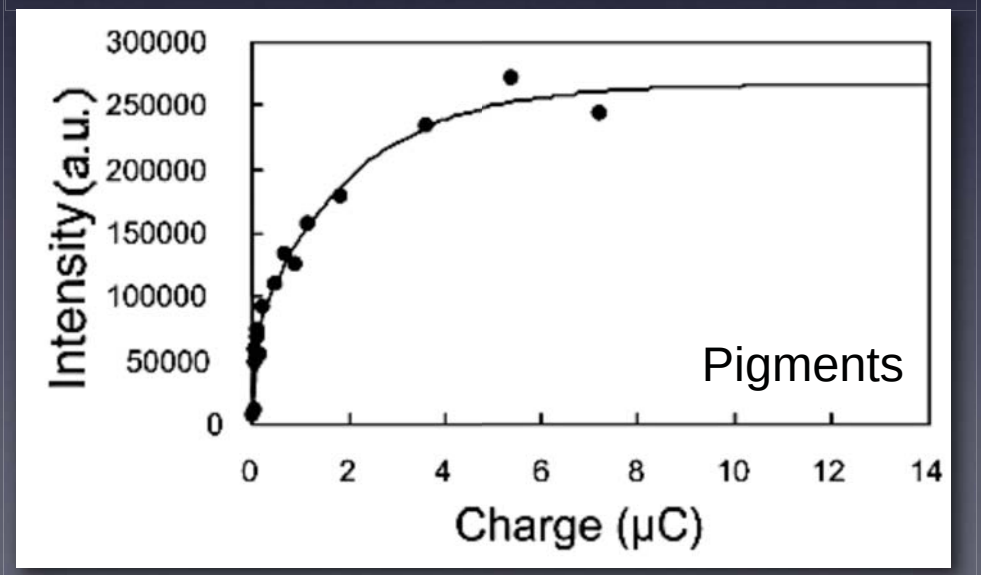

The chromatic variation or the intensity of the dark spot saturates with increasing beam charge

Recovery of damage

Once the proton beam irradiation stops, the “dark spots” progressively fade out

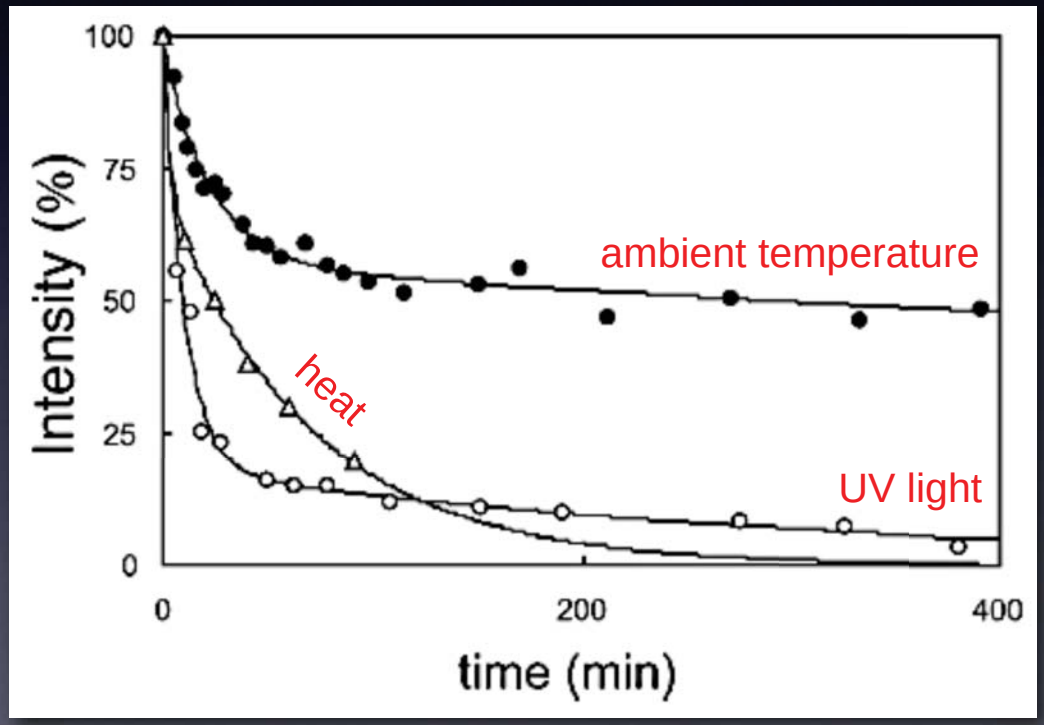

The apparent damage produced in valuable artistic objects can be anyway recovered even at ambient temperature.

Airborne particulate matter (aerosol)

Solid or liquid particles with a diameter from 10^{-3} to 10^{2} µm

Origin: primary or secondary

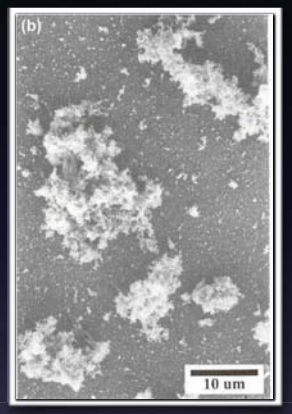

Diesel engine emission

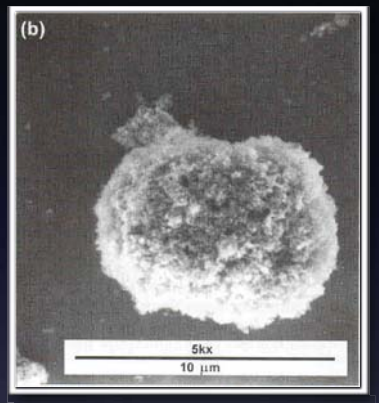

Black carbon

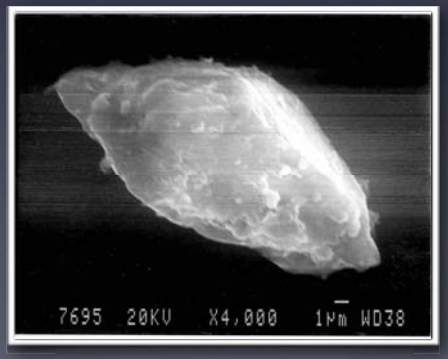

Mineral dust

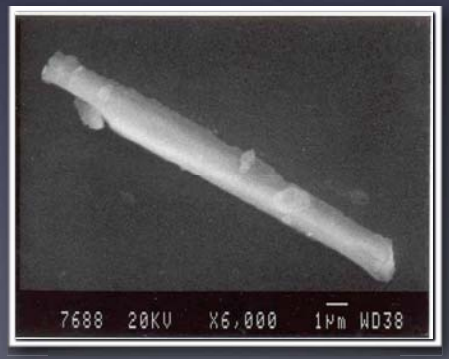

Vegetal fibre

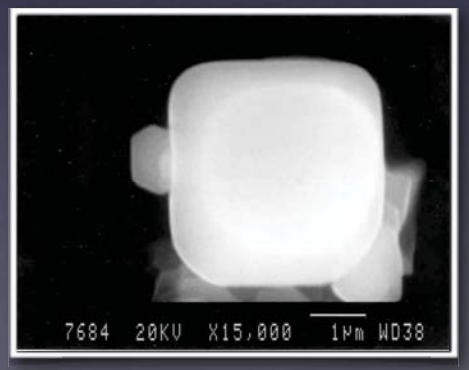

NaCl crystal

Aerosol average distribution

Aerodynamic diameter: diameter of a sphere of unit density (1 g/cm^3) that has the same gravitational settling velocity as the particle in question.

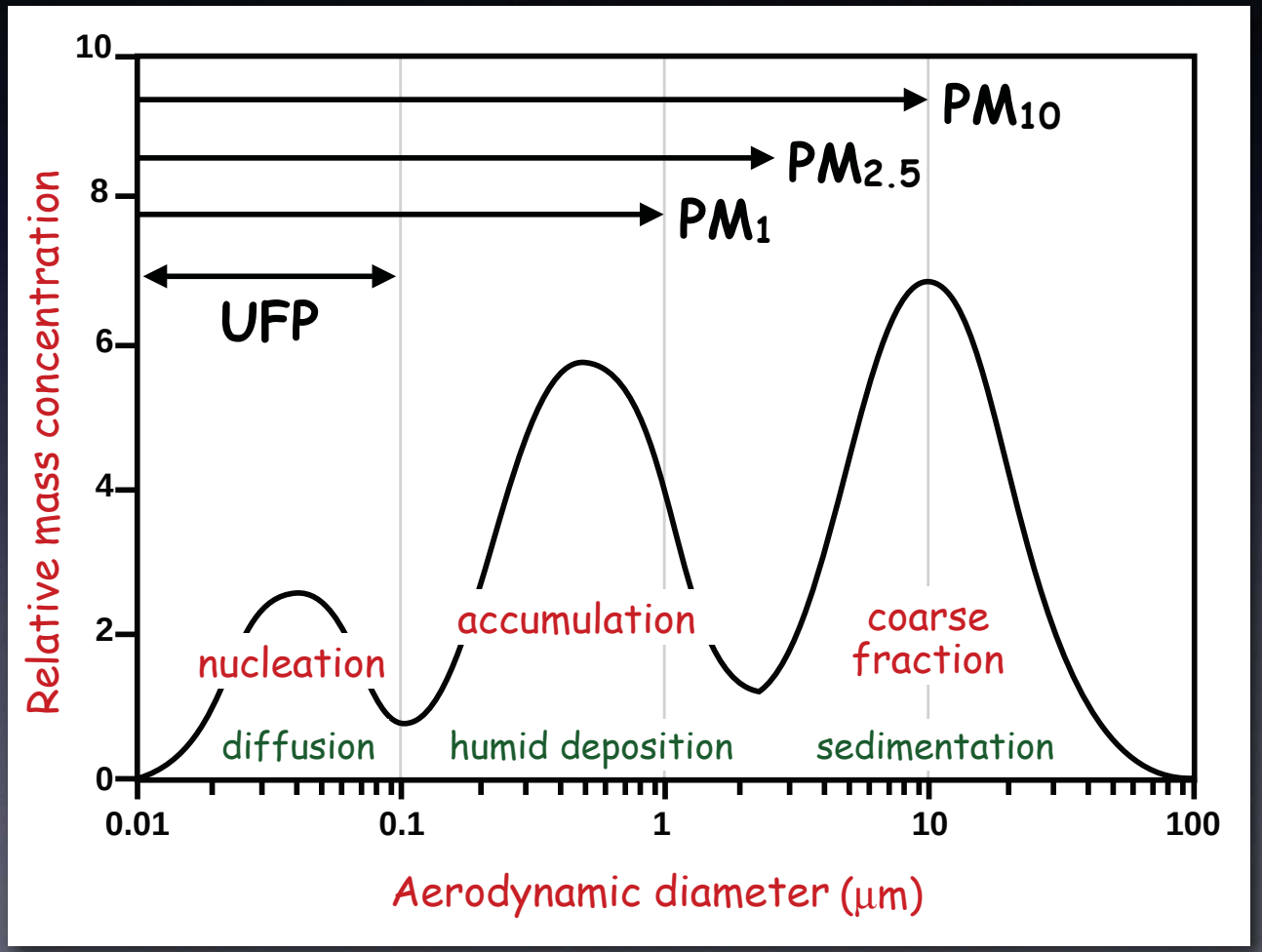

Natural sources of aerosols

Sea Spray

Volcanic eruptions

Forest fires

Desert dust transport

Anthropogenic sources of aerosols

Traffic

Thermoelectric power plants

Waste incinerator

Domestic heating

Industrial activities

Aerosol impact on environment

- Cloud formation
- Absorption and scattering of solar radiation

Climate forcing

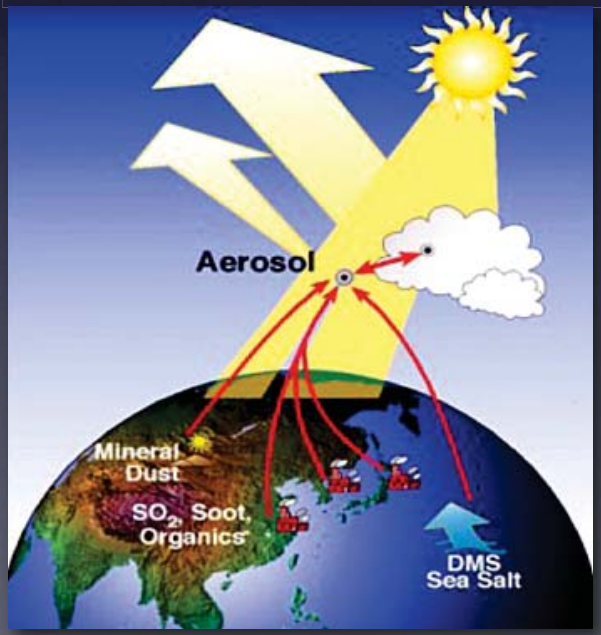

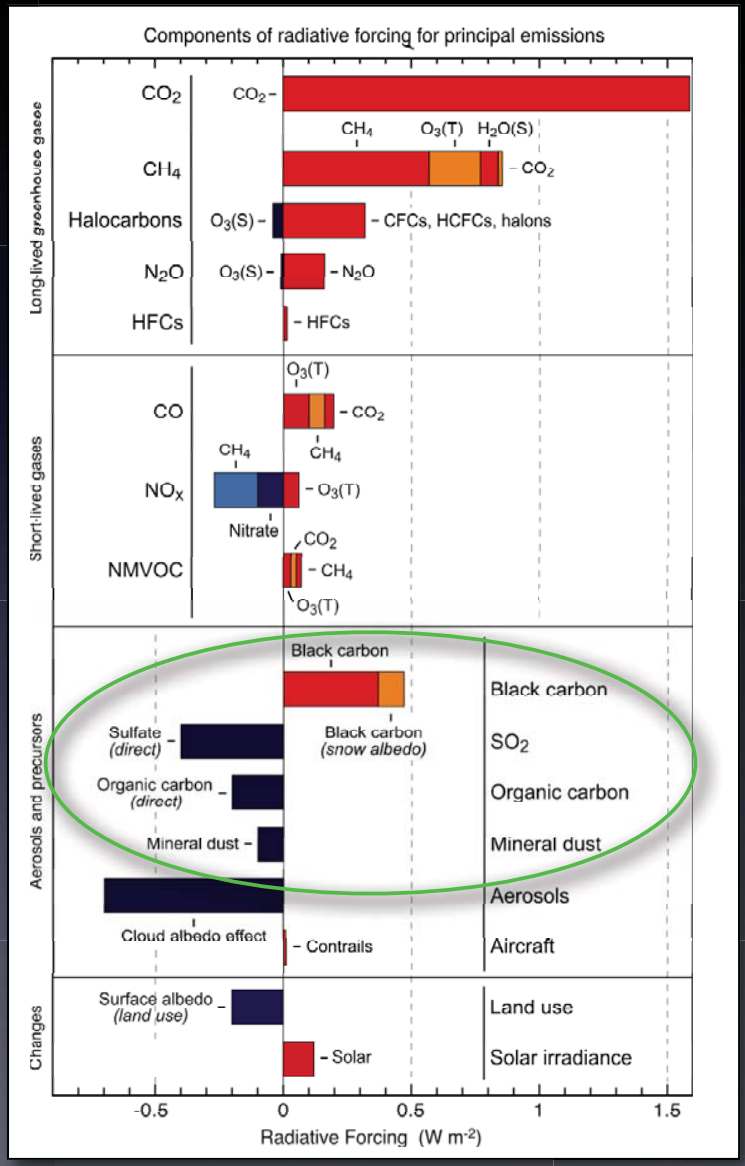

IPCC 2007

Aerosol impact on human health

- Chronic or severe respiratory diseases
- Toxic or carcinogen effects

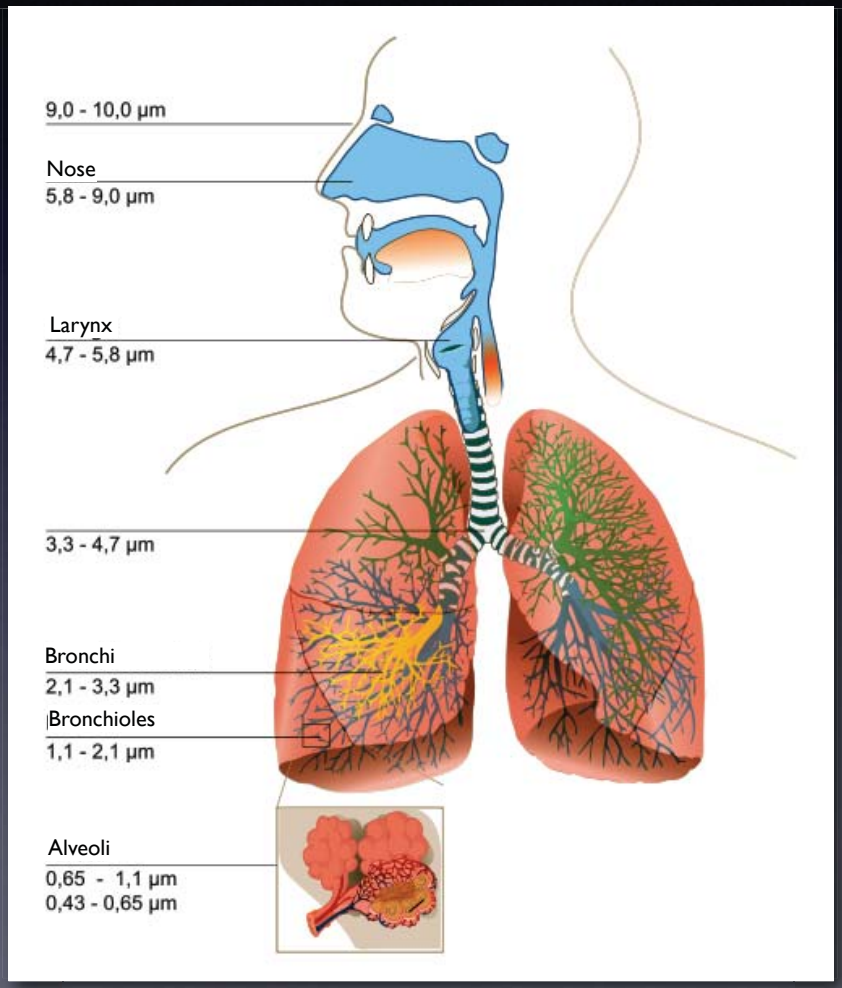

EU LIMIT VALUES FOR PARTICULATE MATTER CONCENTRATION

New European regulation (2008/50/CE)

PM_{10}

- Annual avg. <40 µg/m^3
- Daily avg. <50 µg/m^3 (not more than 35 days/year)

$PM_{2.5}$

- Annual avg. <25 µg/m^3 within 2015 ($PM_{2.5}$<10 µ/m^3 according to WHO)

Aerosol impact on cultural heritage

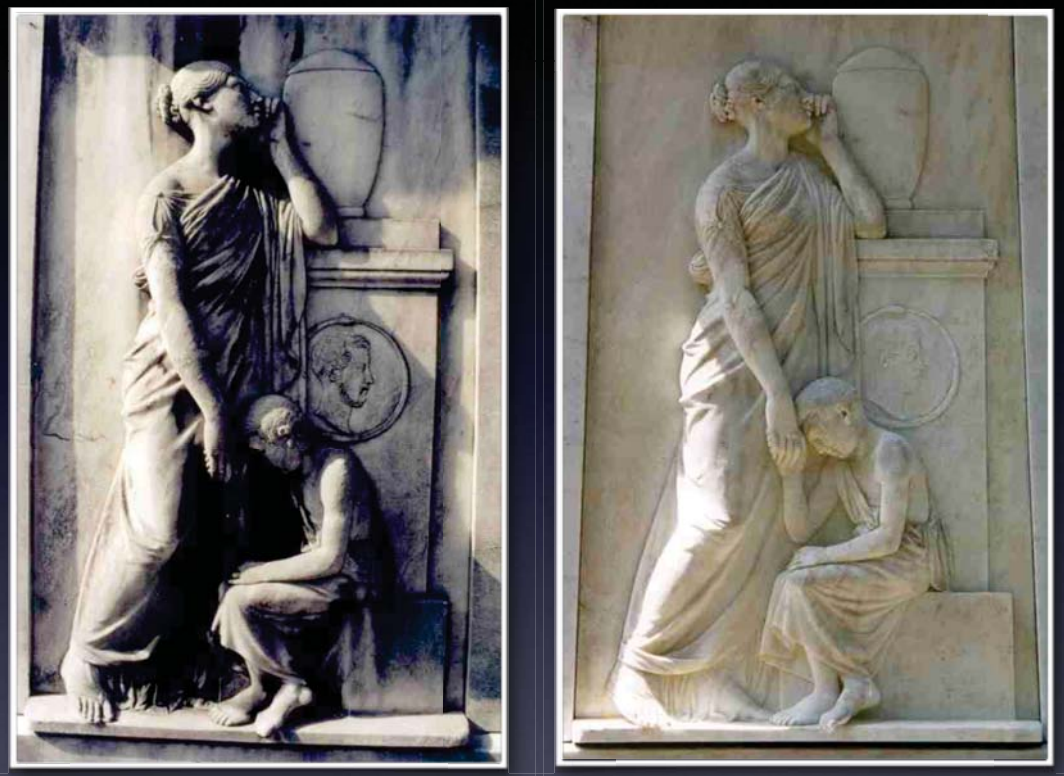

Funerary monument from 1837, English Cemetery, Florence (before and after restoration)

- Soiling
- Black crust formation
- Soluble salt crystallization

- Aesthetic damages
- Chemical reactions and physical interaction with the materials

What do we need...

Many good quality data concerning:

- PM concentration and composition
- size distribution
- optical properties
- time and space evolution
- ...

Identification e quantification of PM emission sources through receptor models

OUTPUT

Contribution to pollution abatement policies to improve air qualitity

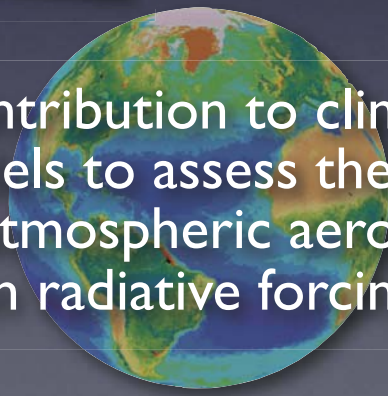

Contribution to climate models to assess the role of atmospheric aerosols in radiative forcing

Why IBA techniques?

- Aerosol sampling campaign produce huge amounts of small samples data (10-300 μg/cm^2)

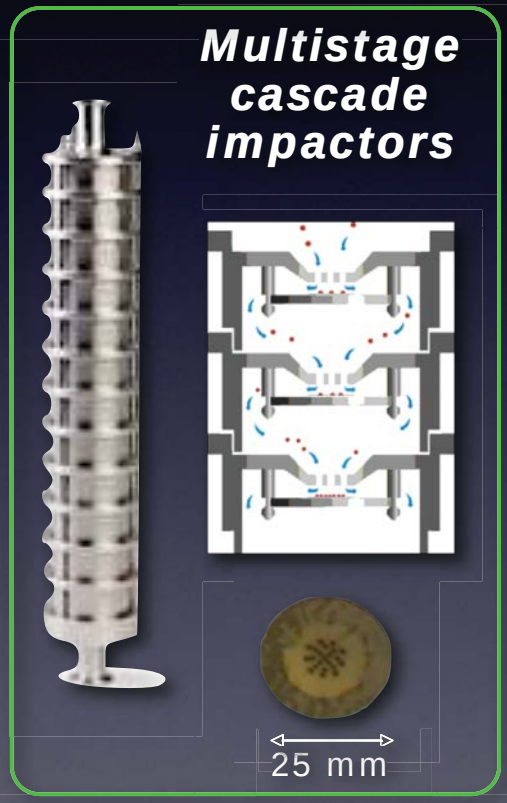

- Multielemental, fast, high sensitive, quantitative, non-destructive techniques are necessary

IBA in the context

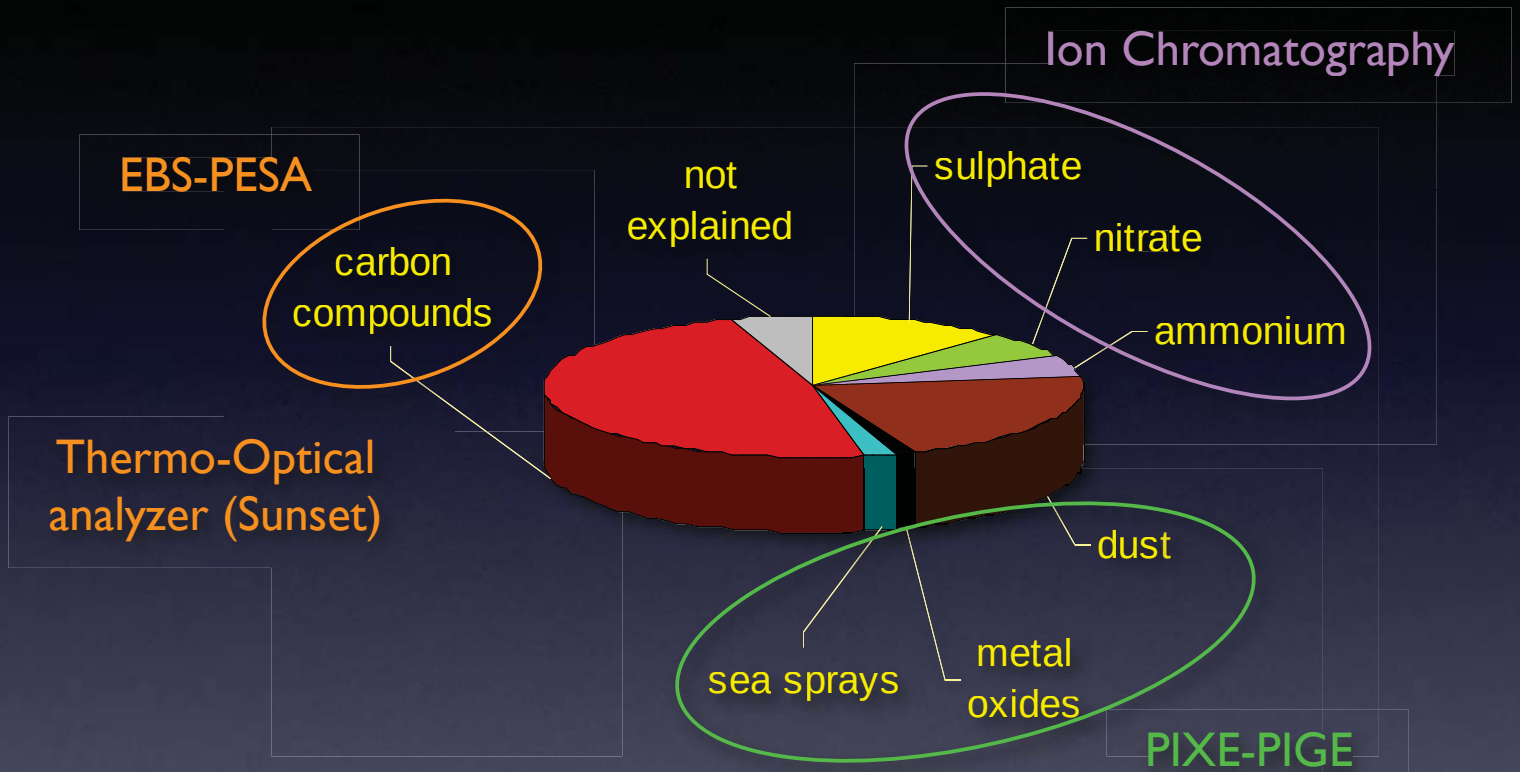

- Aerosol campaigns need an integrated approach involving different analytical techniques
- PIXE is the most widely used IBA technique (it detects all elements from Na to Pb)

PM_x daily samples

PM_1

$PM_{2.5}$

PM_{10}

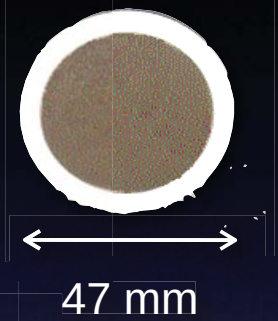

Typical filters:

Nuclepore ($C_{15}H_{14}CO_3$)

Cellulose ($C_{12}H_{30}O_{15}$)

Teflon (CF_2)

Quartz fiber (boro-silicate)

- Beam current 5 ÷ 50 nA
- Beam size: 1 mm x 2 mm (scanning the sample)
- Measuring time: 5 ÷ 10 minutes

1 year of daily samples: 2-3 days

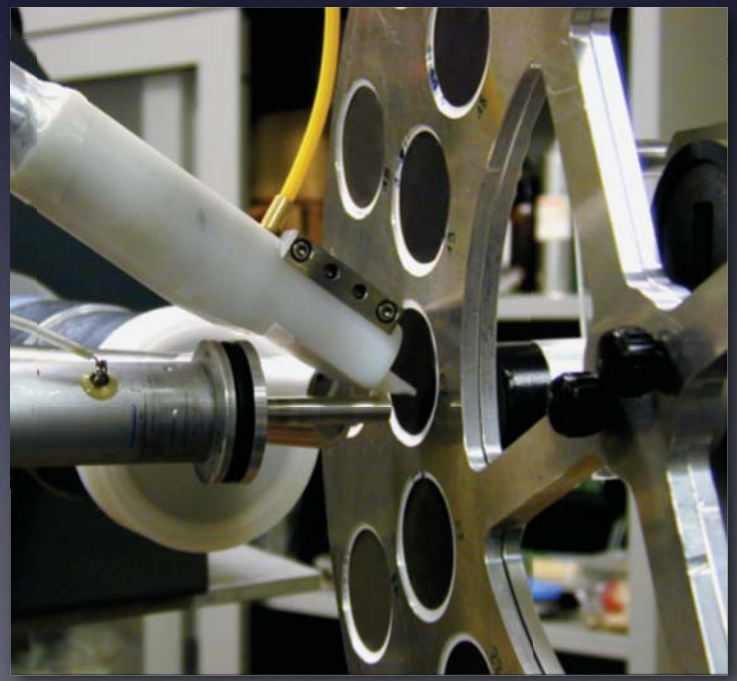

Saharan dust transport events

Increase in PM10 concentration

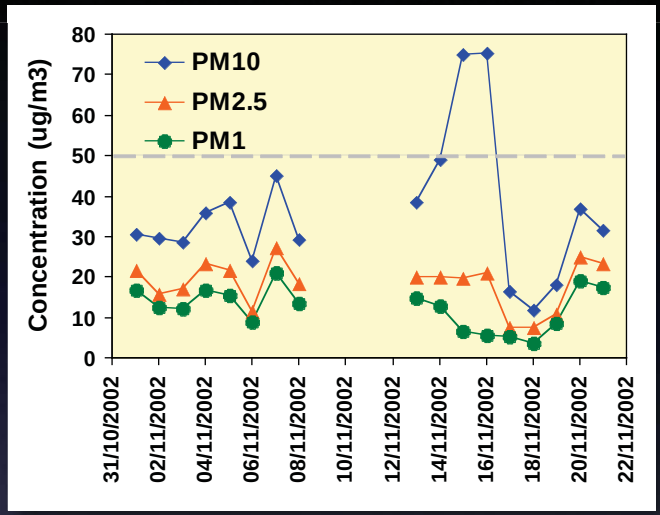

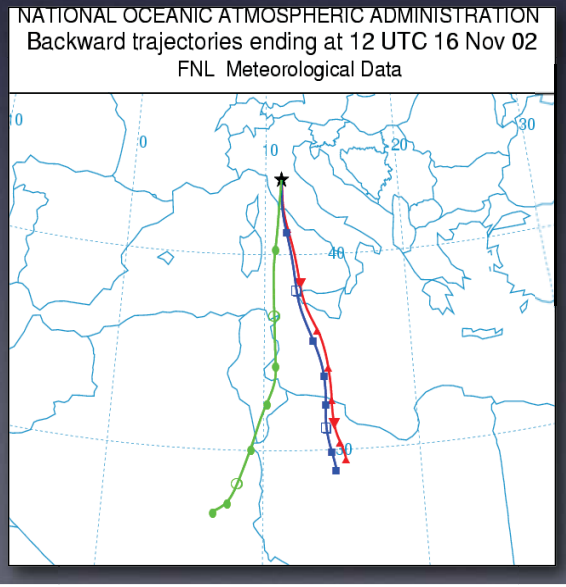

Air masses coming from Sahara

Increase of soil related elemental concentrations

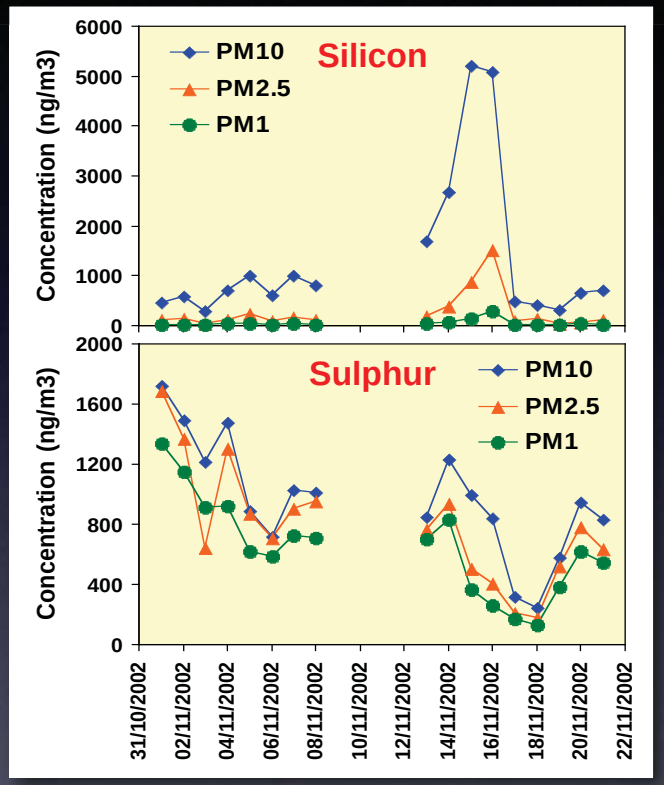

Change in elemental ratios

	Ti/Fe	Si/Fe	Al/Fe
15-Nov-02	0.09	2.79	1.07
16-Nov-02	0.10	2.52	1.01
other days	0.05 ± 0.02	1.81 ± 0.43	0.56 ± 0.22

Identification of aerosol sources

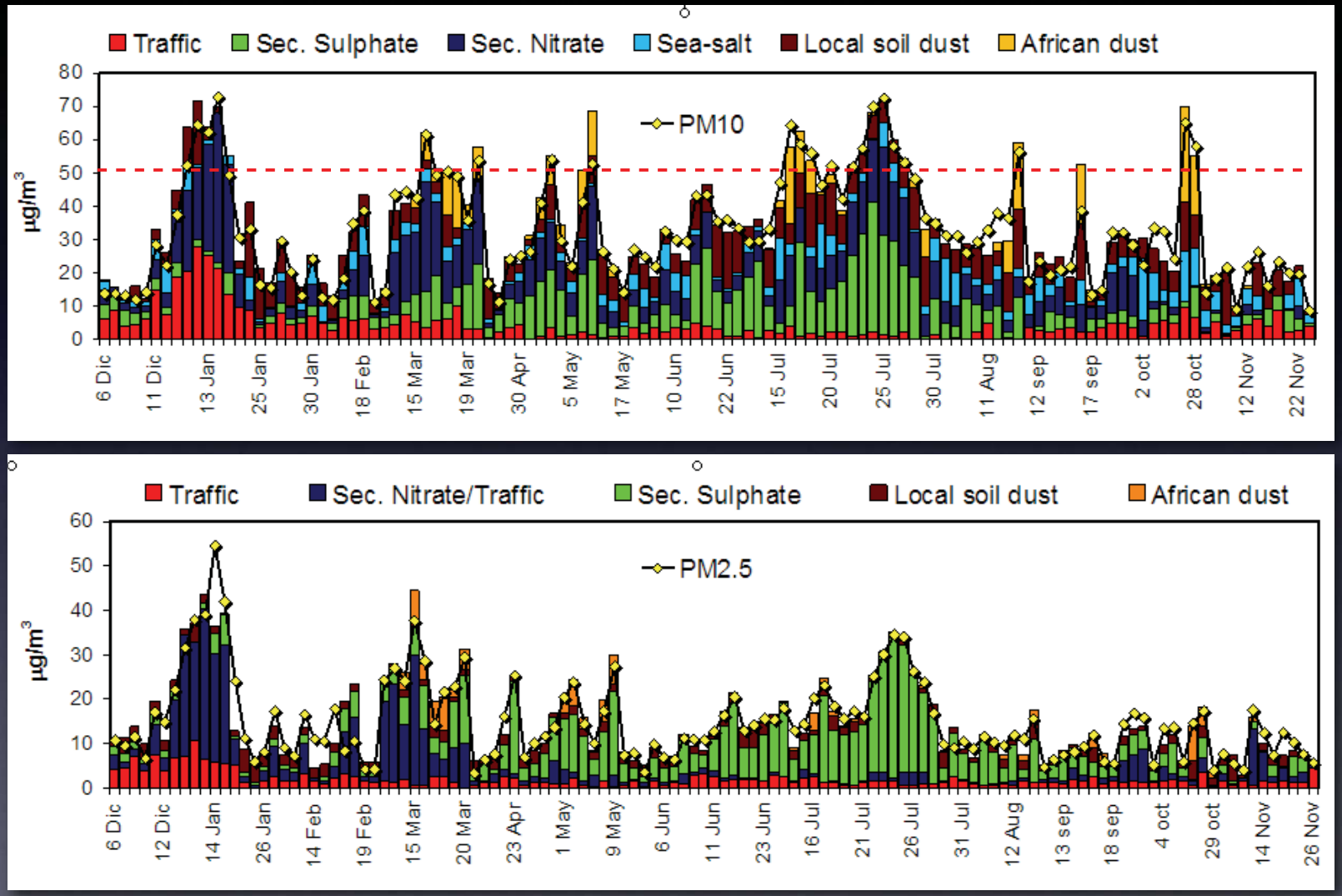

PM10 and PM2.5 daily samples collected simultaneously for one year (Dec. 2004 – Dec. 2005) in Elche, Spain

Fine and coarse hourly samples

Continuous "streaker" sampler

Kapton foils
Nuclepore

$PM_{2.5\div10}$

$PM_{2.5}$

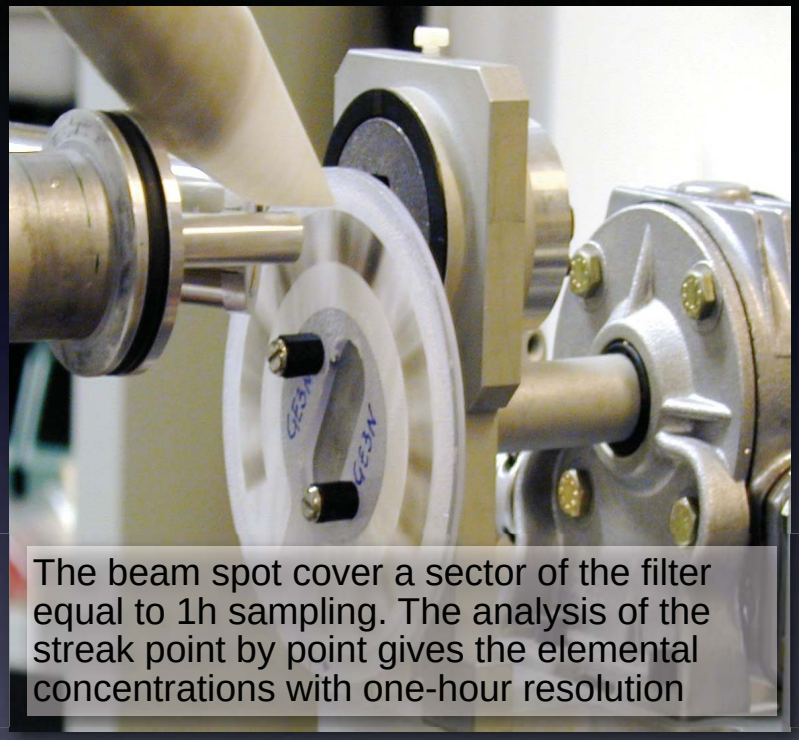

The beam spot cover a sector of the filter equal to 1h sampling. The analysis of the streak point by point gives the elemental concentrations with one-hour resolution

- Beam current 20 ÷ 50 nA
- Beam size: 1 mm x 2 mm
- Measuring time: 3 minutes

1 week at 1h resolution:
9 hours (168 spots)

Elemental time series

Size fractionation
+
High time resolution
+
Low elemental detection limit
+
Broad range of elements
=
New insight into short-term dynamics of atmospheric pollution by trace elements

Fugitive industrial emissions

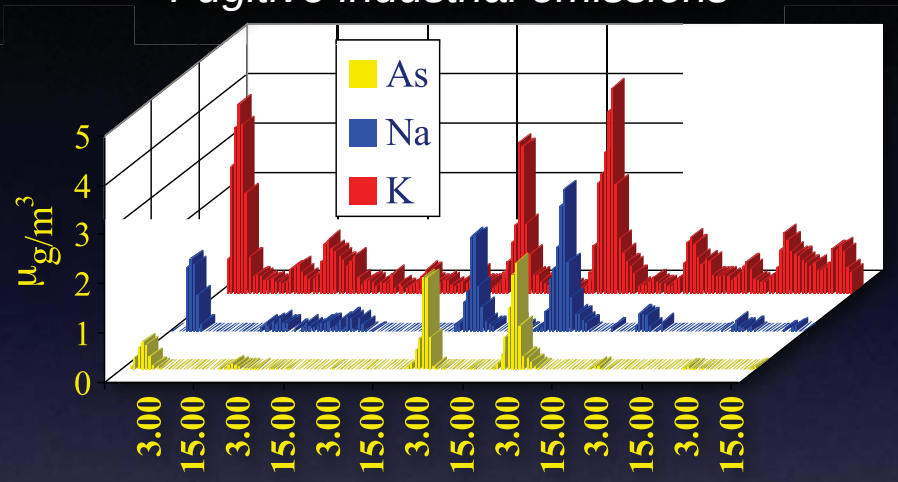

Wood burning for domestic heating

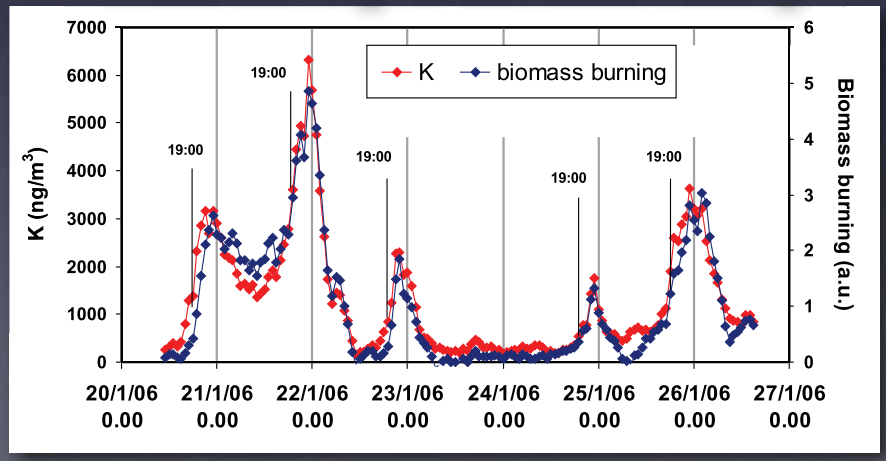

Identification of industrial emissions: steel plants in Taranto (Italy)

Taranto

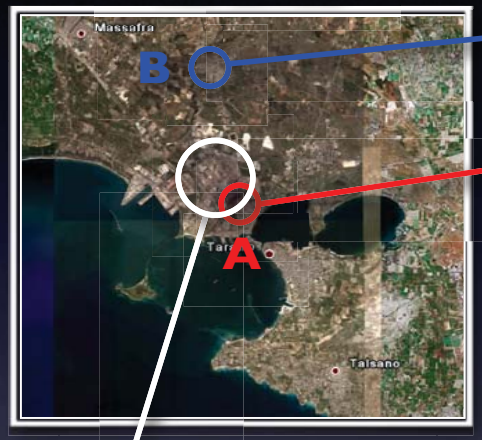

Site B: small town 7 km N of Taranto

Site A: urban district adjacent to the industrial area

Industrial area

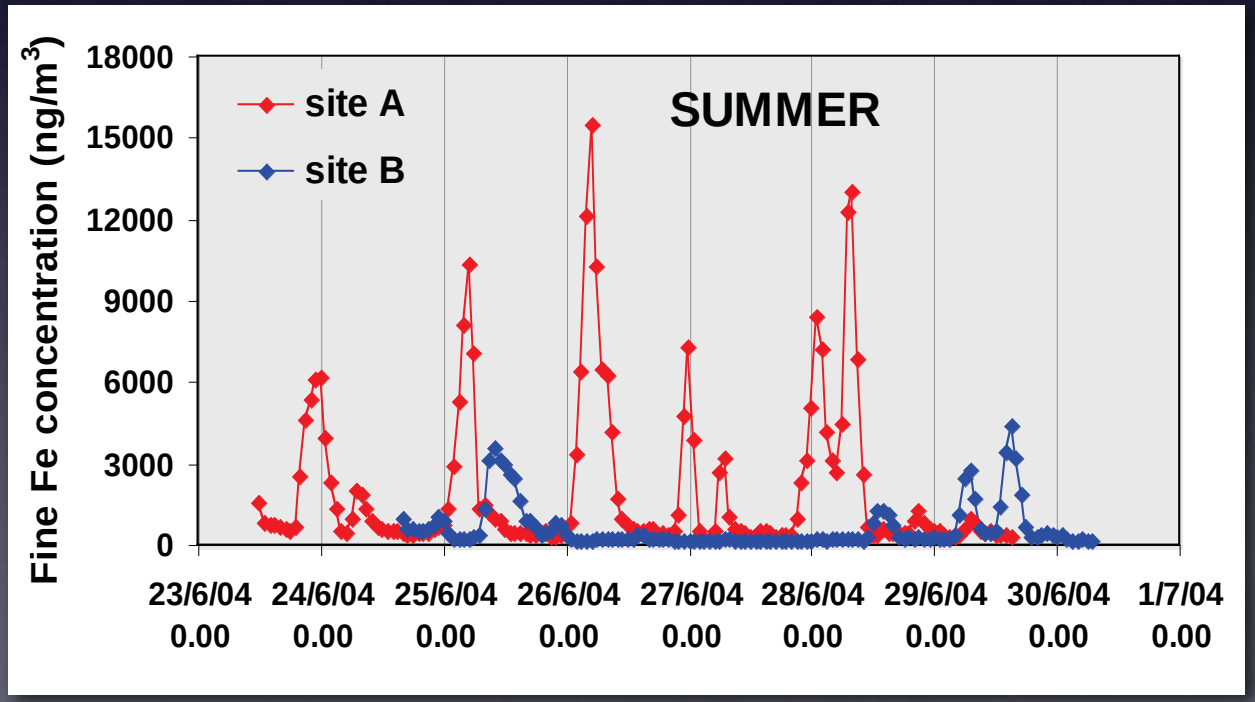

Impact of tourism on cultural heritage

Michelozzo's Courtyard
(Palazzo Vecchio, Florence)

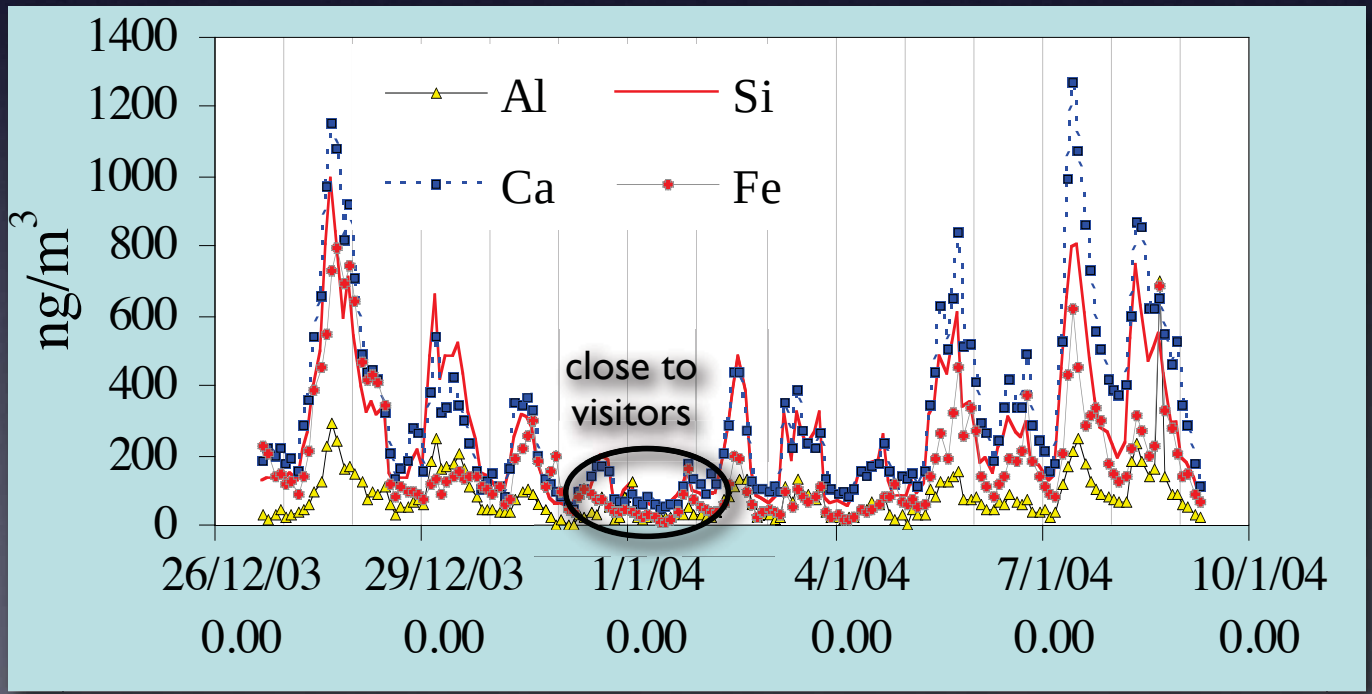

Identification of anthropic emissions: fireworks

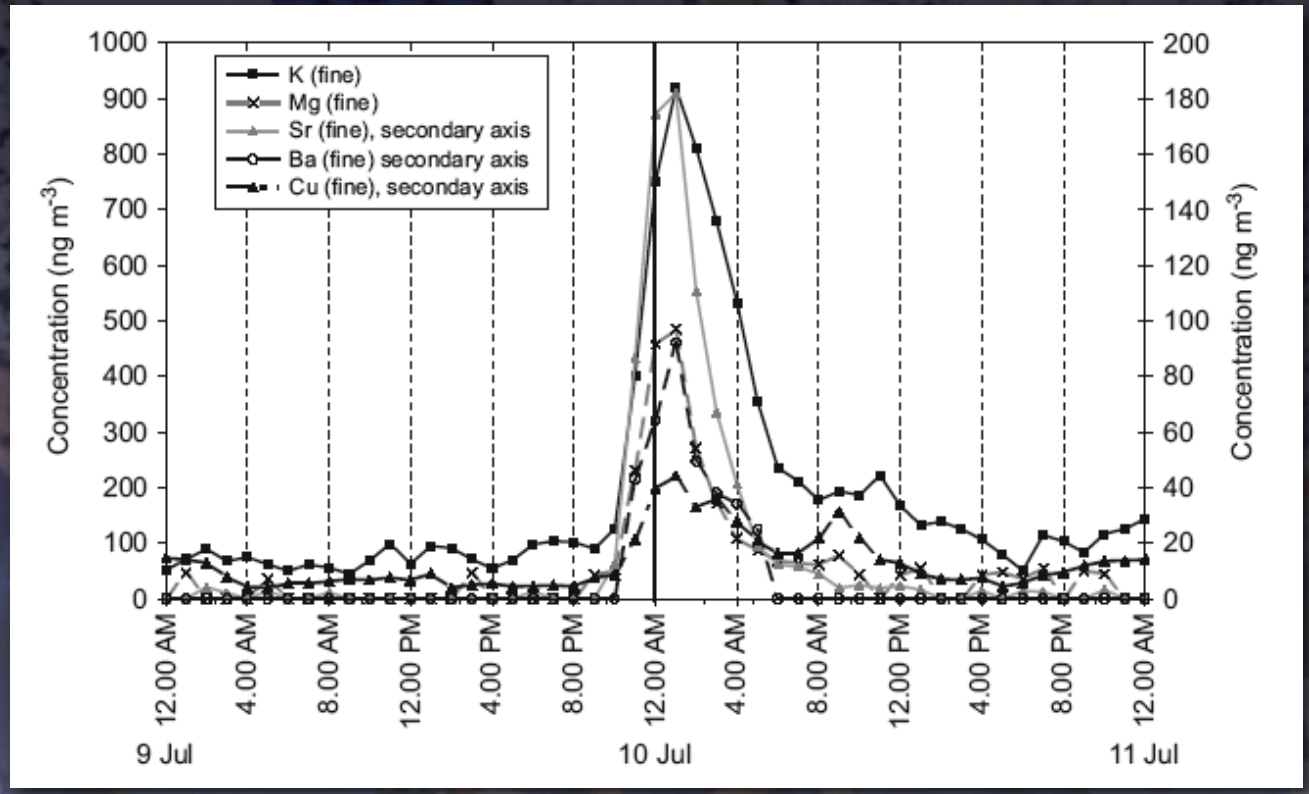

During the night between 9 and 10 July 2006 fireworks were burnt to celebrate the Italian football team, winner of the FIFA World Cup

Multi-stage cascade impactors

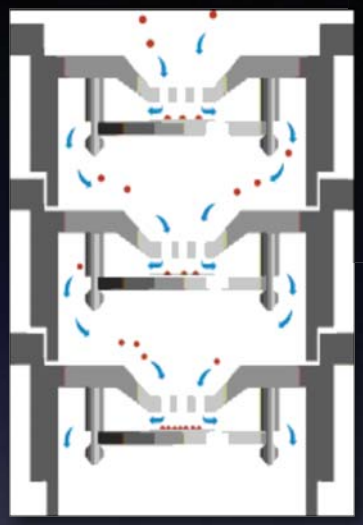

Kapton, Mylar or policarbonate foils

- SDI (Small Deposit area Impactor)
  - 12 stages from 45 nm to 8.5 μm (11 l/min.)
  - Small particle collection area (< 8 mm)
- Developed to collect aerosol (in remote areas) for PIXE in-vacuum analysis with large beams
- In an external set-up it is not possible to work with large beams

Multi-stage cascade impactors

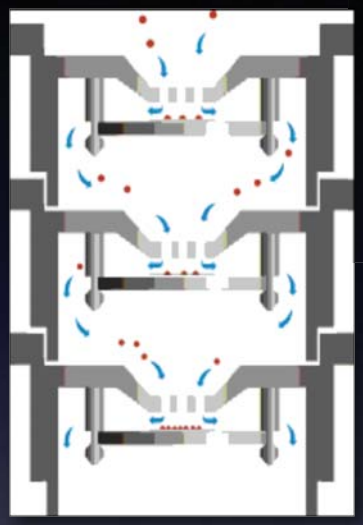

Kapton, Mylar or policarbonate foils

- SDI (Small Deposit area Impactor)
  - 12 stages from 45 nm to 8.5 µm (11 l/min.)
  - Small particle collection area (< 8 mm)
- Developed to collect aerosol (in remote areas) for PIXE in-vacuum analysis with large beams
- In an external set-up it is not possible to work with large beams

Homogeneus scanning of the deposit area

Dimensional distributions

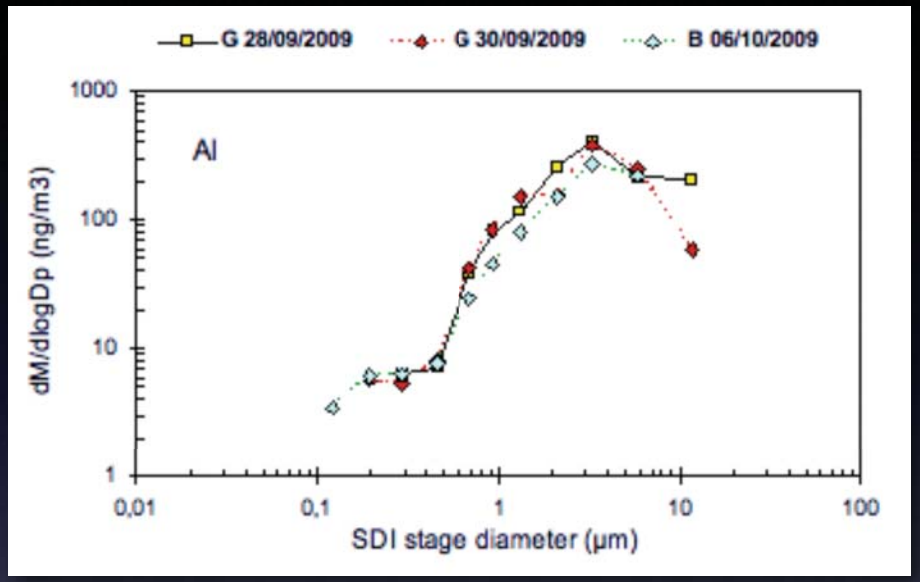

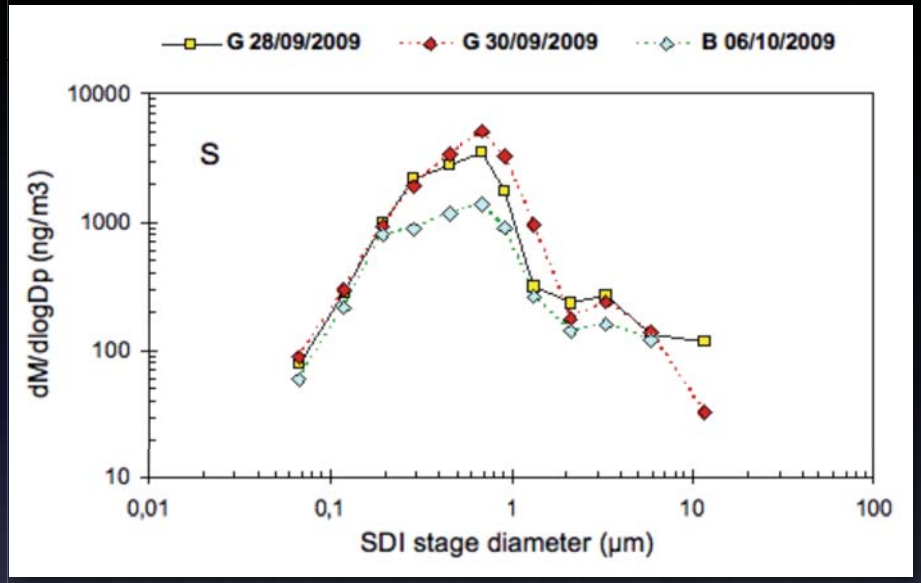

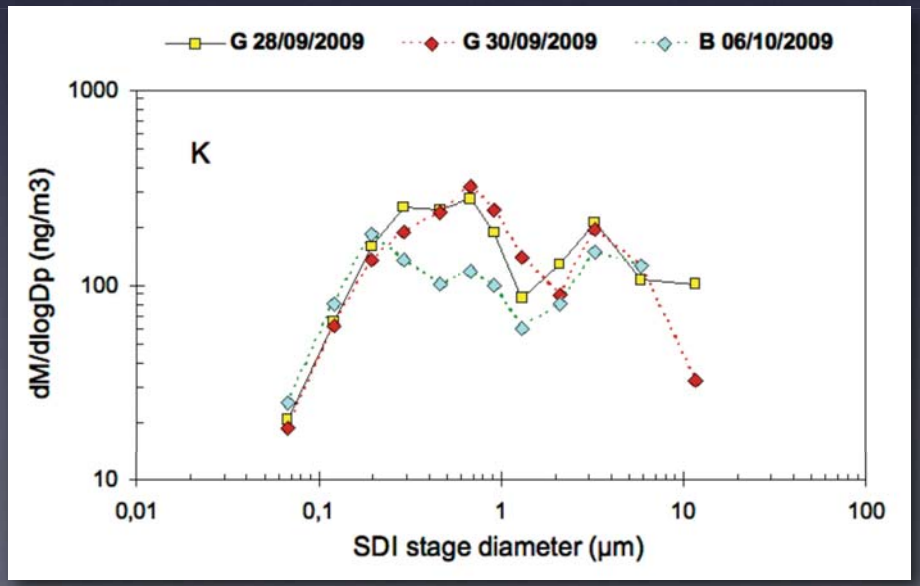

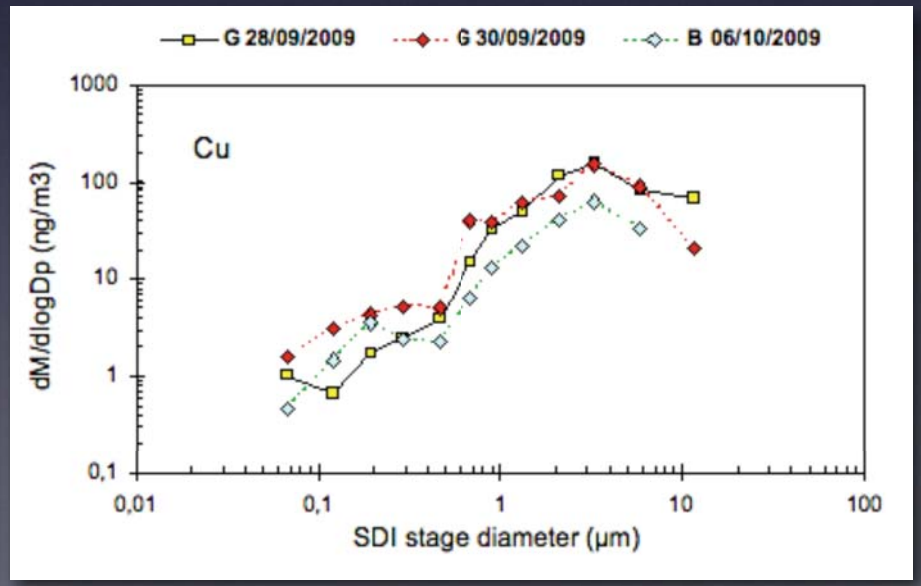

Matrix effects in PIXE

- Aerosol deposit can be considered a thin target ($\Delta E \leq 120$ keV for protons of few MeV energy in PM_{10})
- Small cross section variations within energy loss inside the sample
- Self-absorbtion of emitted radiation inside aerosol particles:
  - *it is a problem for a PIXE quantitative analysis for low-Z elements: Na, Mg, Al, Si*
  - *it can not be calculated considering an average matrix composition*

mandatory for studying mineral dust

PIGE for atmospheric aerosols

PIGE measurements can be used to correct the underestimation of PIXE due to low-energy X-rays absorption in the aerosol particles

Aerosol particles are a thin target (for 3 MeV protons ΔE is about 120 keV for "coarse mode" particles, i.e. PM10)

$$n_\gamma = n_p N \Delta\Omega \epsilon \int_{E_0-\Delta E}^{E_0} \frac{\mathrm{d}\sigma}{\mathrm{d}\Omega}(E,\theta)\frac{\mathrm{d}E}{S(E)}$$

If the PIGE cross sections are constant over the energy range ΔE then:

$$n_\gamma = n_p \sigma \Delta\Omega N t$$

The unknown concentrations can be deduce by comparing the Υ-ray yield to those of **thin** elemental standards

Spreading the beam for PIGE

- Finding energy intervals where prompt gamma-ray emission cross sections are **costant** and **high** enough.
- Prerequisite to provide an analytical method with good sensityvity and not affected by sample weight and matrix effects, suitable to large-scale analysis.
- Smooth the fluctuations in the PIGE cross sections (i.e. use a diffuser).

Use an external beam !

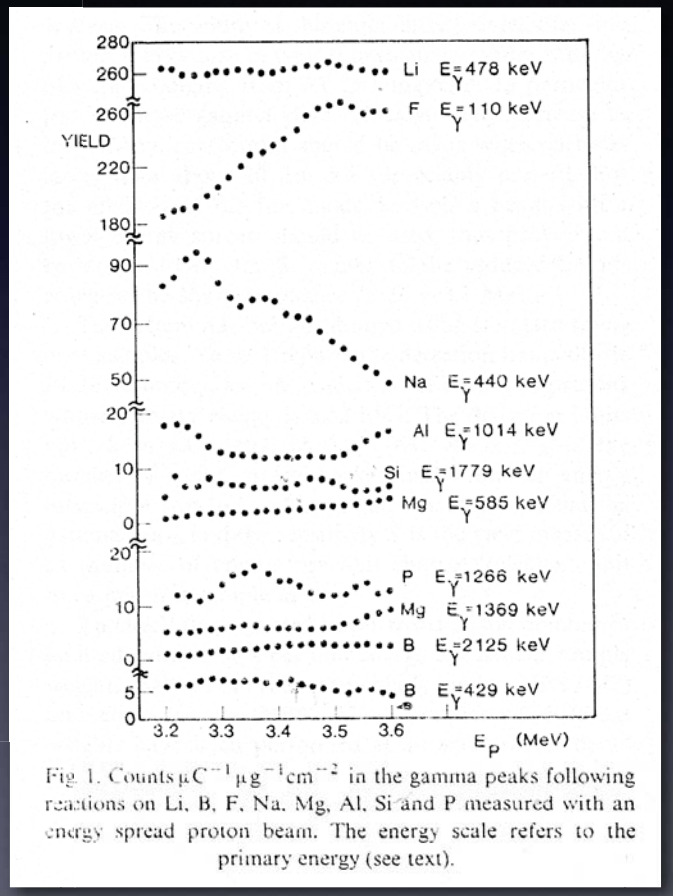

Fig. 1. Counts $\mu C^{-1} \mu g^{-1} cm^{-2}$ in the gamma peaks following reactions on Li, B, F, Na, Mg, Al, Si and P measured with an energy spread proton beam. The energy scale refers to the primary energy (see text).

C. Boni et al., NIM B 40/41, 1989

PIGE yields with external proton beam

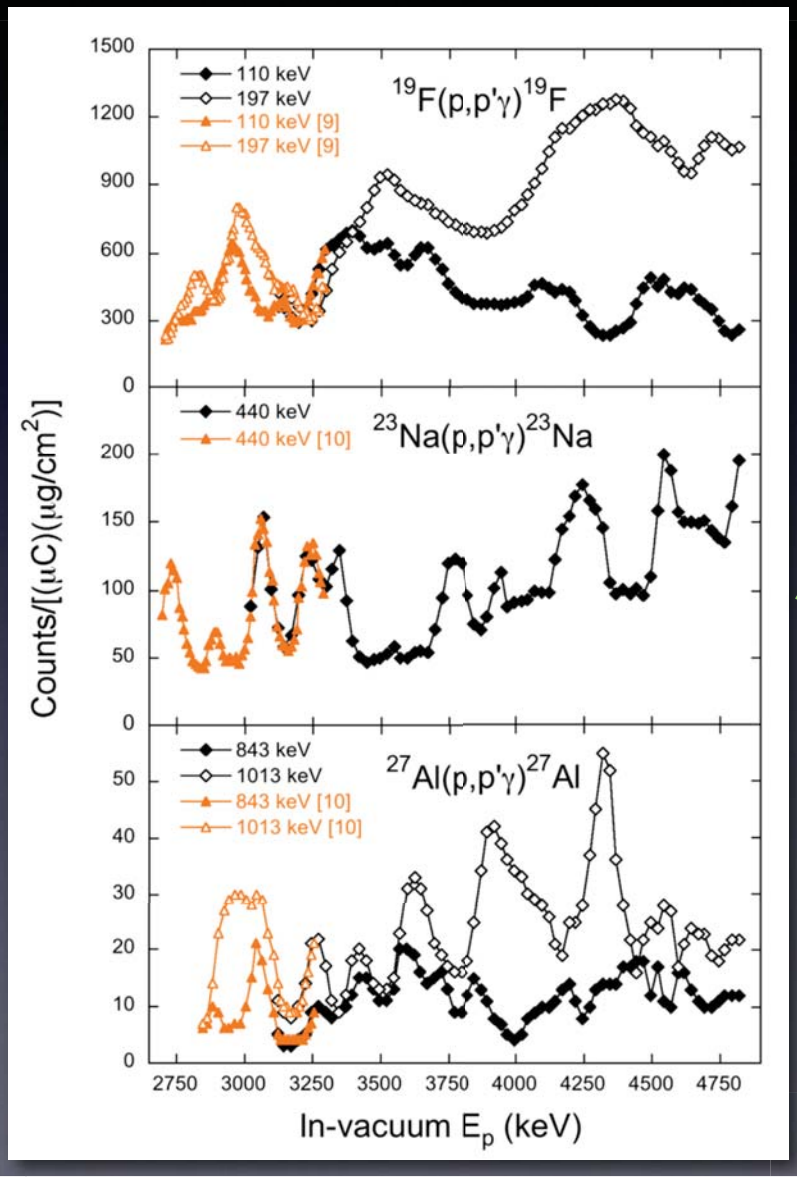

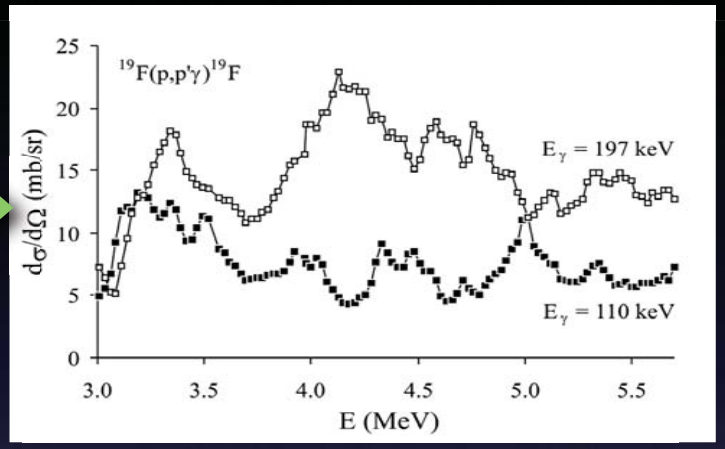

A. Caciolli et al., NIM B 249, 2006

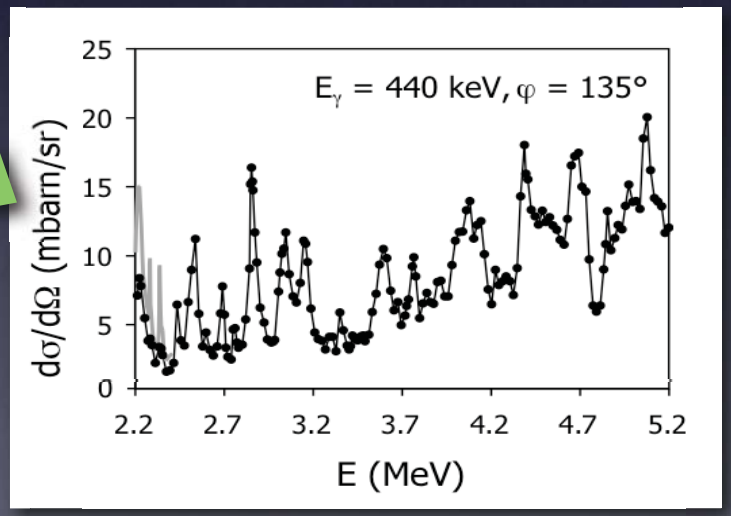

A. Caciolli et al., NIM B 266, 2008

G. Calzolai et al., NIM B 268, 2010

Energy plateau region for PIGE

Reaction	E_γ (keV)	E_p (keV)	E_p on target[a] (keV)	Width (keV)	Average yield [counts/(μC·μg/cm^2)]
$^{19}F(p,p'\gamma)^{19}F$	110	4020	3863	175	380
		4395	4248	100	250
	197	3945	3785	125	700
		4420	4274	150	1250
$^{23}Na(p,p'\gamma)^{23}Na$	440	2990	2791	70	50
		3520	3346	100	50
		3670	3501	100	55
		4045	3889	75	90
		4470	4326	100	100
		4695	4556	100	150
$^{27}Al(p,p'\gamma)^{27}Al$	843	4370	4223	75	14
		4745	4607	75	10
	1013	3065	2870	120	29
		3820	3657	75	18
		4695	4556	75	23

[a] The proton beam energy E_p on target is calculated taking into account the energy loss in the 7.5 μm Upilex exit window and in the external path of 5 mm of air and 5 mm of He.

Energy plateau for Na measurement

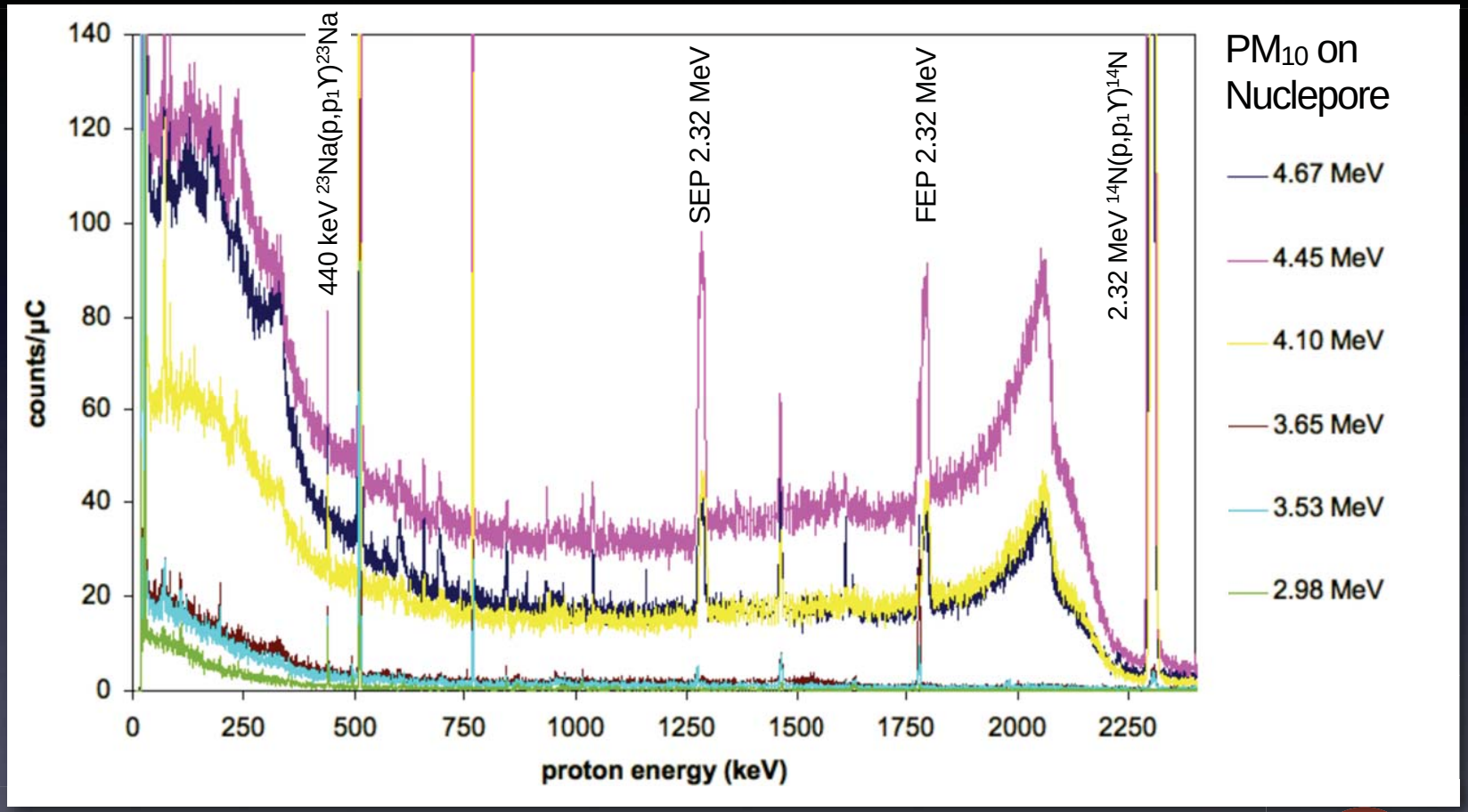

E_p (MeV)	4.67	4.45	4.10	3.65	3.53	2.98
MDL (ng/cm^2)	73	133	93	70	60	37

Measurement of Na in PM_{10} samples

Sampling site	E_p (keV)	PIGE (μg/cm^2)	PIXE (μg/cm^2)	PIXE/PIGE
Lampedusa (Re)	3520	19.6 ± 0.9	13.3 ± 0.2	0.68 ± 0.04
Lampedusa (Re)	3670	20.0 ± 0.8	13.3 ± 0.2	0.67 ± 0.03
Lampedusa (Re)	4045	20.7 ± 0.7	13.2 ± 0.1	0.64 ± 0.02
Lampedusa (Re)	4470	20.9 ± 0.8	13.3 ± 0.1	0.64 ± 0.03
Lampedusa (Re)	4695	20.8 ± 0.5	13.5 ± 0.2	0.65 ± 0.02
Sesto F.no (U)	4045	8.4 ± 0.6	5.5 ± 0.1	0.65 ± 0.05
Livorno (Ru)	4045	16.0 ± 0.6	11.2 ± 0.1	0.70 ± 0.03
Prato (T)	4045	7.3 ± 0.5	5.1 ± 0.1	0.69 ± 0.05

- PIGE reproducibility independent from the used plateau
- The self-absorption effects are almost the same for all the samples: Na concentration is underestimated by 30-35%

Measurements of Al in dust particles

Airborne mineral dust collected in-flight over Sahel desert

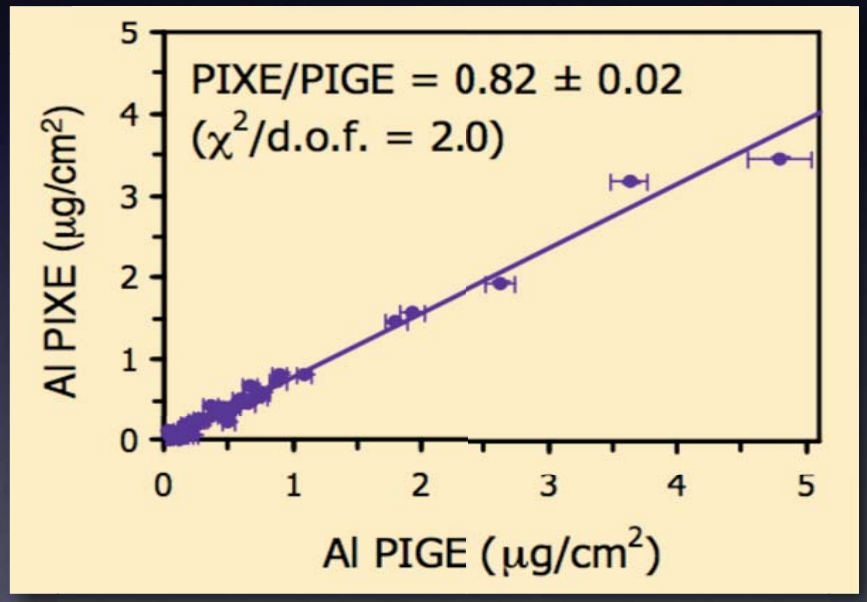

Mineral dust archived in Antarctic ice cores

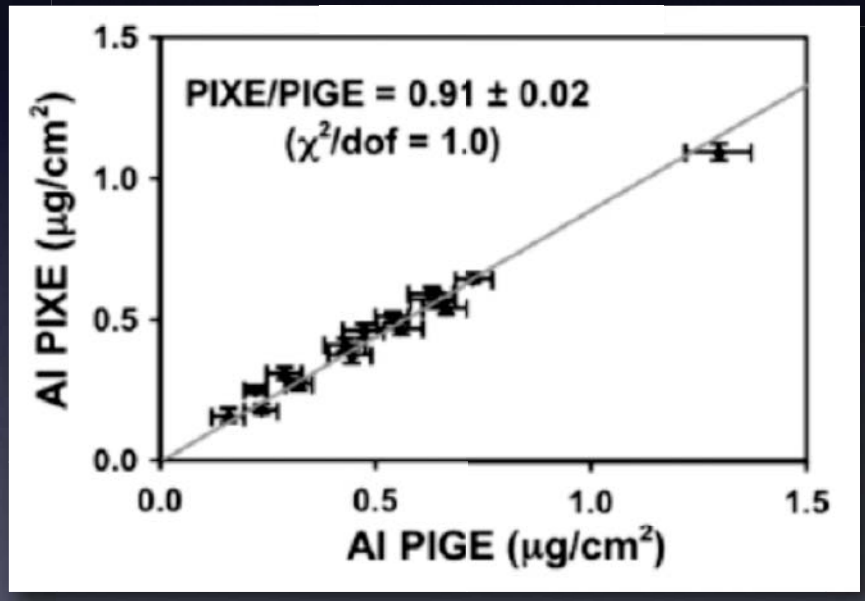

Correct the concentration of low-Z elements obtained by PIXE

Accurate study of geochemical composition of mineral dust

Study of geochemical composition of mineral dust

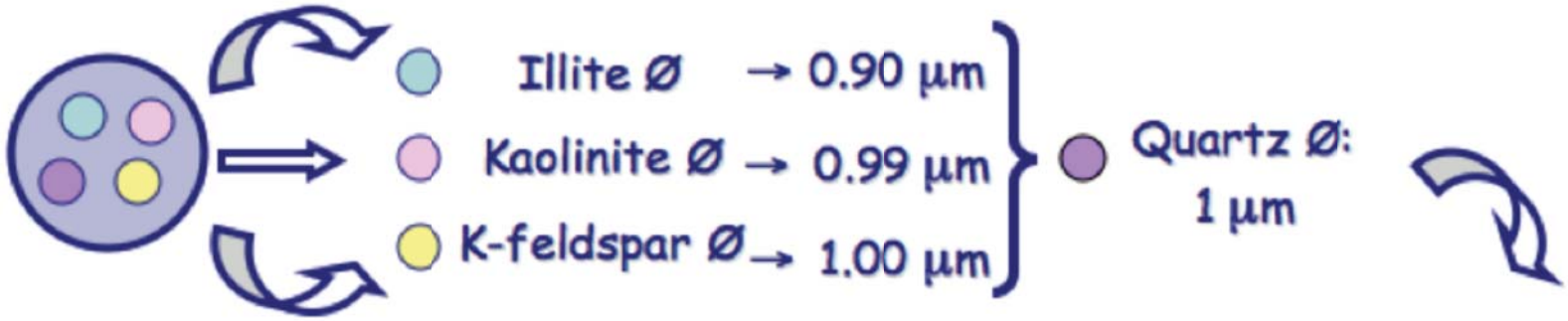

$$\left(\frac{PIXE}{PIGE}\right)^{Al}_{\substack{ice\\dust}} = 0.91$$

$$AF = \frac{1-\exp(-a\cdot D)}{a\cdot D},\ a = \frac{2}{3}\cdot\mu\cdot\rho$$

B. Holynska and A. Markowicz, XRS 10, 1981

	Na	Mg	Al	Si	K
Kaolinite			0.91	0.90	
K-feldspar	0.79		0.91	0.92	0.97
Illite		0.87	0.91	0.91	0.97
Quartz				0.94	

Scheme of the evaluation of the attenuation for the light elements in a dust sample, in the hypothesis that it is mainly composed by a mix of pure minerals, namely Kaolinite, Illite, K-feldspar and Quartz.

Study of desert aerosol composition

Mineral dust is one of the major components of atmospheric aerosols (~40% on a global scale): it has important effects on the radiative budget of the atmosphere and thus on climate change.

Estimates of the global mean direct radiative forcing by mineral dust vary in a wide range (+0.09 to –0.46 W/m^2), owing to uncertainties in the mineralogical composition and size distribution.

An accurate quantitative analysis of airborne dust is needed.

Fingerprinting the desert dust

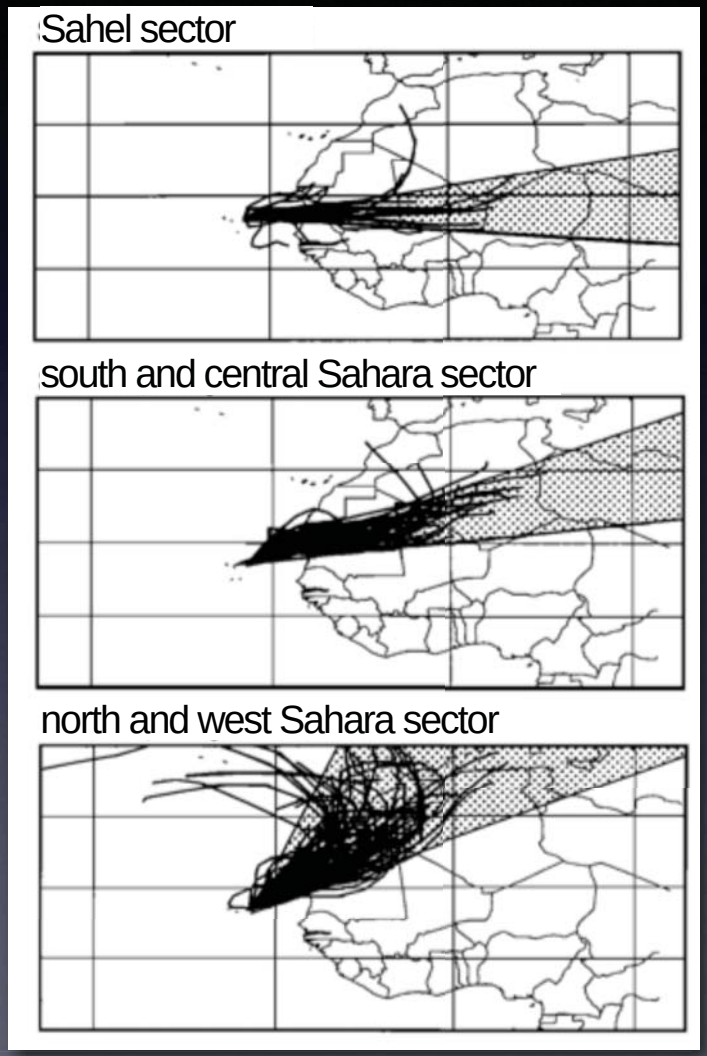

- Interelemental ratios in mineral dust measured at a receptor site can be used to differentiate source regions.

Table 1. Elemental Ratios of Dust Collected at Sal According to the Sectors of Origin Presented in Figure 2*

	Sector 1	Sector 2	Sector 3
Si/Al			
Mean	2.03	2.21	2.32
s.d.	0.09	0.07	0.10
Ca/Al			
Mean	0.20	0.36	0.60
s.d.	0.05	0.07	0.19
Fe/Ca			
Mean	2.71	1.43	0.90
s.d.	0.59	0.32	0.30
K/Ca			
Mean	0.96	0.62	0.43
s.d.	0.21	0.10	0.11

- If not corrected, elemental ratios prevent the possibility of distinguishing the origin of the dust.

I. Chiapello et al., J. Geophys. Res. 102, 1997

Study of ice core dust composition

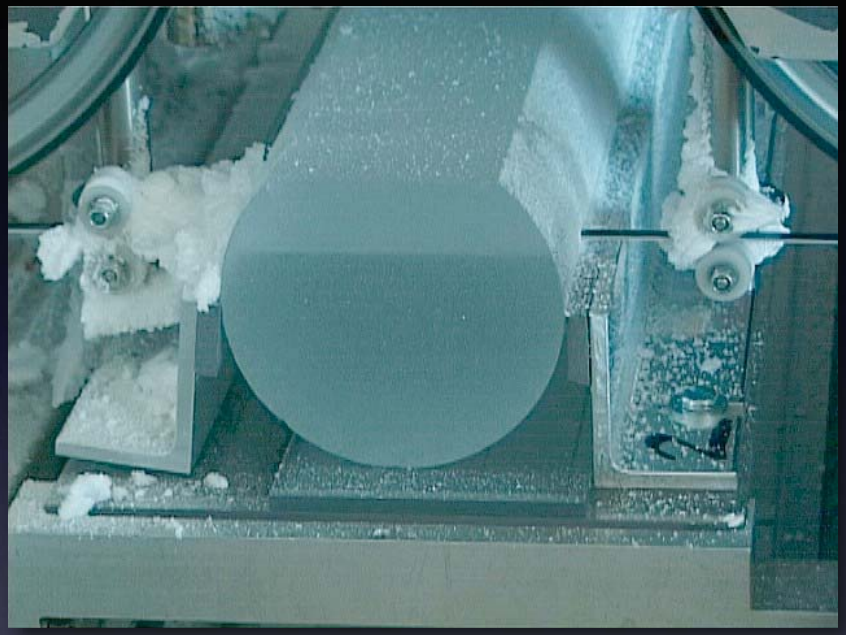

EPICA ice core (lenght 3190 m).
Ice sampled to an age of 800 kyr BP.

Polar ice cores are extensive archives of records of past atmospheric compositions, allowing paleoclimate research.

Snow, accumulated and compressed into solid ice, contains traces of the gases and the aerosols being in the atmosphere at the deposition time.

No post-depositional processes affect dust.

Study of ice core dust composition

Italian-French "Station Concordia" at Dome C.

No local dust sources in Antarctica.

Dust particles reach the inner Antarctic areas after long-range transport from continental areas in Southern Hemisphere.

From the analysis of the geochemical composition of ice core dust it is possible to infer the dust source location.

Ice core and PSA dust composition

The study of the composition of dust particles deposited over the Antarctic ice sheet and archived in ice core samples (spanning the last 220 kyr) helps to investigate global climate changes (EPICA project)

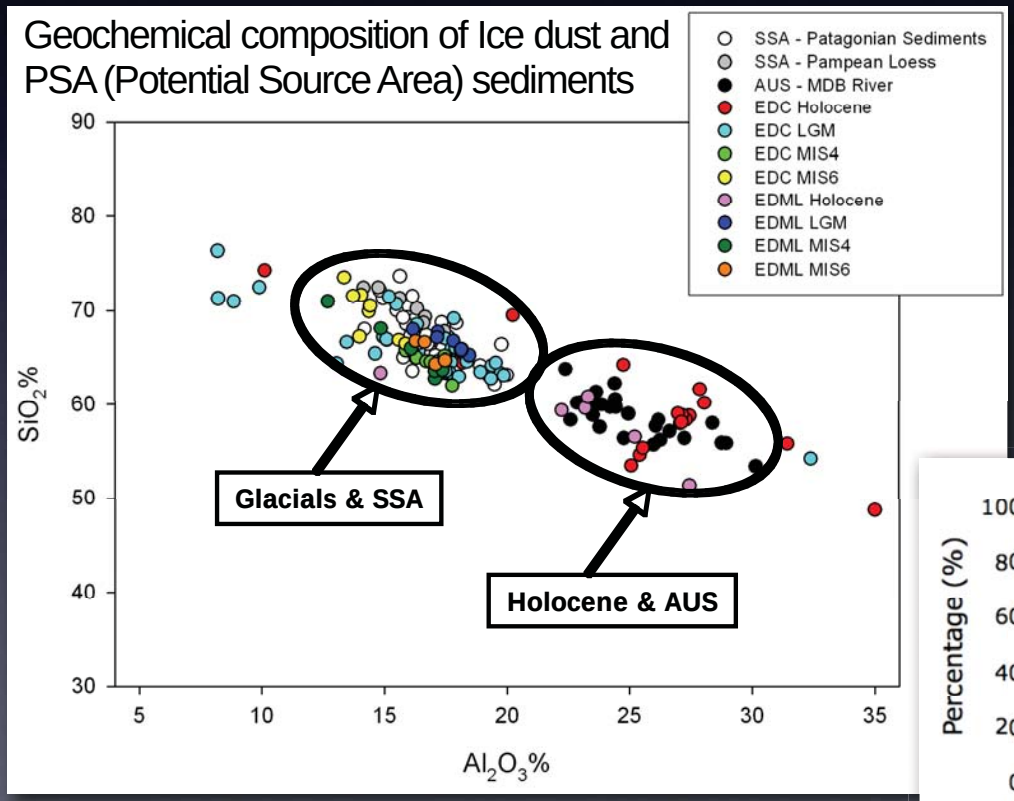

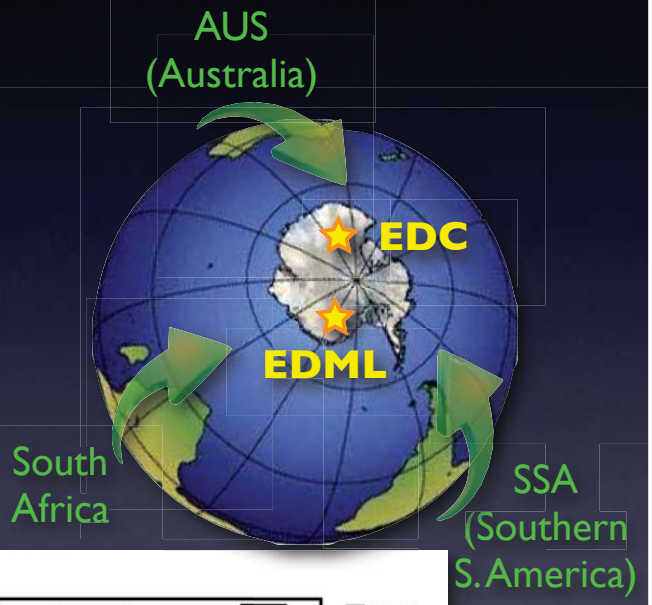

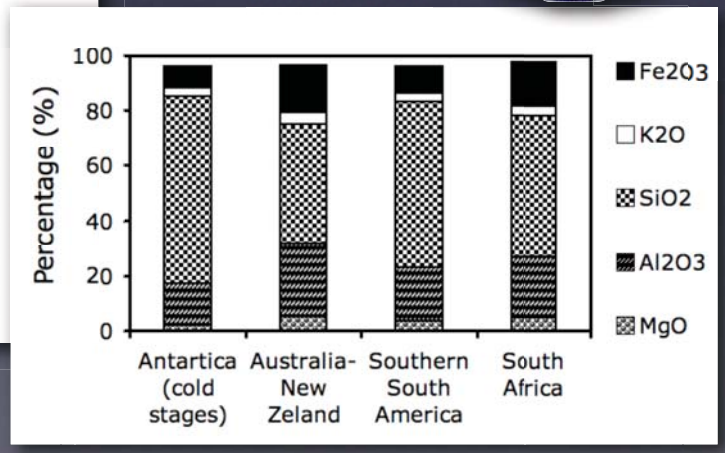

F. Marino et al., Geophys. Res. Lett. 36, 2009

Elastic scattering techniques & the aerosols

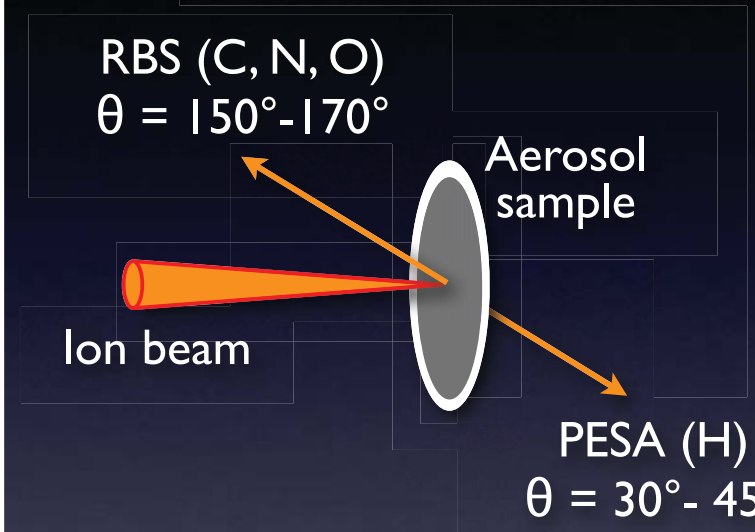

- RBS and PESA are "killing apps" to determine the light elements in aerosol samples
- Use of proton beams is mandatory to perform simultaneous PIXE measurements

- *C and O by 1.15 MeV protons backscattering, θ = 150° (Rubin et al., Anal. Chemistry 29, 1947)*
- *C by 16 MeV protons backscattering, θ = 120° (Andrae and Barnard, NIM 181, 1981)*
- *H, C, N and O by 30 MeV alpha particles forward scattering/recoil, θ = 64° (Cahill et al., NIM B 3, 1984)*
- *C and O by 3-4 MeV protons backscattering (Boni et al., NIM B 15, 1986)*

Typical filtering / collecting substrata

Name	Composition	Thickness (mg/cm^2)
Quartz and Glass fibre	Silicate and Borosilicate	5 - 7
Cellulose Acetate	$C_{12}H_{30}O_{15}$	~ 5
Cellulose Nitrate	$C_2H_{15}N_5O_{20}$	~ 5
Cellulose Mixed Ester	85% cell.nitrate 15% cell.acetate	~ 5
Teflon (ring supported)	PTFE: $(CF_2)_n$	0.5 - 0.7
Nuclepore	$C_{15}H_{14}CO_3$	~ 0.9

Teflon filter is an ideal substratum for H, C, N, O measurements

Choosing proton energy for RBS / PESA

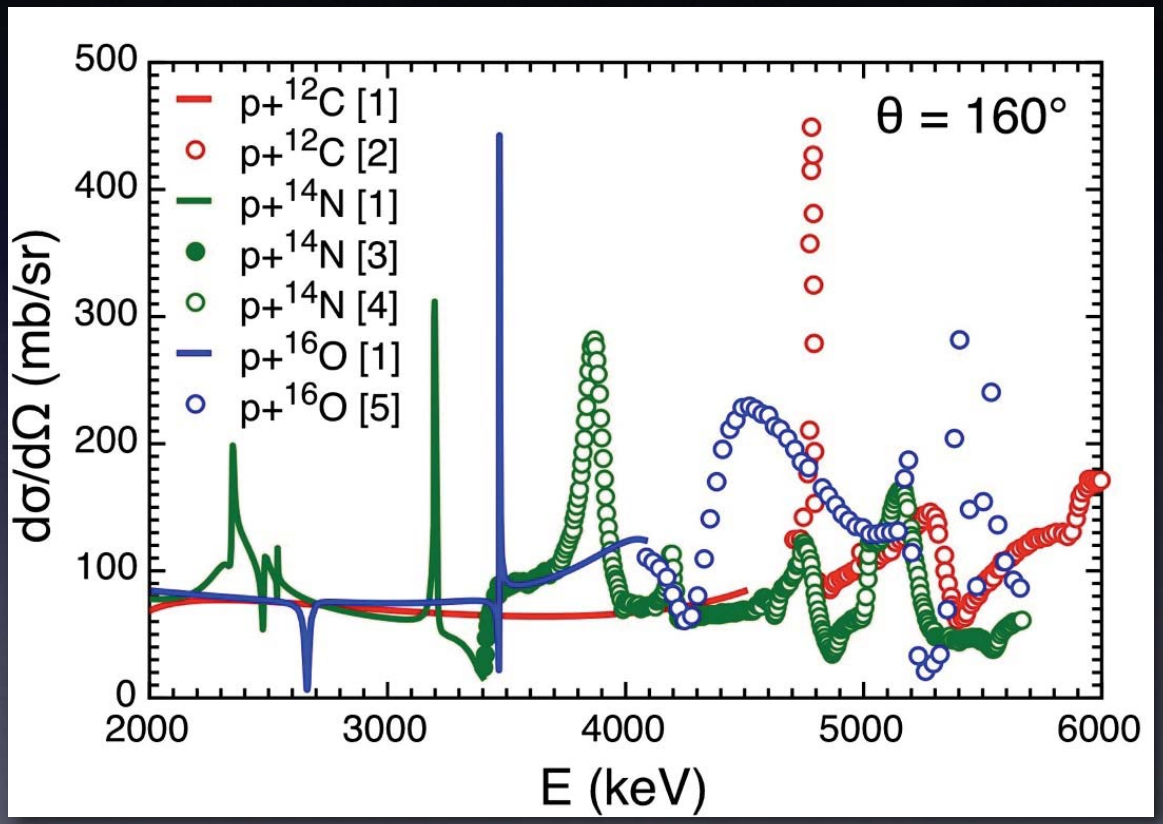

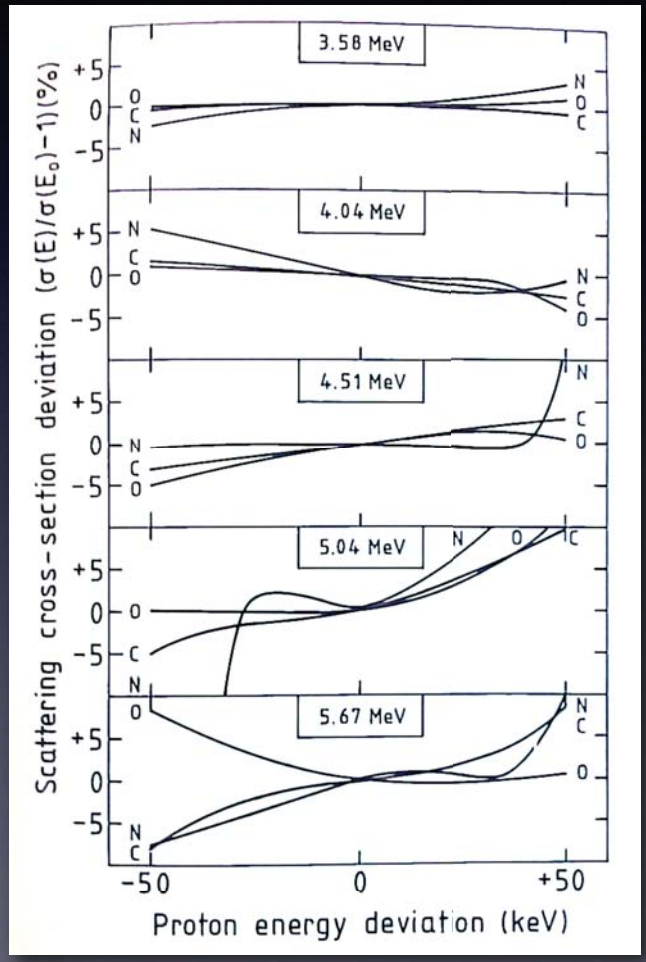

Martinsson, NIM B 15, 1986

[1] SigmaCalc (www-nds.iaea.org/sigmacalc/)
[2] Swint et al., Nucl. Phys. 86, 1966
[3] Bashkin et al., Phys. Rev. 114, 1959
[4] West et al., Phys. Rev. 179, 1969
[5] Harris et al., Nucl. Phys. 38, 1962

Sensitivity values for C, N, O, H by RBS / PESA

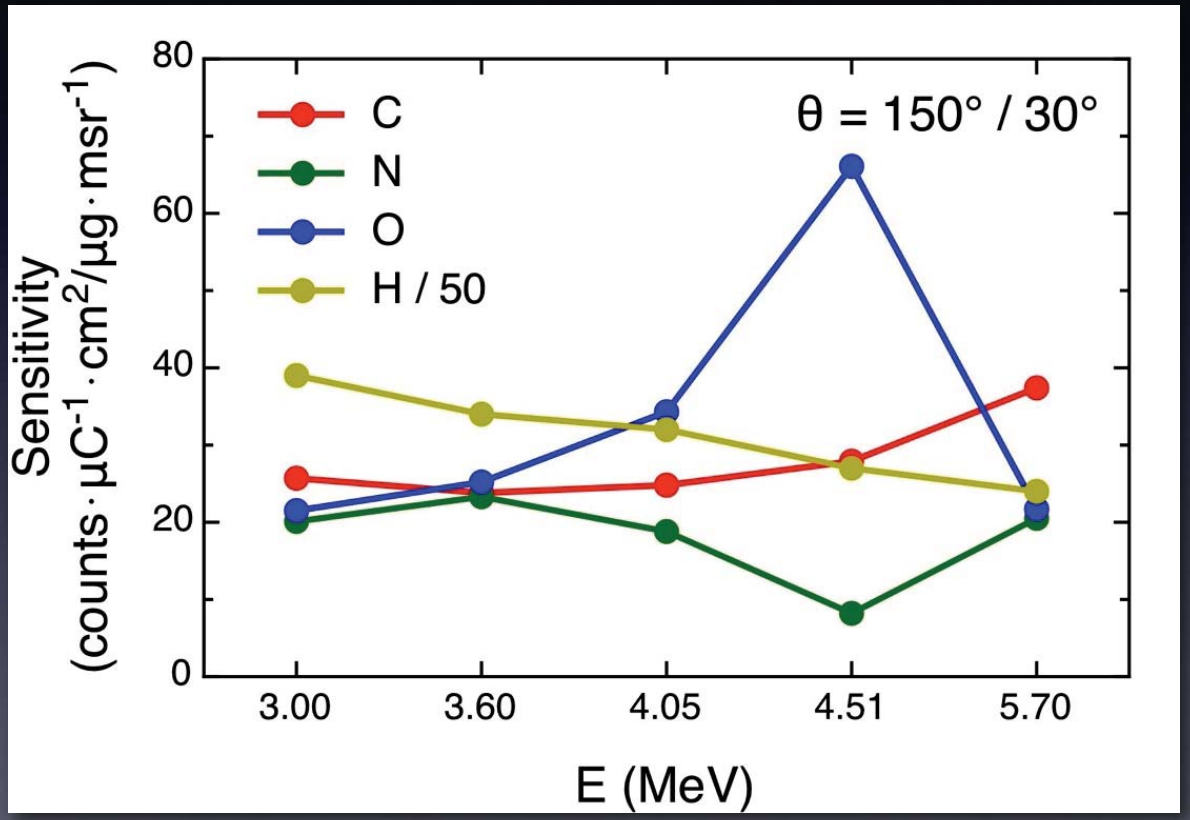

Measured with a thin Upilex-S standard ($H_{10}C_{22}N_2O_4$, 7.5 μm)

RBS/PESA on Teflon (CF_2) filters

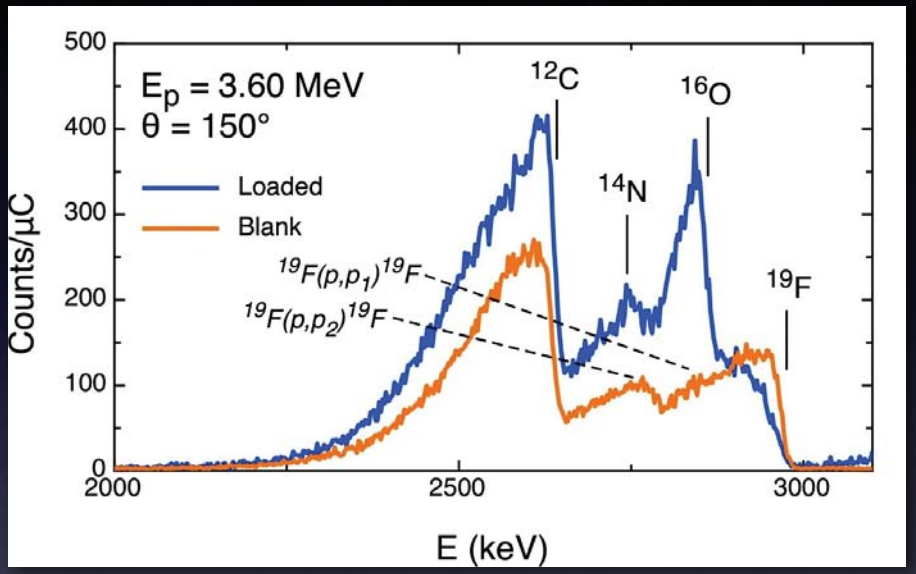

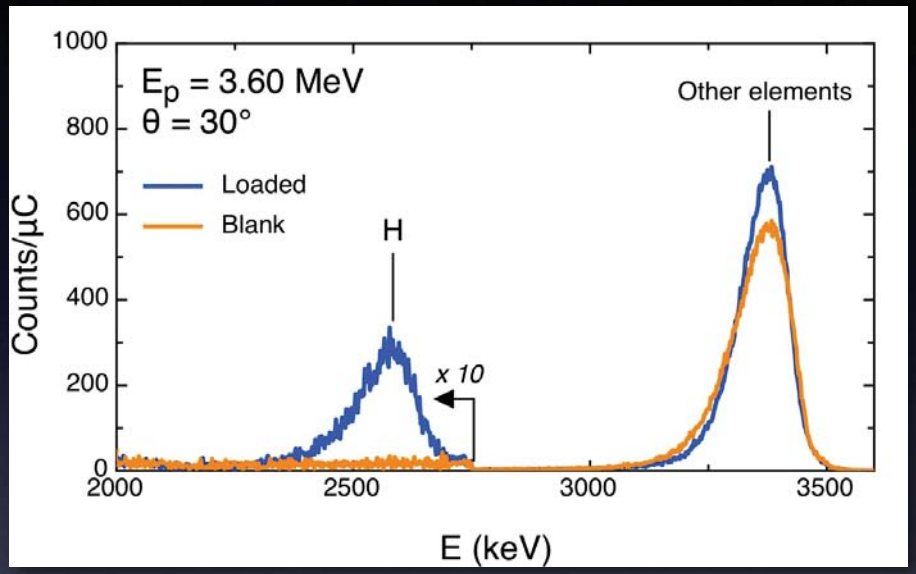

- Teflon (CF_2) filter is the ideal collecting substratum for RBS and PESA measurements
- Background in the RBS spectra due to:
  - *p elastically scattered by C and F of the filter*
  - *p inelastically scattered, (p,p') reactions, by F of the filter*

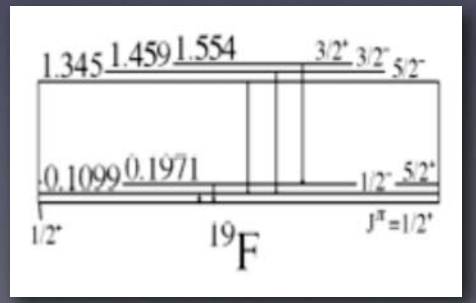

Quantitative analysis of C and other light elements

Fitting and simulations codes of RBS and PESA spectra (i.e. SIMNRA v6.05 by M. Meyer) implementing validated microscopic data and advanced physical models and effects

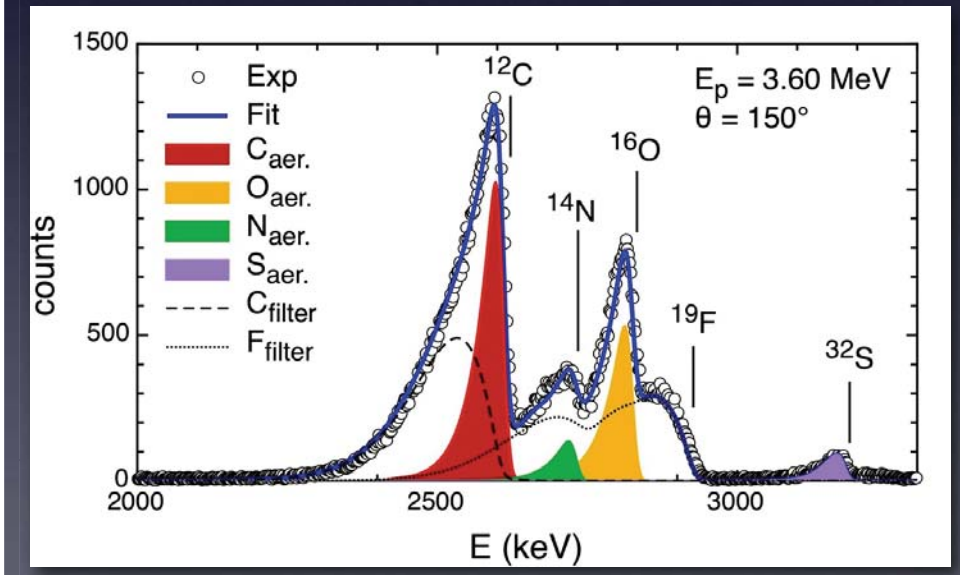

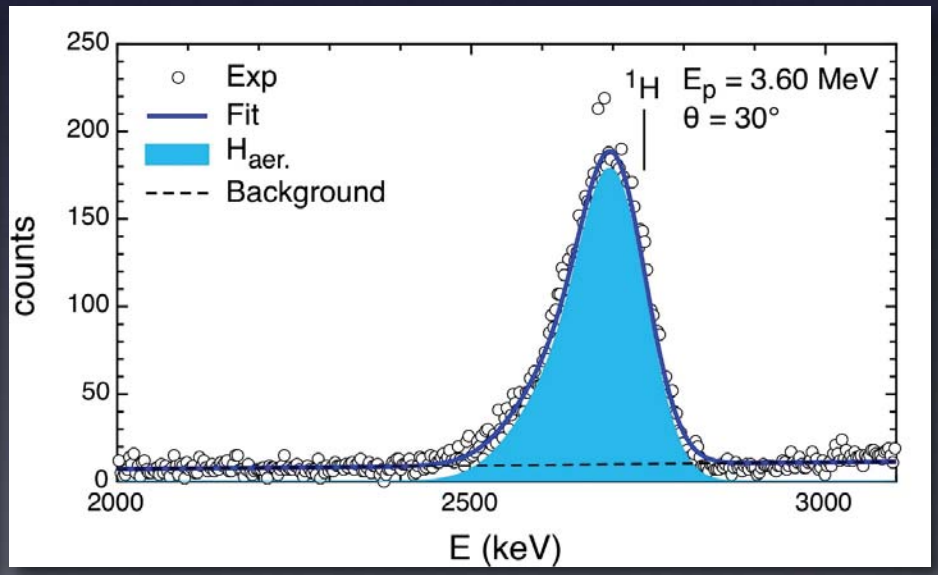

Typical detection limits and uncertainties

i = 5-10 *nA*
t = 5-6 *min.*

	Detection limit ($\mu g/cm^2$)	Detection limit ($\mu g/m^3$) *	Uncertainty
H	0.10	0.02	5-10%
C	4.0	1.0	5-10%
N	2.0	0.5	10-30%
O	2.0	0.5	10-20%
Z > 10	0.005 - 0.05	0.001 - 0.01	5-20%

* Considering a 47 mm diameter Teflon filter and sampling for 24 h at 2.3 m^3/h (European standard, EN12341)

Gravimetric mass reconstruction

The coupling of IBA techniques (PIXE, PIGE, RBS and PESA) allows the "mass closure": the sum of the mass of all the measured elements is equal to the gravimetric mass within 20% for all the samples (and within 10% for 85% of the samples)

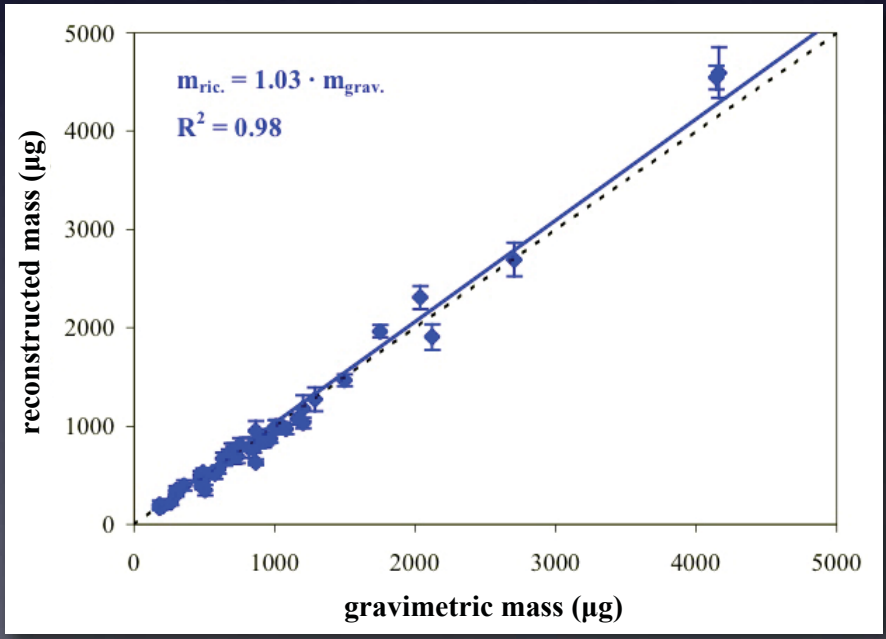

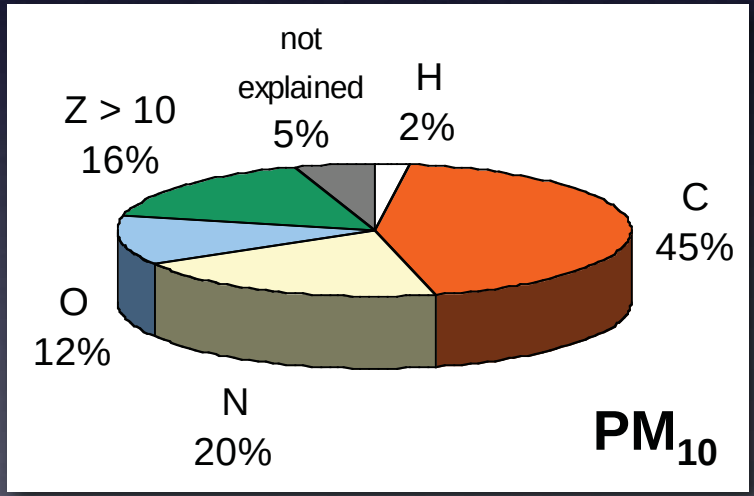

Airborne particulate matter characterization in the industrial district of Montelupo Fiorentino, Florence, Italy (September 2002 - June 2003)

Thanks for
your attention!

Bibliography

- R. Tesmer, M. Nastasi ed.s *"Handbook of Modern Ion Beam Materials Analysis"* MRS
- S. A.E. Johansson, J.L. Campbell, K.G. Malmqvist ed.s *"Particle-induced X-ray emission spectrometry (PIXE)"* John Wiley & sons
- W.-K. Chu, J.W. Mayer, M.-A. Nicolet *"Backscattering Spectrometry"* Academic Press
- G. Deconninck et al. *"Prompt gamma-ray spectroscopy and its use in elemental analysis"* At. Energy Rev. suppl. no. 2 (1981) 151